Applied Catalysis B: Environmental 343 (2024) 123576

Contents lists available at ScienceDirect

Applied Catalysis B: Environmental

journal homepage: www.elsevier.com/locate/apcatb

Electrochemical hydrogenation of levulinic acid, furfural and 5-hydroxymethylfurfural

Yunfei Zhang [a], Yi Shen [a,b,*]

[a] School of Food Science and Engineering, South China University of Technology, Guangzhou 510640, China
[b] China-Singapore International Joint Research Institute, Guangzhou Knowledge City, Guangzhou 510663, China

ARTICLE INFO

Keywords:
Levulinic acid
Furfural
5-hydroxymethylfurfural
Electrocatalysis
Hydrogenation

ABSTRACT

Platform molecules from lignocellulosic biomass, such as levulinic acid (LA), furfural (FF), and 5-hydroxymethylfurfural (HMF), hold great potentials as precursors to various fuels and high-value compounds through catalytic hydrogenation. However, the existing thermochemical conversions of these carbonyl-containing short-chain organics such as thermal catalytic hydrogenation involve energy-intensive and expensive processes. Electrocatalytic hydrogenation (ECH) emerges as an environmentally friendly, cost-effective, and safe process. The ECH of these organics can contribute to mitigating fossil-energy dependencies, fostering sustainable energy production, and yielding socio-economic benefits. ECH of these organics are thus intriguing, but there is a need to objectively evaluate this field. This review summarizes the product outcomes and critical reaction parameters (e.g., electrode materials, temperatures, electrolyte compositions) associated with ECH of LA, FF, and HMF. Emphasis is placed on the mechanisms related to the varying substrates. Special attention was paid to the correlations of catalytic performance with catalyst structures. After a thorough literature survey, strategies for catalyst design are discussed to enhance selectivity by promoting desired product formation and suppressing competing reactions. Moreover, current challenges, unresolved issues, and future perspectives on ECH of LA, FF, and HMF are proposed. It is expected that this work will afford useful information on the synthesis of electrocatalysts for electrochemical conversions of biomass.

1. Introduction

The utilization of non-renewable fossil resources, such as oil and natural gas, has been instrumental in driving the rapid growth of modern industries [1–3]. However, the increasing consumption of these limited resources, arisen from economic expansion and population growth, has resulted in the depletion of fossil reservation [4,5]. It has also led to substantial ecological costs and significant environmental risks, posing serious impediments to the sustainable development of human society [6,7]. Consequently, there is an urgent need to develop renewable alternatives to fossil fuels. Lignocellulosic biomass stands out as a promising candidate for replacing fossil resources [8–11]. Lignocellulosic biomass, being the most abundant energy resource on the earth, has the potential to serve as a raw material for the synthesis of high-value-added chemicals and liquid fuels (as shown in Fig. 1) [12–14]. One of the major advantages of biomass lies in its ability to produce various carbohydrates through heat treatment or acid hydrolysis [15–17]. The resulting carbohydrates can serve as primary resources for the production of platform molecules, fine chemicals, and liquid biofuels [18–20]. In addition to commercially available bioethanol, extensive research is being conducted on various carbohydrate-based fuel systems [21–26].

Ethanol derived from corn or sugar cane, serving as biomass components, has been studied to blend with petrol [27–35]. Nevertheless, the relatively low energy density of this fuel and its limited blending capacity (often less than 10 %) have stimulated the exploration of alternative biomass-based fuels [36–41]. Some platform molecules, derived from lignocellulosic biomass such as levulinic acid (LA) [42–46], and furanic compounds like furfural (FF) [61–64] and 5-hydroxymethylfurfural (HMF) [72–76], have promising applications in biofuel production through catalytic reduction. N-octane, a liquid biofuel, can be synthesized by combining electrocatalytic hydrogenation (ECH) of LA with the Kolbe reaction (as depicted in Fig. 2a) [50,51]. The conversion of LA paves the way for investigating hydrocarbons and valeric acid derivatives, including valeric esters, as potential biofuels for transportation [47–49]. This process utilizes valeric acid (VA) as an

* Corresponding author at: School of Food Science and Engineering, South China University of Technology, Guangzhou 510640, China.
E-mail address: feyshen@scut.edu.cn (Y. Shen).

https://doi.org/10.1016/j.apcatb.2023.123576
Received 2 September 2023; Received in revised form 23 November 2023; Accepted 27 November 2023
Available online 29 November 2023

intermediary [43,52]. Biofuels like 2-methylfuran (MF) and 2-methyltetrahydrofuran (MTHF), derived from FF reduction (Fig. 2b), have high energy densities that make them promise for various applications [67–70]. In particular, the energy density of MF is 28.5 MJ/L, which not only exceeds bioethanol's 23 MJ/L but also closely competes with gasoline's 32.9 MJ/L [71]. MTHF with an octane number of 74, can be incorporated into *p*-series gasoline fuel [71]. Another notable biofuel, 2, 5-dimethylfuran (DMF), produced from the reduction of HMF, has an energy density of 31.5 MJ/L, bringing it closer to gasoline's range. In addition, the other reduction byproducts of LA and furanic compounds have significant applications in fine chemicals, food, polymers, and pharmaceuticals [53–60]. VA, derived from LA reduction, is used in polymer synthesis and flavor/fragrance production, while gamma-valerolactone (GVL), another LA derivative, serves as a valuable solvent. Furfuryl alcohol (FA) from FF reduction has applications in polymers, pharmaceuticals, and adhesives [65,66]. HMF serves as a platform for various value-added chemicals, such as 2,5-dihydroxymethylfuran (DHMF) [77–79], and 2,5-dihydroxymethyltetrahydrofuran (DHMTHF) [80–82]. Other derivatives include 2,5-hexanedione (HD) and 5,5'-bis(hydroxymethyl)hydrofuroin (BHH) [86,87]. DHMF and DHMTHF play pivotal roles in the synthesis of biodiesel, polyesters, and polyurethane foams [88,89], [90,91]. HD acts as a precursor for many biofuels and chemicals, and BHH shows potential in diesel and jet fuel precursors [93]. Catalytic hydrogenation of LA, FF, and HMF has been studied through various approaches [25,95–99]. Therefore, the reduction of carbonyl-containing short-chain compounds, including LA, FF and HMF, into valuable chemical substances holds significant importance.

Various methodologies have been studied for the catalytic hydrogenation of LA, FF, and HMF [60,61]. Conventional thermal hydrogenation typically requires high temperatures and substantial quantities of hydrogen [62,63]. However, the high temperature and pressure conditions pose inherent safety risks, including explosion and leakage hazards, in industrial production [64,65]. Moreover, elevated temperatures during the catalytic hydrogenation may lead to catalyst poisoning and carbonization, compromising the activity and stability of the catalyst [66,67]. Additionally, the continuous supply of hydrogen throughout the reaction escalates the overall economic burden associated with catalytic hydrogenation technology [68]. In contrast, ECH of biomass derivatives offers several advantages over conventional thermal catalysis [69,70]. One notable advantage is the exploitation of H_2O as an in-situ hydrogen donor, eliminating the need for an external hydrogen gas supply and the associated procurement and storage costs [71,72]. Additionally, the electrocatalytic process can be conducted under mild conditions of ambient temperature and pressure, eliminating the necessity for the extreme temperature and pressure regimes involved in the traditional thermocatalysis [73,74]. Consequently, the electrochemical approach enhances the safety of hydrogenation of biomass derivatives. Another significant advantage of electrocatalysis lies in the facile control of product selectivity and substrate conversion by manipulating the experimental parameters, such as potentials and pH values of the electrolytes [75]. Modulating the electrode potential allows for a facile approach to control the reaction pathway, enabling the target products under appropriate potentials [76]. Furthermore, the electrical energy required for the electrocatalytic process can be derived from renewable sources, such as wind energy, solar energy, and tidal energy, making the entire process environmentally sustainable and aligned with the principles of green chemistry [77].

While the ECH presents numerous advantages over thermocatalytic reduction, the field of research on ECH of LA and furanic compounds is still young. Most existing research has primarily explored parameter effects, emphasizing catalysts, reaction conditions, and reactors. The diverse array of studied parameters complicates the comparison of findings in this domain. Two significant challenges persist: firstly, the issue of mass imbalance arising from side reactions and product volatilization during the ECH of LA and furanic compounds; and secondly, efficiency reduction due to the hydrogen evolution reactions (HER). Such complications have left much of the existing literature without broad, conclusive insights. Review papers have been published with sections on the ECH of LA and furanic compounds, with a primary focus on catalyst selection and development. However, other experimental parameters also play crucial roles in determining ECH outcomes. This review presents a systematic overview of the reduction products from the ECH of LA, FF, and HMF. Important parameters that influence product selectivity and Faradaic efficiency (FE) in the ECH processes of these compounds are analyzed. This paper provides insights into the possible mechanisms of ECH for LA, FF, and HMF. Recommendations are provided for enhanced target products selectivity, mitigation of undesired reactions, and optimal catalyst design. Moreover, the current challenges and prospects for industrial-scale implementation are also discussed.

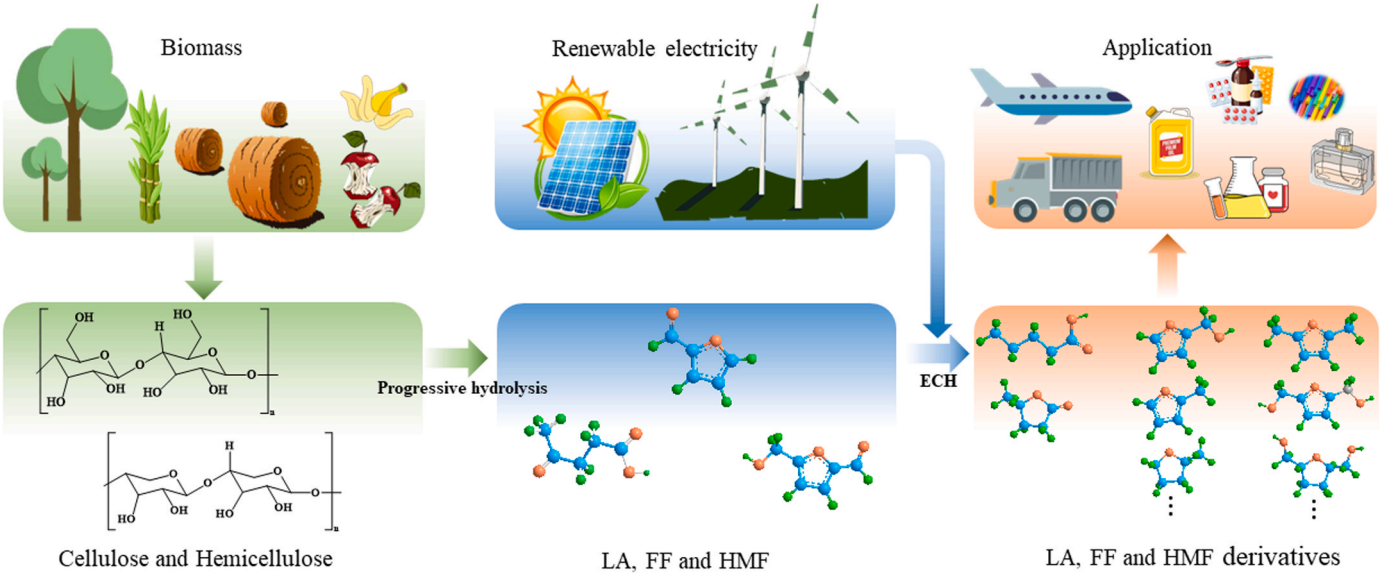

Fig. 1. Biomass as a source of cellulose and hemicellulose possible precursors to fuels, chemicals, and materials.

2. ECH processes

During the ECH process, chemisorbed hydrogen (H_{ads}) is generated in situ on the electrode surface through the process of proton or water electroreduction via the Volmer step, as illustrated in Fig. 3a [78–80]. The resulting H_{ads} species plays a pivotal role as a hydrogen source for the subsequent ECH of LA, FF, and HMF (pathway in the pink area of Fig. 3b). However, a significant challenge arises from the competition with the HER. The Tafel step and Heyrovsky step involve the consumption of H_{ads} to generate H_2, thereby facilitating the HER pathway [78–80]. Consequently, this occurrence reduces the surface density of H_{ads} and impairs the FE of the ECH process. In addition to the competition with the HER, Chadderdon et al. have proposed another competing reaction known as electroreduction processes [81,82]. As depicted by the pathway in the blue area of Fig. 3b, in an acidic environment, carbonyl-functionalized compounds undergo adsorption on the electrode surface and engage in electron transfer processes. Upon interacting with 1-proton and 1-electron (H^+/e^-), the carbonyl-containing compounds form radical intermediates, which subsequently undergo C-C coupling with another radical intermediate to yield dimeric species [82,83]. The radical intermediates can also participate in the formation of alcohols by further reacting with a H^+/e^- pair, representing an indirect pathway for the production of the alcohols. In neutral or alkaline electrolytes, carbonyl-functionalized compounds cannot directly adsorb onto the electrode surface. The electroreduction involves water as the source of hydrogen and proceeds through an outer-sphere electron transfer process [81–83]. This electroreduction process has detrimental effects on the product selectivity and FE of ECH involving carbonyl-functionalized compounds.

3. ECH of LA

Sugars, typically composed of five or six carbons, are derived from the continuous hydrolysis of lignocellulose biomass and could serve as the primary feedstock for LA production [61,84–90]. The ECH of LA produces relatively simple products, mainly GVL by 2-electron reduction and VA by 4-electron reduction [91]. Typically, the sum of the selectivities of GVL and VA exceeds 90 %, and there are scarce reports on LA dimerization during the electrochemical process. The reaction rates and product selectivities in the ECH of LA are influenced by various reaction parameters, including electrode materials, electrolyte pHs, initial concentrations of LA, applied potentials of the working electrode, among others.

3.1. Effects of electrode materials

Electrochemical conversion is a heterogeneous process in which the electrode material's inherent properties play a crucial role in the conversion of LA [39]. Structural characteristics of the electrodes notably determine both reaction efficiency and product distribution. An array of catalyst materials, encompassing non-precious metals like Fe, Cu, Al, Pb, Zn, Sn, Ni, Co, Ti, Cd, and Hg, as well as rare metals like Pt, Pd, and Ag have been rigorously explored [38,39,78,92]. Additionally, carbon has been examined as an electrode material for LA ECH. Carbon felts (CFs) represent as a suitable support for metal catalysts. Table 1 compiles the performance of the metals for LA ECH. In a comprehensive study by Bisselink et al., they evaluated the electrocatalytic performance of various metals for the ECH of LA, determining that Cd, In, and Zn wires manifested superior selectivity toward VA with remarkable LA conversion in 1 M H_2SO_4 [92]. In the investigation by Dos et al., the ECH performance of different metal plates (Cu, Fe, Ni, and Pb) and carbon for LA conversion were assessed [92]. Their findings indicated the superior catalytic activity of Pb in 0.5 M H_2SO_4 for LA ECH. In contrast, Fe, Ni, and Cu had limited catalytic activity. Notably, carbon achieved a 39.0 % LA conversion in 0.5 M H_2SO_4, identifying GVL as the primary product, coupled with a current efficiency of 18.0 % [39]. Such findings underscore the potential of employing metal-carbon composites for converting LA to GVL, broadening perspective in the research topic. Du et al., observed that Pt, Ti, and Co exhibited marginal electrocatalytic activity in 0.2 M H_2SO_4 for LA ECH [93]. It's essential to note that, regardless of H_2SO_4 concentration used as the electrolyte in the ECH of LA, VA and GVL are consistently the primary products. VA selectivity notably surpasses that of GVL. Although it is theoretically possible for LA to form dimers during the ECH process, such a phenomenon has not been reported in the literature. The selection of electrode material profoundly impacts the balance between ECH and HER. Yet, limited studies on other advanced electrocatalysts, such as alloys and single atom catalysts, are seldom reported for the ECH of LA. Future research in this direction is

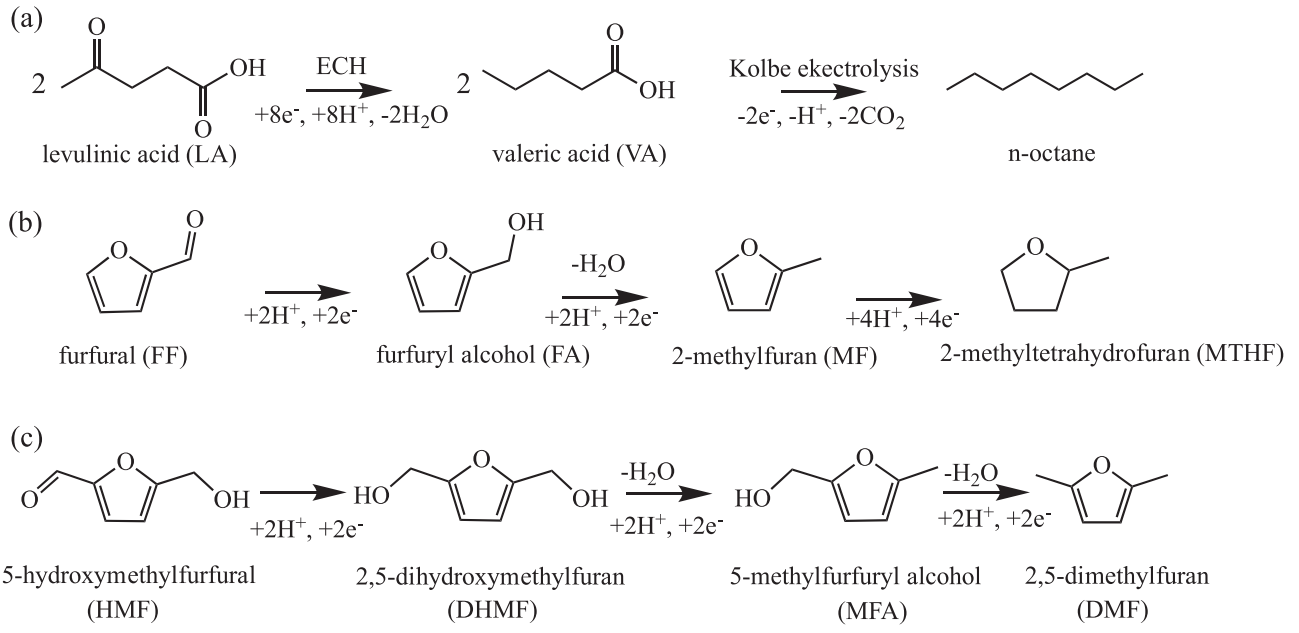

Fig. 2. (a) Schematic illustration of the two electrochemical routes for the conversion of LA to N-octane [38], Schematic illustration of the conversion FF to MTHF (b) and HMF to DMF (c), respectively [59].

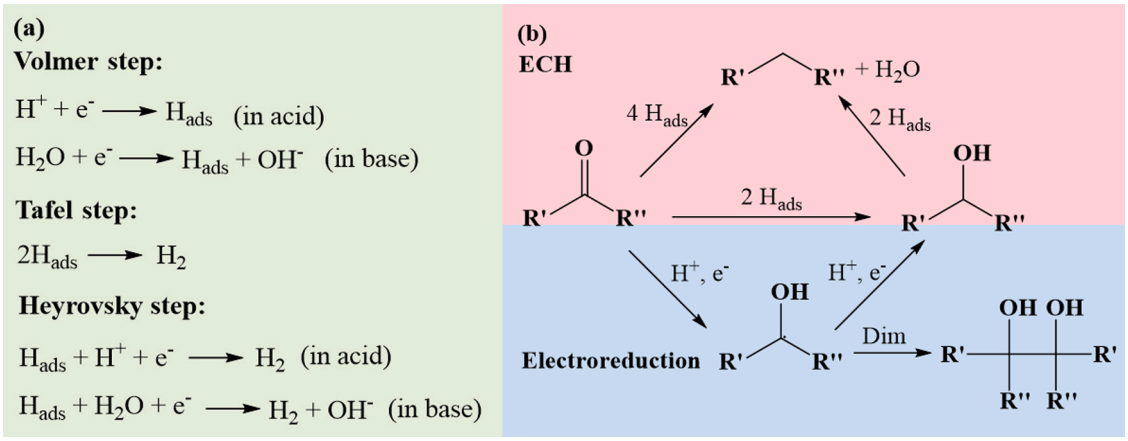

Fig. 3. (a) Pathways of H_{ads} generation and consumption [78] and (b) Proposed pathways of electrocatalytic conversion of carbonyls in acidic electrolytes [81].

Table 1
Catalytic performance of various cathodes for the conversion of LA.

Cathode metal	Reaction medium	LA Conc[a]/M	Electrolysis conditions	T[b]/h	Conv[c]/%	FE or CE/%	Selec[d]/%		Ref
							VA	GVL	
Pb (rod)	SA	-[e]	8 °C; −1.8 V vs. Ag/AgCl	-	-	27.0	97.2	-	[38]
C	0.5 M H_2SO_4	0.5	−1.8 V vs. Ag/AgCl	4	39.0	18.0	0	69.0	[39]
Cu (sheet)					7.3	1.3	8.3	9.6	
Fe (sheet)					19.9	0.5	9.6	7.8	
Fe (sheet)	1 M KOH				24.5	18.5	-	74.5	
Ni (sheet)	0.5 M H_2SO_4				8.0	1.1	17.3	3.2	
Pb (sheet)					71.6	56.4	81.6	18.4	
Pb (sheet)	1 M KOH				19.6	21.1	-	48.7	
Pb (plate)	0.5 M H_2SO_4	0.2	Flow-cell; −1.3 V vs. RHE	2	18.6	86.5	95	-	[78]
			Half-cell; −1.3 V vs. RHE		12.7	84.2	94.5	-	
	Buffer (pH 7.5)		Half-cell; −1.3 V vs. RHE		1.3	6.2	-	10.8	
			Flow-cell; −1.3 V vs. RHE		4.5	18.2	-	4.0	
Pb (plate)	$KHCO_3$ +$KClO_4$	0.1	4 F/mol; −1.9 V vs. RHE	-	92.0	47.1	-	-	[83]
Pb/CFs	0.1 M H_2SO_4	0.1	−1.3 V vs. RHE	2	45.0	87.6	77.0	2.3	[100]
Cd/CFs					52.1	49.7	37.3	0.5	
Co/CFs					41.3	10.2	13.2	31.1	
Ni/CFs					13.5	6.7	50.8	27.7	
Cu/CFs					9.6	7.1	66.9	1.5	
Bi/CFs					18.2	8.9	31.2	3.9	
Pt/CP					17.1	6.5	35.9	30.9	
Pd/CP					10.1	4.5	62.2	-	
Pb (wires)	1 M H_2SO_4	0.5	50 °C; 8 F/mol	-	98.6	46.1	94.0	2.5	[92]
Cd (wires)					98.0	44.8	91.9	3.0	
In (wires)					88.4	43.6	99.1	0.0	
Zn (wires)					65.1	30.8	95.5	2.1	
Al (wires)					14.0	5.6	74.0	21.0	
Ni (wires)					7.3	2.7	71.0	22.0	
Pb (plate)	0.5 M H_2SO_4	0.2	50 °C; −1.8 V vs. Ag/AgCl	1	56.0	72.0	97.0	-	[93]
Co (sheet)	0.2 M H_2SO_4		−1.8 V vs. Ag/AgCl	2	> 5	> 0.8	> 55	> 44	
Pt (sheet)					> 4	> 0.2	100	-	
Zn (sheet)					> 19	> 20	100	-	
Cu (foam)					> 10	> 0.3	-	100	
PbS	$[Bmim]BF_4$	-	−2.15 V vs. Ag/Ag^+	4	-	78.6 GVL	-	-	[107]
Pb (plate)	0.5 M H_2SO_4	0.2	Flow-cell; −1.5 V vs. RHE	8	> 86	> 52	> 97	> 3	[108]
		1.0			> 39	> 48	> 88	> 12	
Pb_1-In_2-600	0.5 M H_2SO_4	0.2	−1.3 V vs. RHE	2	> 41.5	> 84	> 97	> 2.8	[104]
$In_{72.4}Pb_{27.6}$	0.1 M H_2SO_4	0.1	−1.3 V vs. RHE	3	60.5	64.0	91.2	0.60	[101]
β-PbO/Pb	0.5 M H_2SO_4	0.1	−1.4 V vs. RHE	4	~ 100	57.58	95.0	-	[111]

[a] Concentration of LA; [b] Reaction time; [c] Conversion of LA; [d]Selectivity of products; [e] the value was either not mentioned or not detected in this literature.

highly desirable and would profoundly enrich the understandings on the correlation of catalyst structures with catalyst performance for electrochemical conversion of LA.

The surface morphology, such as particle size of the catalyst, is an integral aspect to consider when evaluating electrochemical processes. It's established that smaller metal particles boast a larger specific surface area, providing a greater density of active sites for LA adsorption, which in turn enhances the ECH process [65,94–99]. However, the application of ultrafine metal nanoparticles for LA ECH is not extensively explored, possibly due to their complex interaction with the electrolyte. It's worth highlighting that LA undergoes efficient conversion in acidic conditions. However, these conditions might also lead to the dissolution of ultrafine metal nanoparticles. Therefore, it is urgent to conduct in-depth studies to decipher these intricate interactions and maximize the application of metal nanoparticles in the ECH of LA. To obtain catalysts with tunable particle sizes, we employed electrodeposition techniques to prepare the

electrodes with varying metal loadings on CFs, resulting in the metal/CF catalysts [100]. They were subsequently used to scrutinize the ECH of LA. Fig. 4 illustrates the results from the linear cyclic voltammetry scan (LSV) in 0.1 M H_2SO_4. The introduction of LA into the electrolyte led to a discernible reduction in current density for the Cd/CFs, Co/CFs, and Ni/CFs, while the Bi/CF and Cu/CF were virtually unaffected [100]. In contrast, the Pb/CF showcased a significant surge in current density upon the inclusion of LA in the electrolyte [100]. These observations were resonated with the cyclic voltammetry (CV) profiles documented by Xin et al. (Fig. 5a), where the presence of LA in an acidic medium markedly raised the current density on the Pb electrode. This phenomenon did not occur at the Cu electrode [78]. We further fabricated micrometer-scaled Pb-In bimetallic catalysts and evaluated their electrochemical performance. The $In_{72.4}Pb_{27.6}$/CF catalyst exhibited superior electrochemical activity compared to the individual Pb and In catalysts [101]. The enhanced efficiency of In-Pb bimetallic catalysts over the monometallic components is attributed to the synergy between Pb and In atoms, leading to reduced charge transfer resistance and an enlarged electrochemically active area [102,103]. As a result, we observed a remarkable LA conversion rate of 86.1 % coupled with a remarkable VA selectivity of 99.7 % [101]. Yuan et al. devised a bimetallic catalyst combining PbO and In_2O_3, achieving an LA conversion of 46.1 % and a VA selectivity of 97.8 % [104]. Bimetallic and polymetallic electrode materials bear distinct merits due to their intricate structures and surface properties, outperforming their single-metal counterparts [105,106]. While various nanoparticles have been explored in electrocatalytic conversion of substrates, the application in the ECH of LA is still limited. The synthesis of advanced electrode materials and in-depth understanding the effects of particle size on LA's catalytic efficiency present a promising research direction.

3.2. Effects of reactor

The design of the reactor has a crucial role in determining the efficiency of the ECH of LA. An optimized experimental setup can significantly improve mole balance closure and product selectivity. The ECH of LA has been studied using continuous, batch, and semi-batch reactors. Continuous reactors, often referred to as flow-cell reactors, typically comprise two channels for electrolyte circulation. These reactors are especially beneficial for scale-up applications and mitigating mass transfer issues. Xin et al. utilized a tailored flow-cell to study the ECH of LA [78]. Their results indicated that the flow cell exhibited a slower decline in FE over time compared to the H-type half-cell setup. The enhanced efficiency in the ECH of LA within the flow-cell is likely due to the specialized design and operational parameters. Notably, the flow-cell has a high flow rate of 30 sccm, an increased electrode area of 6.5 cm^2, and a compact cathode chamber with a volume of 12 mL [78]. Such design features facilitate a consistent supply of LA to the working electrode, while minimizing mass transfer restrictions from hydrogen bubble disruptions at the lead electrode. On the other hand, batch and semi-batch reactors are typically employed for fundamental and kinetic studies. A majority of the studies utilized batch reactors, and thus most results highlighted in this section were derived from experiments conducted in batch setups.

3.3. Effects of electrolytes

Apart from the electrode materials, the pH of electrolytes also plays a role in determining product distribution, selectivity, and FE. Herein, the primary focus is the results obtained from Pb electrodes in H_2SO_4, buffer solutions, and KOH solutions. It's essential to highlight that all the employed electrolytes were aqueous without any organic additives. When the pH of the electrolyte was less than 7.0, the selectivity of VA consistently exceeded 90 %. For instance, Nilges et al. [38] and Bisselink et al. [92] conducted ECH of LA in 0.5 M and 1.0 M H_2SO_4 solutions at a constant current density, achieving VA selectivities of 97.2 % and 94.0 %, respectively. Similarly, Xin et al. [78] and Dos et al. [39] employed a constant potential of −1.5 V vs. RHE in a 0.5 M H_2SO_4 solution,

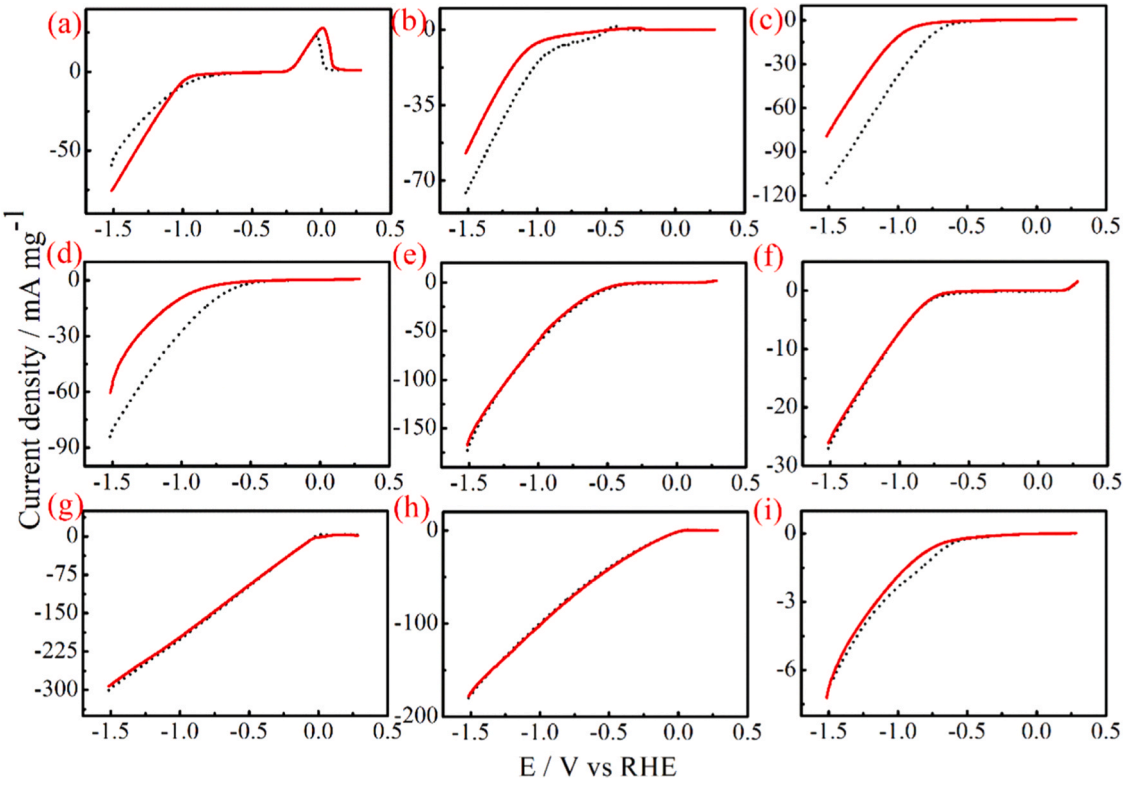

Fig. 4. LSV curves of (a) Pb/CFs, (b) Cd/CFs, (c) Co/CFs, (d) Ni/CFs, (e) Cu/CFs, (f) Bi/CFs, (g) Pt/CP (h) Pd/CP, and (i) CFs electrodes, recorded at 50 mV s^{-1} in 0.1 M H_2SO_4 + 0.1 M LA (Solid lines) and 0.1 M H_2SO_4 (dotted lines), respectively [100].

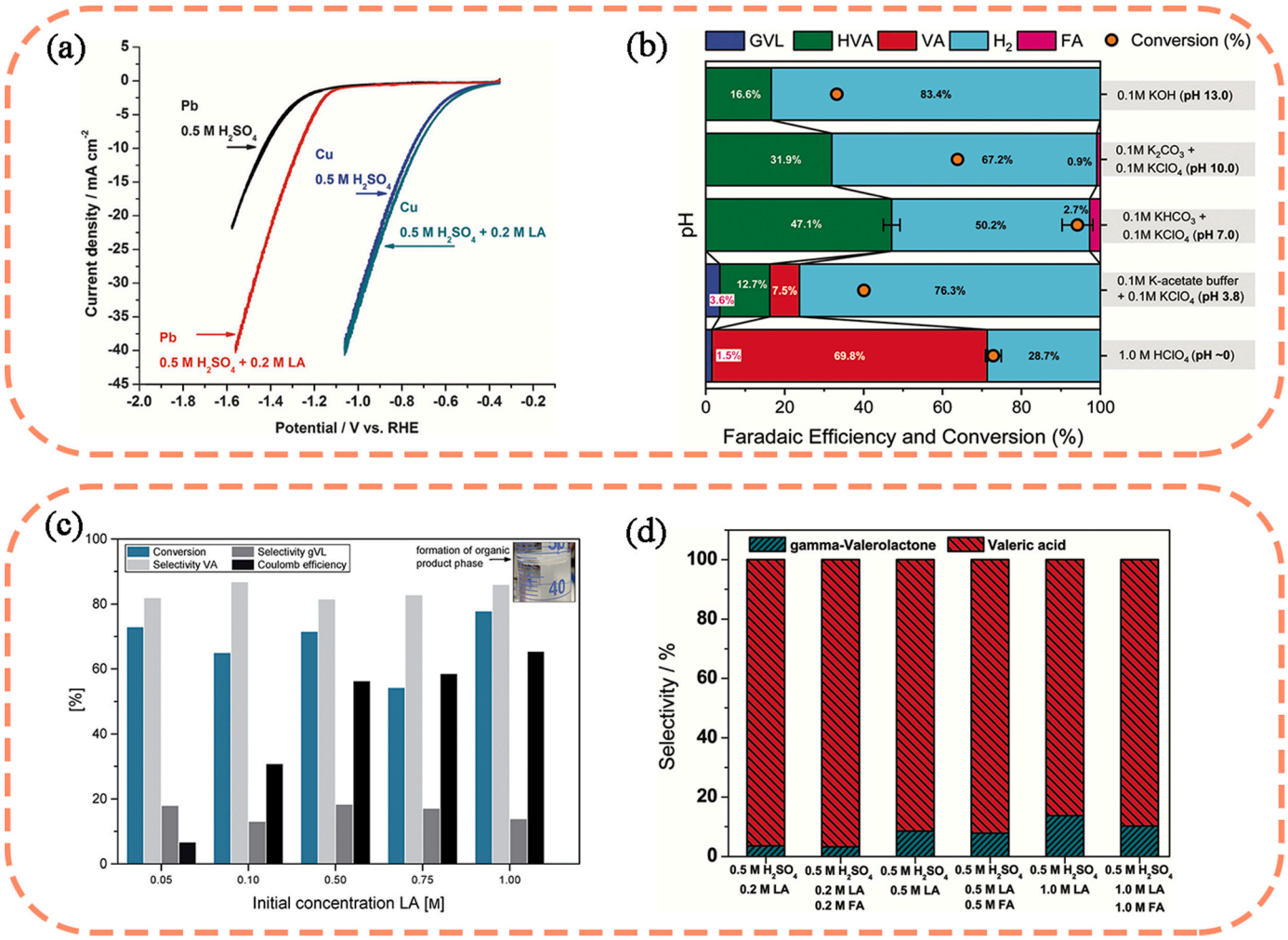

Fig. 5. (a) CVs of the ECH of LA on Pb and Cu in an acidic electrolyte (pH = 0) at a scan rate of 50 mV s^{-1} [78], (b) pH effects for electrolysis performed with 0.1 M LA, at −1.9 V vs. RHE, with passage of 4 F/M LA [83], (c) ECH of LA at Pb-electrode in a divided H-Cell at different LA initial concentrations [39] and (d) Selectivity of the ECH of LA on a Pb electrode in an electrocatalytic flow cell reactor at −1.5 V vs. RHE [108].

obtaining VA selectivities of 97.1 % and 81.6 %, respectively. Substituting 0.5 M H_2SO_4 with 1.0 M $HClO_4$, the VA selectivity remained above 90 %. This trend indicates that the pH, rather than the specific anions, determines VA selectivity. In buffer solutions with pH values ranging from 7.0 and 7.5, VA was undetectable, and the LA conversion rate was below 5 %. When the pH exceeds 7.0, VA remained absent. These results underscore that the selectivity towards VA and GVL is profoundly influenced by the electrolyte's pH, with acidic conditions favoring VA formation. Interestingly, when alternative electrodes like carbon were used in a 0.5 M H_2SO_4 solution, VA was absent, but the GVL selectivity reached to 69.0 %.

The selectivity of GVL exhibits an inverse trend to that of VA, with higher selectivity observed under alkaline conditions. Under acidic conditions, the GVL selectivity remained below 5 %. However, as the pH was ranged from 7.0 and 7.5 (in buffer solutions), GVL selectivity was maximized at 100 %. In 0.1 M and 1.0 M KOH solutions, GVL selectivity was measured at 100 % and 48.7 %, respectively. In 1.0 M KOH solutions, even though GVL was the only product, the reduced selectivity could be attributed to side reactions in the strong alkaline environments. With alternative electrodes, such as Fe, GVL selectivity of 74.5 % was achieved in a 1.0 M KOH solution [159]. While 4-hydroxyvaleric acid (4-HVA) has been identified as a major intermediate in the LA conversion process, it hasn't been extensively discussed as a final product. Yet, Lucas et al. posited 4-HVA as a product species of the ECH process for LA. Detection of 4-HVA was confirmed at pH 3.8, while at pH values of 7.0 or higher, 4-HVA was the sole product with a selectivity reaching to 100 % (as shown in Fig. 5b) [83].

Doping the electrolyte with organics, including acetonitrile, methanol, etc., has been found to enhance the ECH process by minimizing species loss and promoting mole balance. For instance, Wu et al. explored the electrochemical behavior of LA on a PbS electrode, employing an ionic liquid methanol aqueous solution system, specifically [Bmim]BF_4-MeCN-H_2O, as the electrolyte [107]. This study yielded GVL as the only product, boasting a FE of 78.6 %.

3.4. *Effects of applied potential and LA initial concentration*

The FE or Coulombic efficiency (CE) are vital metrics in assessing the ECH of LA. These parameters are primarily governed by the applied potentials and the initial concentrations of the substrates. The applied potential can modulate both the ECH and the HER on the catalyst surface. Typically, the ECH of LA operates at potentials considerably more negative than those required for the HER process. This represents a challenge for ECH study as there's a need to achieve desired reaction rates at relatively low potentials while minimizing HER processes. As elaborated in the Section 2, both ECH and HER share the Volmer reaction mechanism, where protons electrochemically adsorb onto the electrode surface. ECH takes precedence over HER when these H_{ads} react with LA. The ECH efficiency is compromised when HER dominates.

The applied potential is a pivotal factor in the ECH of LA. It

influences the rate of LA adsorption, the kinetics of the HER, and the selectivity of products [39,78,83,92,108]. Appropriately adjusting the overpotential can optimize the FE of the ECH process for LA. To illustrate this effect, Pb was employed as the working electrode in 0.5 M H_2SO_4. At −1.1 V vs. RHE, the FE for the ECH of LA was 27.9 %. As the potential was shifted to −1.3 V vs. RHE, the FE was increased to 83.8 %. However, further decreasing the potential to −1.5 V vs. RHE caused a slight drop in FE to 78.3 %. This implies that as the potential becomes more negative, HER becomes increasingly competitive [100, 101]. Furthermore, the applied potential influences the product selectivity of VA and GVL. An increase in overpotential is favorable for VA selectivity, but compromises that of GVL. Thus, in 0.5 M H_2SO_4, it's reasonable to maintain the applied potential between −1.3 to −1.5 V vs. RHE to reduce competitive effects from HER.

The initial concentrations of the substrates influence the ECH of LA. The data presented here is based on the experiments conducted under the conditions of −1.8 V vs. Ag/AgCl, using a 0.5 M H_2SO_4 electrolyte, and using Pb as the working electrode. At an initial LA concentration of 0.05 M, the CE of ECH was 6.8 %. However, when the LA concentration was increased to 0.5 M, the CE notably increased to 56.4 %. A subsequent increment in LA concentration to 0.75 M witnessed only a slightly CE enhancement to 58.6 % (as shown in Fig. 5c). Besides, LA conversion was decreased from 71.6 % to 54.3 %. The observations clearly suggested that the initial LA concentration also impacted product selectivity. Specifically, GVL selectivity increased with increasing LA concentration, whereas VA selectivity decreased (as shown in Fig. 5d) [108]. A noteworthy competitive reaction during the ECH process is HER. The HER competition is accentuated at lower LA concentrations, leading to diminishing ECH CE values. Enhancing the initial LA concentration progressively mitigated the HER competitiveness, resulting in improved CE values. Nevertheless, using 0.75 M LA, the conversion rate of LA experienced a decline. The LA concentration plays a pivotal role in determining the adsorption of the molecules on the active sites [107]. High initial substrate concentrations can lead to occupation of the active sites, potentially retarding the reaction rate. Thus, to avert the risk of saturating the electrode with the substrate, it's suggested to keep the LA starting concentration below 0.75 M. Concurrently, to ensure effective electron utilization in ECH against HER competition, the initial LA concentration should remain above 0.1 M.

3.5. Effects of reaction temperatures and durations

The efficacy of the ECH of LA is also influenced by reaction temperatures. While reaction temperature and duration play roles in determining product distribution, they substantially affect the ECH rate and the FE [108–110]. Reaction temperature is pivotal in dictating the kinetics of both ECH and HER. Elevating the temperature tends to accelerate the overall reaction rates. A study by Lucas et al. evaluated the FE of ECH and HER at temperatures of 20 °C and 50 °C [83]. Their findings indicated that with increasing temperature, the FE for ECH and HER processes approximately doubled. Notably, the ECH showed more significant increases in FE compared to the HER. While extending the reaction duration can enhance the conversion of LA, an overly extended reaction time may introduce unwanted side reactions and lead to the degradation of electrode materials.

3.6. Mechanism of the ECH of LA

According to Bisselink et al. [92], Fig. 6 illustrates the pathway through which LA is converted to VA and GVL at a electrode. For the ECH of LA in acidic solutions, the primary focus is on reducing the carbonyl groups. However, this process differs from the conventional reduction of the carbonyl groups to methylene [112,113]. The conventional process typically does not involve hydrogen adsorption and may be similar to the Clemmensen reduction [114]. During the ECH of LA, LA undergoes protonation and 1-electron reduction to form a 4-HVA radical. The resulting radicals can either form organometallic complexes with metals, resulting in the formation of VA through 1-electron reduction, or it can undergo further 1-electron reduction to produce 4-HVA [38,39,92]. The electrode surface adsorbs 4-HVA with a weaker strength compared to LA. Therefore, a water molecule is eliminated from 4-HVA to generate GVL. This process does not consume electrons and does not involve an electrochemical reaction [78,100]. Notably, the produced GVL cannot be further converted into VA [78].

Lucas et al. [83] proposed that the mechanism of LA transformation is dependent on the pHs of the electrolytes. As shown in Fig. 7a, in acidic solutions with a pH of 0, one of the primary considerations is the protonation of a portion of LA molecules at the carbonyl oxygen [115]. This protonated form, referred to as LA-H^+, is electrostatically adsorbed onto the cathode surface when under an electric field, specifically below the potential of zero charge (represented as intermediate a*) [83]. The local concentration of protons at the surface can become enriched, driving the equilibrium towards the LA-H^+ direction. However, the mechanism can, in principle, proceed even at very low concentrations of LA-H^+ due to the rapid acid-base balance maintained upon consumption of the protonated LA [83]. The adsorption rates of these species effectively compete with proton adsorption and HER processes, resulting in the superior FE. The intermediate a* is electrochemically reduced to

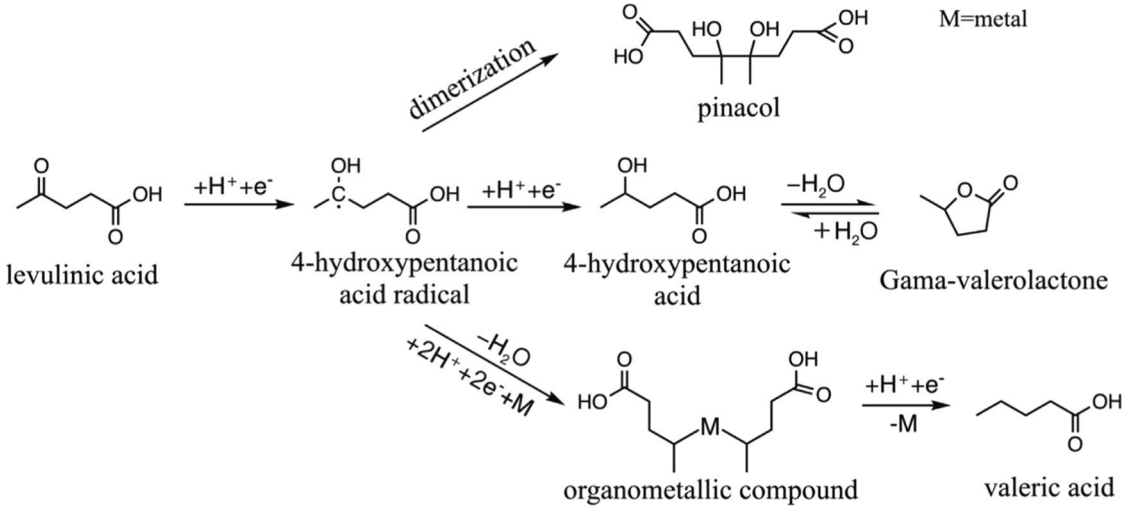

Fig. 6. Conversion of LA to VA and GVL based on the generic carbonyl reduction mechanism [92,114].

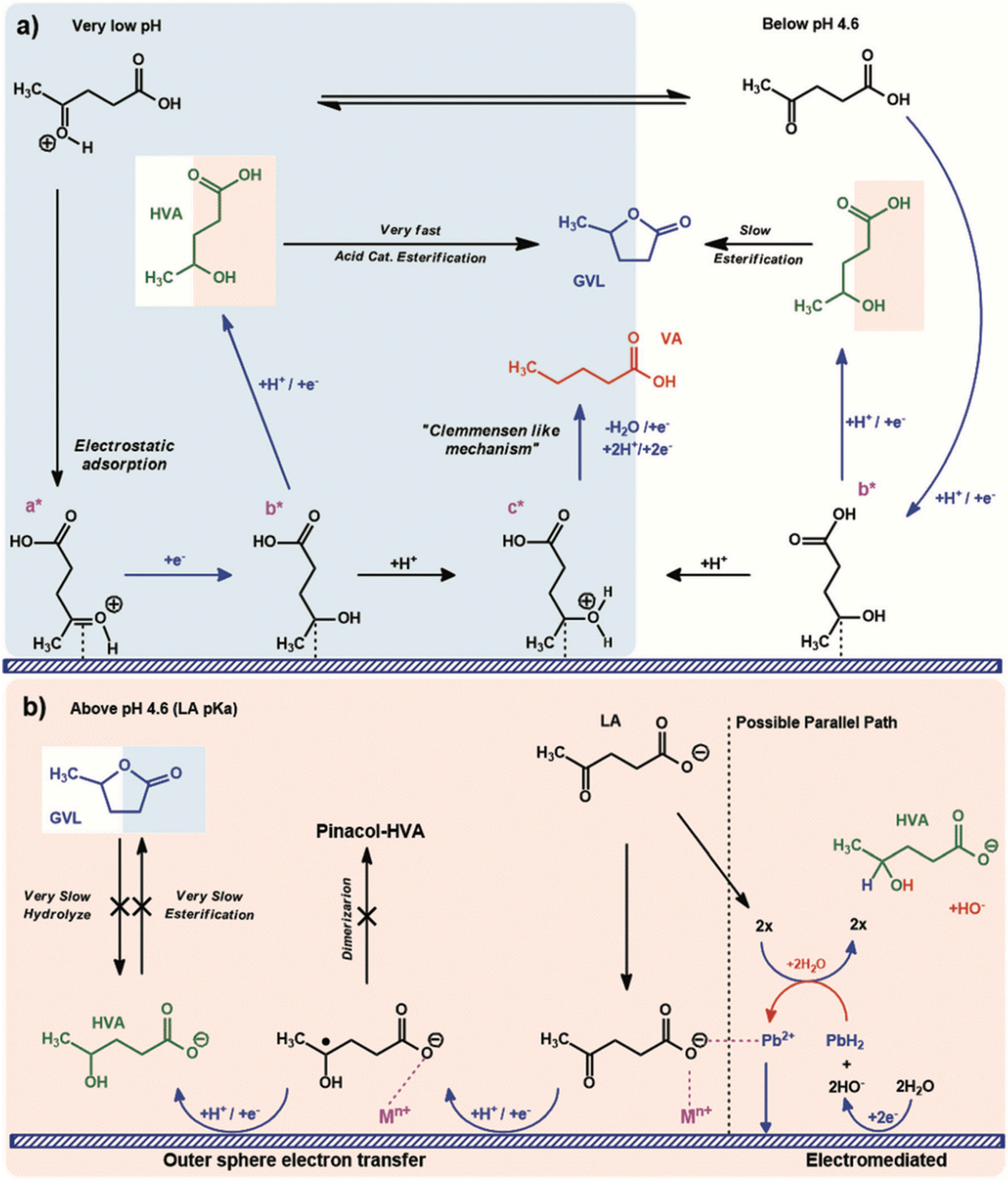

Fig. 7. Mechanism of LA reduction reaction at pHs below (a) and above (b) the LA pK_a~4.6 [83].

intermediate b* (bound by the former carbonyl carbon). Subsequently, b* can undergo further reduction to form 4-HVA or protonation on the alcohol group to generate intermediate c* . The intermediate c* is then deoxygenated via a well-known Clemmensen process, leading to the formation of VA. The 4-HVA derived from intermediate b* is catalyzed by an acid and a homogeneous catalyst, undergoing lactonification to yield GVL [83].

In neutral or alkaline electrolytes, the LA^- species carries a negative charge, rendering its adsorption onto the electrode surface highly improbable [83]. Nevertheless, the reduction of LA persists. Plausible

scenarios involve the adsorption of neutral LA molecules near the electrode surface via acid-base equilibrium or the charge screening effect of base cations in the Helmholtz layer, which facilitates the proximity of LA^- to the electrode surface and enables its reduction via the outer sphere electron transfer pathway [83]. Fig. 7b illustrates the proposed reaction mechanism. The reduction and protonation of LA^- give rise to the formation of a 4-HVA radical (intermediate d*), which can undergo reduction and protonation to yield 4-HVA. In neutral or alkaline environments, the electrochemical reduction of ketones and aldehydes typically generates pinacol products (vicinal diols) through the generation of free radical intermediates, such as intermediate d* . However, the anionic and solvated nature of intermediate d* induces repulsion, thereby expecting a lower dimer yield [83]. Notably, the absence of GVL detection in the reaction and the failure to hydrolyze into HVA under the same experimental conditions suggest that 4-HVA is the ultimate product under neutral or alkaline conditions [83].

4. ECH of FF

The ECH process for FF is notably more intricate than that for LA, given that the latter primarily yields simpler products like VA and GVL, neither of which serve as substrates for subsequent hydrogenation within the system. Conversely, in the process of ECH of FF, apart from the main products, FA and MF, these compounds can instigate secondary reactions. Specifically, FA can undergo further hydrogenation to yield THFA or MTHF, and MF can serve as a substrate for MTHF synthesis, as illustrated in Fig. 8a [116,117]. It's also worth noting that the FF hydrogenation process introduces the polymer hydrofuroin (HF), a potential precursor for sustainable drop-in jet fuels, as shown in Fig. 8c [66,118,119]. Furthermore, the ECH process for FF must account for molar balance completeness, while also considering by-products like pinacol, humins, and other polymers. Table 2 provides the corresponding Gibbs free energy and standard electrode potentials associated with the generation of these species from FF. Notably, the pathway involving MF formation from FA (pathway 3 in Fig. 8a) requires a higher potential than THFA formation (pathway 2 in Fig. 8a), signifying the greater thermodynamic favorability of hydrogenating furan rings to THFA compared to hydrogenating conjugated hydroxyl groups to MF. Similarly, the hydrogenation of furan rings to MTHF (Pathway 4 in Fig. 8a) is more energetically favorable than the non-conjugated hydroxyl hydrolysis to MTHF (Pathway 5 in Fig. 8a) [118]. Although MTHF can be produced from THFA through traditional catalysis, this route is improbable in electrocatalysis. This unlikelihood arises from the fact that H_2 generation, requiring 1.23 V, is thermodynamically much more favorable and hence progresses at a faster rate [120,121]. Therefore, Pathway 5 in Fig. 8a is deemed electrochemically improbable. The research on the ECH of FF is still in the early stages. Previous research in this topic has mainly focused on exploring the parametric effects, investigating various catalysts, reaction conditions, and reactors.

Table 2
Gibbs free energy and stand potentials for the hydrogenation of FF using hydrogen gas and water electrolysis [118].

Reaction	Hydrogen gas		Water electrolysis	
	△G (kJ mol^{-1})	E_{cell} (V)	△G (kJ mol^{-1})	E_{cell} (V)
1. FF → FA	−35.95	0.19	200.38	−1.04
2. FA → THFA	−80.97	0.21	391.69	−1.01
3. FA → MF	−25.27	0.13	211.06	−1.09
4. MF → MTHF	104.78	−0.27	577.44	−1.50
5. THFA → MTHF	160.48	−0.83	396.81	−2.06

4.1. Effects of electrode materials

The electrode materials employed in the ECH of FF play a pivotal role in determining product selectivity. Given the complex nature of the FF ECH process and the varied interests of researchers in specific products, a comprehensive overview of electrode materials is provided here. Beyond the influence of the electrode materials, the pH of the electrolytes profoundly influences both product distribution and selectivity and this aspect will be elaborated in later sections. Various electrode materials have been extensively studied, encompassing both precious metals such as Pt [59,123–125], Au [126], Ag [127], Pd [127], Ru [122], and Rh [122], as well as non-precious metals like Fe [59,80], Co [122], Ni [59,122,123,128], Cu [122–126,128–130], Al [59], Pb [59,123,124], Ti [131], and even non-metallic carbon [59]. Furthermore, various forms of carbon materials, such as graphite felts, carbon paper (CP), and toner, have been investigated as supports for metal catalysts[132], including Au/C [126], Cu/C [126,133], Pt/C [118], Pd/C [118], and others. Electrode materials for FF ECH are not limited to these, and may categories such as alloys, bimetals, oxides, single-atom catalysts, and even materials related to biological enzyme binding were explored. Notable examples include stainless steel [80], TiO_2 [134], La-TiO_2 [79], Ni-Fe [80], Cu-NPNi/NF [128], $Ag_{60}Pd_{40}$ [127], single-copper-atom catalysts [31] and ADH@ZIF-8 [135]. Many of these catalysts are nanoparticulate in nature with large surface roughness and area, thus affording a high density of active sites for the ECH process. Table 3 provides a summary of catalysts, particularly those predominantly produce FA and MF.

Lopez-Ruiz et al. introduced a volcanic plot (refer to Fig. 8b) showcasing the relationship between the turnover frequency (TOF) and binding energy of metals. Pd demonstrates the highest activity in the ECH of FF, owing to its optimal interaction strength with FF [122]. Consequently, a plethora of studies have been conducted on Pd-based materials. Green et al. highlighted that Pd/C manifested outstanding activity that was 4.4 times superior to Pt/C in a flow reactor. This led to a surge in the production of FA and THFA, accompanied by a marginal yield of MF [118]. AgPd nano-alloys have showcased superior catalytic performance compared to their monometallic counterparts, especially at lower overpotentials. The integration of Ag into the alloy modulates the

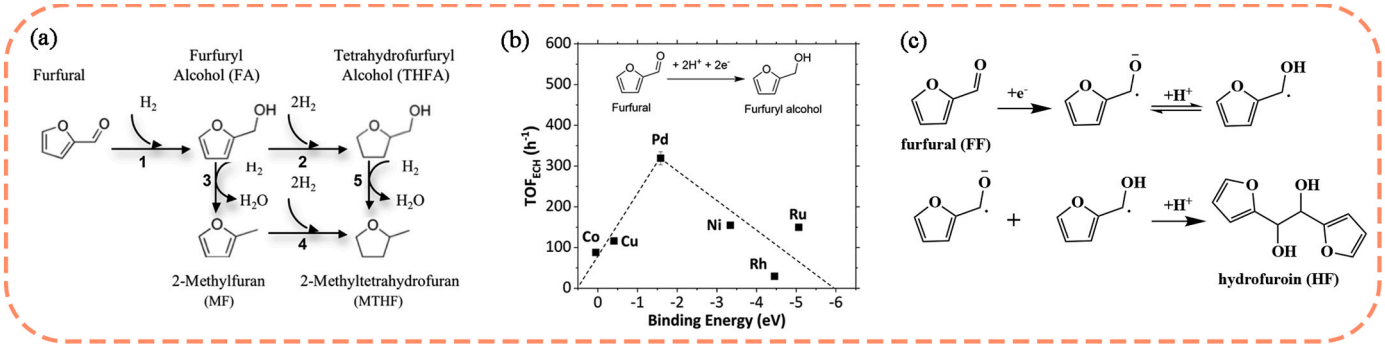

Fig. 8. (a) Reaction scheme for the hydrogenation of FF [118], (b) Volcano plots combining the experimentally measured intrinsic rates of ECH (TOF_{ECH}) of FF [122] and (c) A proposed reaction scheme outlining the formation of HF [59].

Table 3
Catalytic performance of various cathodes for the conversion of FF.

Cathode metal	Reaction medium	FF Conc[a]/M	Electrolysis conditions	T[b]/h	Conv[c]/%	FE or CE/%	Selec[d]/%		Ref
							FA	MF	
Cu (rod)	0.1 M NaOH	0.08	−1.2 V vs. SCE	-[e]	80	10	15	-	[123]
Ni(rod)			−0.9 V vs. SCE		25	16	80	-	
Pb (rod)	0.1 M H_2SO_4	0.08	−1.1 V vs. SCE	-	90	36	45	-	[123]
Pt (sheet)			−0.3 V vs. SCE		8	7	99	-	
3 %Pt/ACF			−0.5 V vs. SCE		82	78	99	-	
5 %Pt/ACF			−0.5 V vs. SCE		75	72	99	-	
3 %EDPt/ACF			−0.5 V vs. SCE		25	21	99	-	
Blank ACF			−0.5 V vs. SCE		0	0	0	-	
Nano TiO_2	[Emim]BF_4	17.4(g)	38 mA cm^{-2}	-	-	61.7	61.7(yield)	-	[134]
La-Nano TiO_2	DMF	10 (g)	50 mA cm^{-2}	-	-	85.7	88.6(yield)	-	[79]
Ti/TiO_2						58.7	59.8(yield)	-	
Cu wire	0.2 M NH_4Cl-ACN	-	−10 mA cm^{-2}	-	93		25.1	1.8	[129]
	0.1 M H_2SO_4-ACN				68	40.6	20	20	
	0.5 M H_2SO_4-ACN				87	56.8	12	31.3	
CuGF	PBS (pH 6.6)	-	Flow cell, -	-	60	-	86	-	[133]
Pt	0.1 M $HClO_4$	0.05	−0.36 V vs. SCE	24.5	9.1	13	98	-	[124]
Cu	0.1 M NaOH	1	Flow cell, −30 mA cm^{-2}	4	100	56	16	-	
Cu	Carbonate (pH 10.0)	0.1	−0.65 V vs. SCE	5.5	90	72	80	-	
Pb	0.1 M H_2SO_4	0.05	−1.5 V vs. SCE	4	96	75	70	-	
Cu	Methanol + KOH	0.5	Flow cell, −30 mA cm^{-2}	4	23	-	19	-	
Bare Cu	0.5 M H_2SO_4	0.1	−0.8 V vs. RHE	1.5	14	> 97	-	-	[130]
Cu/Cu-4 μm					13	> 97			
Cu/Cu-400 nm					28	> 97			
$Ag_{60}Pd_{40}$	neutral buffer	0.1	−0.5 V vs. RHE	1	> 15	> 95	> 90	-	[127]
Cu-NPNi/NP	0.5 M NaOH	0.05	−0.45 V vs. RHE	1	> 70	-	21.6	-	[128]
CP	0.1 M NaOH	0.1	−1.4 V vs. Ag/AgCl	5	-	93	93 % HF yield		[139]
Pb	pH 0.5	0.05	−0.55 V vs. RHE	1	-	38	HF (main product)		[81]

[a] Concentration of FF; [b] Reaction time; [c] Conversion of FF; [d] Selectivity of products; [e] the value was either not mentioned or not detected in this literature.

adsorption strength of aromatic components onto Pd. Moreover, the ligand and ensemble effects inherent to the alloy catalyst diminish the likelihood of site contamination [128]. The bimetallic material Pt-Pd reported by Lenk et al., managed to attain a THFA selectivity of 15.3 %. It's essential to point out that the selectivity for FA in this system still surpasses that of THFA [136]. Muhammand et al. designed a PdNiB/C electrode that facilitated the transformation of FF to FA at the cathode, while HMF was converted to DHMTHF at the anode [23]. In another study, Sarah et al. synthesized Al_2O_3-supported Pb electrocatalysts, which achieved an impressive selectivity of 35 % for MTHF [137].

In Fig. 8c, FA undergoes a reduction to form FA free radicals via a 1-electron transfer. Following this, two FA free radicals combine to yield HF [59]. Notably, this mechanism does not facilitate the required four-electron transfer per furfural molecule, which is crucial for MF generation. Nilges et al. tested several electrode materials for the ECH of FF, including Cu, Ni, Pt, C, Fe, Pb, and Al in 0.5 M H_2SO_4 (with a 20 % acetonitrile phase). MF was emerged as the dominant product on the Cu electrode, while the Pt electrode manifested the best selectivity for FA. Notably, HF was absent on the Cu and Pt electrodes but was detected on other electrodes. Among them, Al and Fe electrodes exhibited the highest selectivity for HF [59]. Due to these findings, many researchers have initiated the synthesis of electrode materials primarily based on Cu or Pt. While FA and MF are the products of interest, secondary reaction products such as MTHF, THFA, and the polymeric HF are also explored. Zhao et al. prepared a 3 %Pt/ACF catalyst via the impregnation technique to introduce Pt onto activated carbon felt fibers (ACF). It showcased a striking FA selectivity of 99 % with a CE of 78 %, outperforming the Pt sheet electrode [123]. Dixit et al. developed a non-precious Cu-NPNi/NF electrocatalyst by co-depositing Ni-Cu onto a nickel foam (NF) followed by Cu layer deposition. This catalyst demonstrated remarkable catalytic activity, surpassing plain copper electrodes and resulting in a comprehensive FF transformation in alkaline media in 2 h [128]. A CuSn/CuF@Cu material reported Li et al. efficiently suppressed HER and facilitated the reduction of FF to MF. Simultaneously, a PbO_2 anode adeptly oxidized FF to maleic acid [138]. In an electrolyte with a pH value of 10, a single Cu atom catalyst demonstrated a FE of 67 % for HF production, whereas a single Co atom catalyst achieved an FE of 58 % under the same conditions. [31].

In essence, the selection and structural optimization of electrode materials remain central to the realm of this research topic. The inherent properties of electrode materials significantly influence products distribution. Currently, a number of novel catalysts based on Pd, Pt, Ag, Cu, and Ni, have drawn particular attention owing to the outstanding activity, which could possibly make further progresses in the field.

4.2. *Effects of pHs of electrolytes*

The choice of catalytic material is crucial in directing the outcome of the ECH process of FF. Meanwhile, other factors, such as the pH and composition of the electrolytes, significantly influence product distribution and selectivity. A wide spectrum of electrocatalysts has been explored for the ECH of FF including materials like C [139], Cu [140], Ni [128], Pb [131], Fe [80], Pt [118]. The product distribution tends to be strongly influenced by the acidity of electrolytes while the effects of the anions in the electrolytes are less profound. For instance, the hydrogenation of FF to FA necessitates the involvement of 2 pairs of H^+/e^-, whereas the transformation of FF to MF demands 4 pairs of H^+/e^-. An electrolyte with a lower pH value is favorable for the formation of H_{ads} on the electrode surface, promoting hydrogenation processes. Consequently, an acidic electrolyte promotes MF formation, whereas alkaline-medium favors FA selectivity. Nevertheless, the optimal pH for generating FA and MF is dependent upon the specific electrode material. An essential consideration for ECH of FF is the challenge posed by non-closure of the mole balance. The introduction of specific solvents, like acetonitrile and methanol, into the electrolyte can address this issue. Research indicated that the variations in the solvent mixture and the solvent-to-water ratio didn't significantly alter product distribution [140].

Brosnahan et al. conducted ECH of FF utilizing an AgPd alloy electrode in different environments including 0.1 M H_2SO_4 (pH = 0.95), 0.2 M NH_4Cl (pH = 4.5), 0.1 M Na buffer (pH = 6.8), and 0.1 M K buffer (pH = 6.9) [127]. They observed a consistent rise in the FE of FA with

increasing pH. Notably, in 0.1 M Na buffer (pH = 6.8) and 0.1 M K buffer (pH = 6.9), the FE value reached around 90 %. In the acidic medium, the carbon balance was found to be notably less than 100 %, manifesting the formation of other furan derivatives like MF, HF, and resins. Concurrently, phosphate buffers with either Na^+ or K^+ ions exhibited analogous results, suggesting limited influence of the electrolyte's cations on the ECH of FF [127]. May et al. concluded that the specific anions had a minimal influence by using HCl and H_2SO_4 as electrolytes for the ECH of FF. Instead, the pH of the electrolyte was emerged as the critical determinant in the process [140].

Jung et al. examined the impact of pH on product distribution utilizing Cu as the working electrode in electrolytes with pH values of 3.4, 1.1, and 0 [129,130]. In a weakly acidic buffer solution, FA emerged as the primary product with a yield of 23.4 %. At a pH of 1.1, FA and MF yields were nearly equivalent, recording at 11 % and 14 %, respectively. However, when the pH of electrolyte was reduced to 0, MF was dominated the products. Zhao et al. [123] and Parpot et al. [124] conducted ECH of FF employing Cu as the working electrode in 0.1 M NaOH. FA remained the major product, but with diminished selectivities of 15 % and 16 % respectively. Dixit et al. achieved a selectivity of 74.3 % for FA using Cu-NPNi/NF as the working electrode in a 0.5 M NaOH electrolyte. Furthermore, other products like HF were identified [128]. Li et al. conducted ECH of FF using a Ni electrode in electrolytes with pH values of 1.0, 5.0, and 9.0 [80]. FA selectivity in these solutions stood at 86 %, 95 %, and 93 %, while MF selectivity was recorded at 14 %, 5 %, and 7 % respectively. Li et al. noted that the conservation of mass in solutions with a pH of 9.5 was limited to 53 %, possibly due to furan destabilization in alkaline electrolytes. Remarkably, an elevation of pH to 11 led to a pronounced drop in reaction efficiency, which is attributed to the inherent instability of FF in basic conditions [80].

The effects of electrolyte pH on secondary products like MTHF, THFA, and HF are seldom investigated. FA, THFA, and MTHF was the detected when FF was used as the substrate. While THFA and MTHF was the products when FA was used as the substrate, the selectivities was 26 % and 74 %, respectively [141]. Using MF as the substrate, MTHF formation is rapid. MTHF was originated from both FA and MF, while THFA was exclusively from FA. Consequently, adjusting the solution's pH to elevate FA and MF yields can potentially enhance THFA and MTHF production. The generation of HF is more prevalent in alkaline electrolytes with prolonged reaction durations. Zamaan et al. employed single Cu atoms as electrocatalysts in a carbonate buffer solution (pH = 10.0) which achieved a FE of 67 % for HF formation [31].

4.3. Effects of applied potential

The electrode potential plays a crucial role in regulating various aspects of electrochemical reactions, including charge transfer kinetics, surface states, and the stability of adsorbed species [81,142]. Consequently, it significantly influences the selectivity observed in complex multi-step reactions. In the specific case of the ECH of FF, the selectivity and FE of the resulting products are intricately linked to the overpotential associated with the HER. Notably, metals like Pt and Ni, which have lower hydrogenolysis overpotentials, predominantly form FA. In contrast, metals such as Pb, Fe and Al, which possess higher hydrogenolysis overpotentials, favor the production of pinacol derivatives [81]. Previous studies conducted by Zhao et al. [123] and Li et al. [129] have postulated a direct relationship among the electrode potential, the overall reaction rate, and its impact on current efficiency and product yield. Optimizing the electrode potential is a critical factor in achieving efficient ECH of organic compounds. Operating below the optimal potential leads to limited surface coverage of H_{ads}, consequently reducing the likelihood of FF interacting with H_{ads} and thereby diminishing the reaction efficiency of ECH. Moreover, when the potential approaches the initial potential, the ECH of FF becomes more competitive than the HER process [130]. However, this advantage is counterbalanced by the excessively slow reaction rate of the ECH of FF [130]. On the other hand, applying a higher potential enhances the yield of FA by facilitating the availability of surface H_{ads} atoms and accelerating the rate of the ECH of FF [129]. It is important to note that excessively negative reduction potentials may induce undesired side reactions at the electrode, thereby impeding the overall ECH reaction rate. Beyond an optimal current density, the adsorption sites become saturated with H_{ads}. Consequently, as the applied potential becomes more negative, H_{ads} may desorb from the cathode to participate in the HER through Tafel or Heyrovsky steps, thereby diminishing the FE for the ECH of FF [80,123]. Green et al. have reported that at low FF conversion and low potential conditions, FA becomes the predominant product with a selectivity of 100 %. However, as the potential is increased to −1.75 V vs. Ag/AgCl, the conversion of FF rises, resulting in a selectivity of 26 % for THFA, 8 % for MF, and MTHF [118]. Dixit et al. have suggested that the C-H coupling necessary for FA production doesn't necessitate a substantial overpotential. They further demonstrated that FF can be transformed to FA at a potential of −1.15 V vs. Ag/AgCl [128]. Additionally, Cu facilitates the specific adsorption of -CHO groups in FF, leading to the positioning of the arylfuran ring at a greater distance from the catalyst surface [119]. In contrast, Pt and Ni promote the adsorption of furan rings. However, compared to Cu, Pt and Ni exhibit less favorable adsorption of complexes on their surfaces, consequently limiting the yield of FA and HF on a Cu electrode [117,119,128]. In terms of intrinsic activity, Cu surpasses Pt and Ni. With increasing overpotential, the selectivity of FA decreases while that of HF increases due to rapid consumption of H_{ads} for H_2 production on a Pt electrode at very high overpotentials [127]. As a result, limited availability of H_{ads} at high overpotentials promotes the generation of HF. Both FF adsorbates (FF_{ads}) and H_{ads} are essential for FA production, and any constraints on the abundance of these species at the electrode surface inevitably reduce the yield of FA [127]. Notably, Pt, with its propensity for H_{ads} formation, exhibits higher selectivity and yield of FA compared to other metals [127].

4.4. Effects of initial concentration of FF

The initial concentration of FF considerably influences the FE value and molar balance closure in ECH. Andrew et al. reported that with Cu as the working electrode and using 20 mM FF as the substrate, molar balance was closed [140]. However, with FF concentrations at 100 mM or 200 mM, molar balance was not closed, recording closure rates of 74 % and 76 %, respectively. Elevating FF concentration from 100 mM to 200 mM had repercussions: it affected the reaction rate, led to organic matter saturation on the electrode surface, and resulted in polymer buildup, which further presented complications like clogging. While Jung et al. [129] suggested that high FF concentrations effectively suppress HER, it is notable that with an initial concentration of 1.0 M FF, the predominant products were HF and resin. This result seems independent of the electrode material, instead associating with the FF concentration and reaction time. From their respective studies, Li et al. [80] and Zhao et al. [123] proposed optimal initial concentrations of 100 mM and 80 mM. Chu et al. provided insights highlighting a direct relationship between FF concentration and cathode peak current, reaching an impressive peak current efficiency of 61.7 % [134]. Consequently, when the objective is generating FA, MF, THFA, or MTHF from MF or FA, it is advised to keep the FF concentration below 100 mM to preclude polymer formation. Simultaneously, the starting FF concentration should exceed 20 mM to ensure effective electron utilization during FF ECH process. Conversely, if HF is the desired product, it is beneficial to elevate the FF concentration while ensuring the ECH reaction time remains optimal to prevent the emergence of humins and other by-products.

4.5. Effects of organic solvents

In addition to the initial reactant concentration, the introduction of organic solvents into the electrolyte can exert a notable influence on

both the product yield and conversion of FF. Prior studies indicated that in the ECH of FF, a molar balance between the consumed FF and the generated species was not attained. This imbalance arises from the degradation or creation of significant high-molecular-weight by-products, especially in aqueous and/or acidic environments [81,118,122–124,127,128,133,140,143]. This limitation can be mitigated by incorporating polar aprotic organic co-solvents, which enhance the solubility of hydrophobic FF and inhibit undesired side reactions and the degradation of biomass compounds. To illustrate this effect, Li et al. [80] demonstrated a significant improvement in the material balance value, from 64 % to 85 %, by applying an octane coating to the electrolyte. Common co-solvents, such as acetonitrile (ACN) [59,129,130] and methanol [80,124], have been extensively investigated. In a study conducted by Jung et al. [129] (refer to Fig. 9a), the increment in acetonitrile volume fraction from 20 % to 50 % resulted in an elevated molar equilibrium of ECH from 48.8 % to 63.0 %. Although this modification enhanced the selectivity of FA and MF, it concurrently led to a reduction in the conversion of FF. The suitability of N, N-dimethylformamide as an electrolyte solvent for carbonyl organics has been suggested by Wang et al. [79] and Lucho et al. [125], despite its potential adsorption onto Pt electrodes. Fig. 9b depicts the CV curves of FF at two distinct concentrations in a DMF solvent. The peak observed at −0.2 V vs. SCE corresponds to the formation of Cu_2O species, while the peak at −0.8 V vs. SCE is associated with FF reduction. The irreversible nature of FF reduction, indicated by the absence of an oxidation peak, remains unchanged regardless of the initial FF concentration [125]. Additionally, alternative electrolytes have been employed in the ECH of FF, including ionic liquid $[Emim]BF_4$ [134], choline chloride/urea [126], choline chloride/glycerol [126], and others. Incorporating organic solvents as reagents promotes molar balance closure and significantly influences unwanted side reactions. Experiments involving organic reagents as electrolytes necessitate the optimization of their ratios. When using these electrolytes, it is imperative to consider the stability of FF within these organic solvents and the stability of the solvents themselves under applied potential conditions.

4.6. Effect of temperature

Temperature exerts a notable influence on the ECH of FF. According to Zhao et al. [144], the value of CE is governed by the delicate balance between electrocatalytic hydrogenation and hydrogen desorption processes. The relative rates of ECH and HER are determined by several factors, including the intrinsic thermochemical properties of the reduction process, the adsorption patterns and energies of the reactants and products, as well as the activity of chemisorbed hydrogen. Within the temperature range of 30–50 °C, the ECH reaction is thermodynamically favorable. However, in the temperature range of 50–90 °C, the HER rate exhibits an increasing trend with temperature, indicating enhanced hydrogen evolution kinetics [123]. However, Green et al. observed an interesting phenomenon where, with increasing temperature from 30 °C to 70 °C, the current density increased while the current efficiency decreased, indicating an accelerated rate of hydrogen production [118]. These findings suggest that the increase in temperature promotes the electrolysis of water and consequent hydrogen generation and the selectivity of the reaction products remained relatively unaffected. The influence of temperature on the ECH of FF is multifaceted, involving complex interplays between thermodynamics and reaction kinetics.

4.7. Mechanism of the ECH of FF

Irrespective of the inherent characteristics of the hydrogenation step,

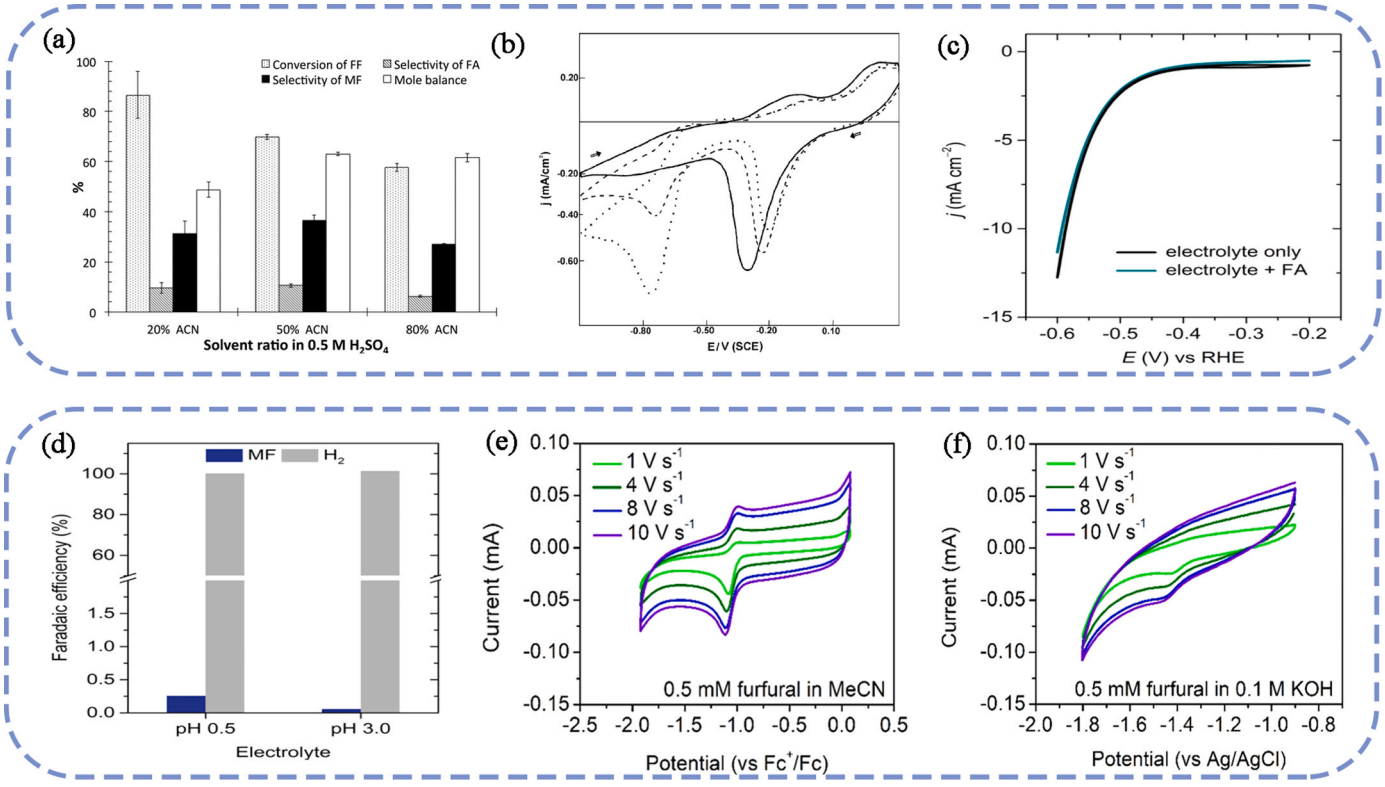

Fig. 9. (a) Impact of ACN ratio in a 0.5 M H_2SO_4 solution on a Cu cathode [129], (b) CV curves of copper in N, N-dimethylformamide with 0.1 M tetraethylammonium chloride, under aerobic conditions, at 25 °C. The CVs are shown for the absence (—) of furfural (FF), as well as in the presence of 3 mM (——) and 9.0 mM (····) FF [125], (c) CV curves obtained on a Cu rotating disk electrode in a pH = 0.5 electrolyte, with and without the addition of 0.01 M FA. (d) FE towards MF and H_2 during the preparative electrolysis of 0.01 M FA conducted on Cu [81], Fast scan CVs illustrating the electroreduction of FF in acetonitrile with a supporting electrolyte of (e) 0.1 M tetrabutylammonium tetrafluoroborate, calibrated using ferrocene (Fc^+/Fc) and (f) in a 0.1 M KOH solution [139].

all mechanisms exhibit two fundamental aspects. Firstly, the electrode surface is subject to a competitive adsorption phenomenon involving organic compounds and hydrogen. Secondly, hydrogenation takes place when organic molecules are adsorbed [122]. Fig. 3b schematically presents two pathways for the reduction of FF on the electrode: ECH and electroreduction. The choice between these pathways predominantly relies on the H_{ads} and the applied potential. ECH necessitates robust interactions between the reactive species and electrode surface, where H_{ads} serves as the primary hydrogen source. The electron transfer process associated with H_{ads} occurs within the internal spherical electrode domain and heavily relies on the surface properties of the electrode material [81]. Conversely, the electroreduction mechanism involves the protonation process in the solution phase, with heterogeneous electron transfer via either an inner or outer sphere process [81]. The outer sphere reaction does not demand a pronounced interaction between the reactant and electrode surface, instead, the electron transfer proceeds via electron tunneling. Consequently, the outer sphere reaction generally exhibits a reduced sensitivity to the properties of the electrode material [81]. ECH exhibits a preference for low hydrogen overpotential electrodes, such as Pt group metals, while electroreduction tends to occur on high hydrogen overpotential electrodes, including Pb, Hg, Cd, and C [81]. However, electrodes with intermediate hydrogen overpotentials (e.g., Ni, Co, Fe, Cu, Ag, and Au) may present a complex scenario where the two pathways can compete [81]. A significant challenge in achieving selective electrocatalytic reduction lies in the simultaneous occurrence of the direct electroreduction pathway, wherein the carbonyl group engages in electron transfer at the electrode interface while protonation takes place in the surrounding solution [81]. In this process, the reaction involving one H^+/e^- pair generates a radical intermediate (C•-OH), which can undergo dimerization through C-C coupling with a second radical or undergo further transformation upon an additional H^+/e^- to yield an alcohol product (see Fig. 8c) [139].

The main competing reaction for the ECH of FF is the HER [145,146]. When Cu is employed as the working electrode, both ECH and electroreduction mechanisms can occur, resulting in the formation of FA, MF, and the dimeric product, HF [81]. FA and MF are products of the ECH process, which requires direct interaction between FF and the Cu surface. The rates of FA and MF formation through ECH reactions depend on the surface coverage of H_{ads} and FF_{ads} on the Cu electrode surface [81]. Increasing the initial concentration of FF appropriately enhances the surface coverage of FF_{ads}, thereby accelerating the rates of FA and MF formation through ECH reactions [81]. The ECH pathway exhibits pH dependence, leading to variations in the production of FA and MF with changes in the pHs of the electrolytes. In highly acidic environments, MF predominates, while FA becomes the major product at an electrolyte with a pH of 3.0. As the pH increases, proton transport in the bulk solution becomes insufficient, resulting in a competition between the hydrogenation pathway (requiring two H_{ads}) and the hydrolysis pathway (requiring four H_{ads}) [81]. The relative availability of H_{ads} and FF_{ads} plays a crucial role in determining the selectivity between these pathways. Furthermore, since both HER and ECH rates are significantly influenced by mass transfer effects, the higher selectivity of FA at electrolytes with elevated pH values can be attributed to the lower relative abundance of H_{ads} compared to FF_{ads}. On the other hand, HF is a product of electroreduction, and its formation does not involve H_{ads}, making it relatively insensitive to the properties of the electrode surface. However, the formation of HF is still influenced by the applied potential, the initial concentration of FF, and the pH of the electrolyte. The rate of HF formation, which does not require H_{ads}, is not significantly affected by pH [81]. Consequently, the increased FE observed for the conversion FF to HF in higher pH environments can be attributed to the reduced contributions from both ECH and HER pathways [81]. To address this, CV tests were conducted using Cu as the working electrode in electrolyte solutions with and without FA, and the results are presented in Fig. 9c. The CV curve obtained for FA closely resembles that of the blank electrolyte, suggesting that the primary electrode reaction in the presence of FA is HER, with minimal transformation of FA. Further analysis of the products revealed that HER exhibited an approximate 100 % FE, while only negligible amounts of MF were detected, corresponding to an FE value of less than 1 % (Fig. 9d) [81]. Therefore, in the ECH process of FF, the conversion of FA to MF is not prominently observed. The substantial production of MF in the ECH of FF occurs in parallel with FA, rather than as a result of the sequential reduction of FA products [81]. Chadderdon et al., through catalytic reduction of FF on Cu electrodes, observed that the selectivity of FA and MF remained consistent with respect to reaction duration and furfural conversion degree. This finding further confirmed that the two products are formed through parallel reactions on a Cu electrode, rather than through consecutive reactions [81].

Shang et al. conducted CV tests using a proton-free acetonitrile electrolyte (Fig. 9e) and a 0.1 M KOH solution (Fig. 9f) [139]. They employed CP as the working electrode with a scanning rate greater than 1.0 V s^{-1}. In the proton-free electrolyte, an interesting observation was made: the FF radical anions formed in situ could undergo oxidization back to its original state after a 1-electron reduction, indicating a quasi-reversible process. This stands in stark contrast to the completely irreversible process observed in an aqueous medium. In the aqueous medium, the formation of the FF radical anions is immediately followed by protonation of the oxygen atom, resulting in the production of a neutral free radical [139]. Fig. 8**c** illustrates the two potential pathways that can be followed subsequently: the first pathway involves a two proton-coupled electron transfer (PCET), leading to the generation of FA; the second pathway involves the dimerization of free radicals, resulting in the production of HF. The selection between these two pathways largely depends on the relative potential required for the formation of H_{ads} on the cathode [139]. Since the HER is more active on the Cu electrode compared to the CP, the potential required for the formation of H_{ads} on Cu is significantly lower than that on CP. Therefore, once the FF radical is formed on the Cu electrode, a subsequent hydrogenation step takes place, favoring the formation of FA. However, at a condition of pH = 13, a CP electrode does not generate sufficient H_{ads} at the potential required for the formation of FF radicals. As a result, dimerization becomes the predominant pathway. It is worth noting that dimerization is a non-electrochemical process.

5. ECH of HMF

Derived from cellulosic species that can be processed into a variety of important chemicals, including transport fuels, polymers, and pharmaceuticals, HMF has emerged as a crucial biomass intermediate [147–152]. The hydrogenation of HMF predominantly yields three products (see Fig. 10) including DHMF, DHMTHF, and DMF [153–155]. Additionally, HMF can be hydrogenated to generate HD or electrochemically hydrogenated and polymerized to form BHH [156]. These compounds possess substantial added value. DHMF, produced through the reduction of the formyl group of HMF, serves as a pivotal starting material for various industrially significant polymerization or etherification processes, such as the production of biodiesel, polyesters, and polyurethane foams [54,55,157,158]. DHMTHF is utilized as solvents, monomers, precursors, and intermediates for the synthesis of other high-value chemicals [56,57,159,160]. DMF is notable for its high energy density, elevated boiling point, and low solubility, making it a potential candidate for liquid transportation fuels with high energy density [43,44,161]. HD can function as a precursor for the production of diverse biofuels and essential base chemicals [162–166]. BHH exhibits desirable properties as a precursor for the synthesis of diesel or jet fuels [58,167,168].

5.1. Effects of electrode materials on the conversion of HMF to target species

The products resulting from the ECH of HMF are more complicated than those from the ECH of LA and FF. Notably, the majority of the

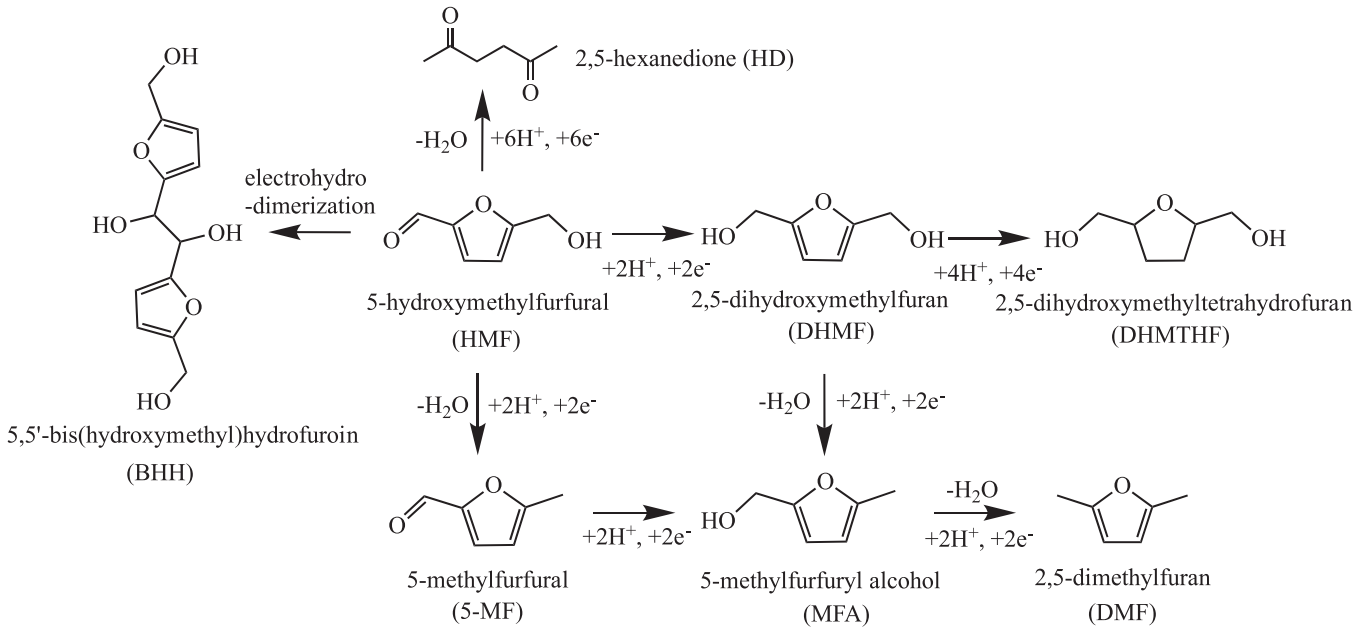

Fig. 10. Schematic illustration of the electrochemical conversion of HMF [153].

studies in this field primarily emphasized the conversion of HMF to DHMF [169–171]. Consequently, following discussion mainly focuses on the pathway from HMF to DHMF. Furthermore, the reaction pathways leading to other products, including DMF, HD, and BDD, are also briefly discussed.

5.1.1. *Electrochemical conversion of HMF to DHMF*

The most favorable pathway for HMF reduction follows the conversion of aldehydes to alcohols, specifically the reduction of HMF to DHMF [44]. Additionally, the aldehyde groups on the side chain of HMF can be converted to DHMF through a 2-electron reduction process. Fig. 10 illustrates the reaction pathway. So far, many studies on the electrochemical conversion of HMF have focused on this particular pathway. The electrochemical conversion of organic compounds is generally influenced by the intrinsic properties of electrodes.

Kwon et al. investigated HMF hydrogenation using various metal electrodes in 0.1 M Na_2SO_4 [180]. While these electrodes manifested comparable onset potentials (−0.5 ± 0.2 V vs. RHE), the intrinsic nature of catalysts determines the specific reaction pathway, leading to the formation of DHMF and other products (e.g., 5-methylfurfural, 2, 5-dimethylfuran, 2,5-dimethyl-2,3-dihydrofuran). Based on their observations, metals were segmented into three groups:

(1) Fe, Ni, Ag, Zn, Cd, and In predominantly generated DHMF.

(2) Pd, Al, Bi, and Pb produced DHMF and other derivatives dependent upon the applied potentials.

(3) Co, Au, Cu, Sn, and Sb mainly yielded other products.

Table 4
Catalytic performances of various cathodes for the conversion of HMF.

Cathode materials	Reaction medium	HMF Conc[a]/ M	Electrolysis conditions	T[b]/ h	Conv[c]/ %	FE or CE/ %	Selec[d]/%	Ref
Ag_{gd}	Broate buffer (pH 9.2)	0.02	20 C passed, − 0.56 V vs. RHE	-[e]	-	99	99 for DHMF	[172]
Ag_{sp}						72	84 for DHMF	
Cu foil						19	39 for DHMF	
Cu foam	Broate buffer (pH 9.2)	0.05	−1.3 V vs. SCE	-	> 90	> 40	44 for DHMF	[173]
Ag foam					> 90	> 60	65 for DHMF	
Ag/Cu ED					> 98	> 80	83 for DHMF	
Ag/Cu GD					> 95	> 80	87 for DHMF	
Ag/C	Broate buffer (pH 9.2)	0.02	−1.3 V vs. Ag/AgCl	0.5	-	96.2	> 85 for DHMF	[174]
Ag_1Cu_1/PA	0.05 M $Na_2B_4O_7$	0.01	−5.4 V vs. RHE	-	93.2	61.8	94 for DHMF	[175]
$Pd_{0.3}Cu$	1 M PBS	-	−0.25 V vs. RHE	-	89	-	99 for DHMF	[176]
Ag-TiO_2 NTs	0.5 M PBS (pH 9.2)	0.02	−1.25 V vs. Ag/AgCl	4	-	82.2	89.8 for DHMF	[177]
AgCu	Broate buffer (pH 9.2)	0.1	−1.16 V vs. RHE	2	62	100	74 for DHMF	[178]
Ru_1Cu Single-Atom Alloy	0.5 M PBS	0.02	−0.3 V vs. RHE	1	65.9	87	-	[55]
CuNi	0.2 M sulfate buffer solution (pH 2.0)	2 (g L^{-1})	−0.8 V vs Ag/AgCl; Charge: 150 C	-	-	88	91.1 for DMF	[44]
Cu	H_2SO_4 + ethanol	0.02	-	2	-	25	35.6 for DMF	[59]
Pt	0.2 M H_2SO_4	0.02	20 C passed, −0.89 V vs. RHE	-	-	0	0 for HD	[162]
Au						2.39	6.92 for HD	
Cu						3.75	8.13 for HD	
Zn						72.4	81.6 for HD	
Ag-aerogel- CN_x	0.5 M H_2SO_4	0.02	−1.1 V vs Ag/AgCl	-	-	78	77 for HD	[179]
Glassy carbon	0.1 M carbonate buffer	0.005	−0.8 V vs. RHE	2	> 42	29	36 for BHH	[58]

[a] Concentration of HMF; [b] Reaction time; [c] Conversion of HMF; [d] Selectivity of products; [e] the value was either not mentioned or not detected in this literature.

In a subsequent study, Kwon et al. explored HMF hydrogenation in 0.5 M H_2SO_4, deriving three groups of [153]:

(1) Fe, Ni, Cu, and Pb largely produced DHMF.

(2) Co, Ag, Au, Cd, Sb, and Bi yielded both DHMF and DMDHF, depending on the imposed potentials.

(3) metals like Pd, Pt, Al, Zn, In, and Sb primarily yielded DMDHF.

Notably, all the electrodes in the acidic environment also produced minor amounts of DHMTHF [29]. Ag exhibited excellent performance for DHMF production in neutral conditions, achieving an impressive selectivity of over 85 % [98]. In acidic environments, Ni and Sb showcased the best catalytic activity. The performance of a given metal is also dependent on the electrolyte environment. The significance of the electrolyte environment in the ECH of HMFs will be elaborated in subsequent sections.

Since Ag and Cu exhibited good catalytic activity for HMF conversion, many studies investigated the electrochemical conversion of HMF to DHMF using catalysts based on these two metals. A number of novel catalysts with varying morphologies were prepared via surface modification techniques to create rough surface structures and load nanoparticles of Ag and Cu nanoparticles onto supporting substrates. Muchharla et al. [181] devised nanostructures of reduced silver (rAg) and reduced copper (rCu) by initially oxidizing Ag and Cu. Subsequent electrochemical reduction of these oxidized materials produced the final electrode materials. Owing to the formation of novel sites in Ag during the oxidation-reduction process, the rAg electrode demonstrated catalytic performance surpassing that of the original Ag electrode for the conversion of HMF to DHMF. However, the resulting rCu exhibited only a marginal enhancement over Cu. Roylance et al. [172] engineered Ag materials with two distinct surface morphologies of a high-surface-area silver electrode (Ag_{gd}) and a flat Ag electrode (Ag_{sp}). LSV results shown in Fig. 11a, b revealed that HMF reduction on these Ag and Cu electrodes is thermodynamically favorable than water reduction. Product analysis indicated that the Ag_{gd} electrode had superior catalytic efficiency for HMF reduction compared to Ag_{sp}, yielding a FE of 99 %, with only trace levels of H_2 and other HMF reduction byproducts. Chadderdon et al. [174] employed carbon black (CB) loaded silver nanoparticles (Ag/C) as a catalyst for the electrochemical reduction of HMF to BHMF, achieving a FE of 96.2 %. CV results of revealed that CB in the Ag/C may play a role in HMF reduction at potentials beyond −1.21 V (see Fig. 11c-e). Moreover, product assessments indicated the CB support in Ag/C actively participated in HMF reduction at pronounced cathodic potentials, leading to increased HMF hydrogen dimerization and diminished BHMF selectivity. Further analysis using the Koutecký-Levich reduction wave revealed an electron transfer number (n) of approximately 2. In contrast, n obtained from the CB electrode was 1, implying different reduction mechanisms. Additionally, at high overpotentials, the HER activity of CB is inferior to silver-based electrodes, with a FE for HER being roughly 2 % at −1.5 V vs. Ag/AgCl [174]. Thus, it's imperative to meticulously regulate cathodic potentials to achieve optimal BHMF selectivity and efficiency. The significance of potentials in HMF conversion will be further discussed in the subsequent sections.

Concerning the utilization of Ag-Cu bimetallic catalysts for the ECH of HMF, Luna and colleagues have made substantial contributions. They synthesized two distinct bimetallic catalysts, namely Ag/Cu ED (electrodeposited sample) and Ag/Cu GD (galvanically displaced sample), through electrodeposition and potential shift techniques [173]. Both Ag/Cu ED and Ag/Cu GD outperformed monometallic Cu foam and Ag foam in terms of FE and DHMF selectivity. The enhancement could be attributed to a potential rise in inherent activity and mass-transfer capability. Interestingly, there were no indications of mass-transport constraints in the Ag/Cu GD or Ag/Cu ED samples, while such limitations were evident from the monometallic Ag and Cu [173]. In a subsequent study, Luna et al. [182] designed a three-dimensional Ag/Cu bimetallic catalyst with a large surface area by electrodepositing Ag onto Cu open-cell foams. In an alkaline medium, the catalyst exhibited superior DHMF selectivity and FE values. While the three-dimensional nature of the bimetallic catalysts didn't influence product selectivity, it did amplify HMF conversion when compared to their two-dimensional counterparts. Employing the resulting catalyst, Luna et al. augmented the applied current density during the ECH of HMF, resulting in an

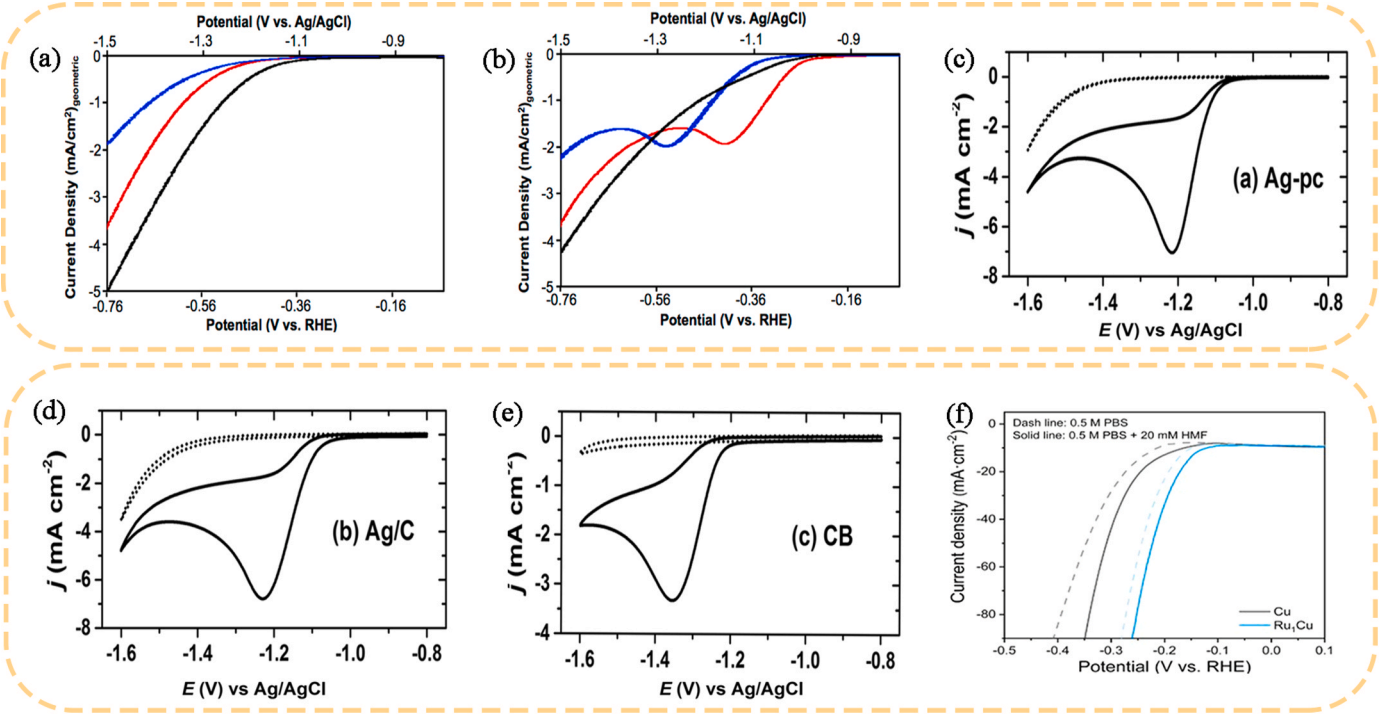

Fig. 11. LSVs recorded from the Cu (black), Ag_{sp} (blue), and Ag_{gd} (red) electrodes in 0.5 M borate buffer (pH 9.2) (a) without and (b) with 0.02 M HMF (scan rate 5 mV s^{-1}) [186], CV curves recorded from (c) Ag-pc, (d) Ag/C, and (e) CB with 20.0 mM HMF (Solid lines) and without HMF (dotted lines) [188] and (f) LSV curves of Cu and Ru_1Cu in 0.5 M PBS with and without 20 mM HMF [89].

elevated yield of DHMF [183]. Additionally, Luna et al. [184] crafted a three-dimensional Cu-CeO_2/Cu catalyst by depositing CeO_2 onto a Cu open-cell foam. Such a design not only offered an abundance of reactive sites but also bolstered conductivity. Remarkably, the catalyst's proficiency in converting HMF to DHMF surpassed that of the Ag-Cu composite. Zhang et al. [178] synthesized bimetallic Ag-Cu catalysts by replacement reaction of Cu nanoparticles with $AgNO_3$ solutions. It was observed that the electrochemical efficacy of the Ag-Cu catalysts for HMF conversion was intricately linked to the concentration of the $AgNO_3$ solution and the duration of the substitution process. Specifically, when Ag was replaced in a 5 mM $AgNO_3$ solution for 20 s, the Ag-Cu catalyst yielded a FE nearing 100 % for the conversion of HMF to DHMF [178]. Li et al. [175], on the other hand, fabricated nano--alloys—Ag_3Cu_1/PA, Ag_1Cu_1/PA, and Ag_1Cu_3/PA—with varying Ag/Cu ratios supported by pyrolyzed biomass alginic acid sodium (PA). Notably, the Ag_1Cu_1/PA catalyst demonstrated a DHMF selectivity of 94 %, an HMF conversion rate of 93.2 %, and an FE of 61.8 %. This bimetallic catalyst exhibited superior performance compared to its monometallic counterpart, Ag/PA, which achieved a 53.89 % DHMF selectivity, 90.6 % HMF conversion, and a 25.79 % FE.

Beyond Ag-Cu catalysts, the ECH of HMF has been explored using other bimetallic combinations like Pd-Cu and Rh-Cu, as well as single atom alloy (SSA). The $Pd_{0.3}Cu$ electrode developed by Yue et al. [176] exhibited superior hydrogenation potential and current response compared to both Cu and Pd nanoparticles. The enhanced electron transfer rate of $Pd_{0.3}Cu$ is evident, given its smaller Tafel slope (208 mV dec^{-1}) compared to Pd (229 mV dec^{-1}) and Cu (226 mV dec^{-1}). Additionally, the performance of $Pd_{0.3}Cu$ for the ECH of HMF surpassed that of both Pd and Cu under identical conditions. Such enhancements are likely due to the modifications on the electronic structure of the alloy surface, increased electrochemically active surface area, and superior conductivity. Zhang et al. [185] fabricated Rh-Cu bimetallic nanoparticles which achieved a notable FE of 92.6 % for the electrochemical conversion of HMF to DHMF in 0.5 M Na_2SO_4 solution. In another study, Ji et al. [55] introduced a Ru_1Cu SAA catalyst which demonstrated an impressive FE of 85.6 % and a yield rate of 0.47 mmol cm^{-2} h^{-1} at −0.3 V vs. RHE for DHMF production. Notably, the SAA catalyst hindered HMF dimerization and showcased superior performance at elevated HMF concentrations. The presence of the single Ru atom appeared to bolster catalytic properties, suggesting its essential role in promoting hydrolytic dissociation. LSV curves (see Fig. 11f) revealed that the addition of 20 mM HMF enhanced the current density of both Ru_1Cu SAA and Cu, suggesting that the electrochemical conversion of HMF is more favorable than the HER [55]. Li et al. designed Cu$(OH)_2$-ER/CF catalysts via a sequential electrochemical oxidation and reduction process, attaining a FE of 92.3 % and a conversion rate of 98.5 % in a 0.1 M KOH solution [186]. Furthermore, Zhao et al. [177] fabricated Ag-TiO_2 by anchoring Ag nanoparticles onto one-dimensional TiO_2 nanotubes, leading to a homogeneous dispersion of Ag nanoparticles free of agglomeration. Consequently, the Ag-TiO_2 exhibited improved activity, resulting in a significant DHMF yield.

To conclude, the research efforts are devoting to searching for advanced catalysts with outstanding conversion and selectivity. Currently, most studies revolve around Ag and Cu as foundational catalyst materials. There remains substantial space for synthesizing advanced catalysts with tunable composition and structures to further improve the catalytic performance. This offers promising avenues for future research on this topic.

5.1.2. Electrochemical conversion of HMF to DMF

In the electrochemical conversion of HMF, there are multiple pathways that can lead to the formation of different products. One pathway involves a series of 2-electron/2-proton reduction steps, leading to the production of DHMF, while another pathway involves a 6-electron/6-proton process, ultimately resulting in the formation of DMF. Fig. 10 illustrates the reaction pathway from HMF to DMF [59]. Nilges et al. conducted experiments using a Cu electrode in a 0.5 M H_2SO_4 solution with a water-to-ethanol ratio of 1:1. They achieved a DMF selectivity of 35.6 % [59]. Along with DMF, some by-products such as DHMF, 5-methylfurfural (5-MF), and methyl furfuryl alcohol (MFA) were also detected. The selectivity of DHMF was 33.8 %, which is comparable to that of DMF [59]. Zhang et al. investigated the use of a CuNi alloy electrode for the electrochemical conversion of HMF to DMF [44]. CuNi alloys are known for their excellent performance for thermochemical catalysis. The results demonstrated that the CuNi alloy electrode exhibited good electrocatalytic activity and stability in the reduction of HMF, yielding a high FE value of 88.0 % and a DMF selectivity of 91.1 % [44].

5.1.3. Electrochemical conversion of HMF to HD

HMF also can be electrochemically reduced to HD through a 6-electron/6-proton process. This conversion involves the reduction of the alcohol and aldehyde groups to alkyl groups and the opening of the furan ring, as illustrated in Fig. 10 [162]. In a study conducted by Roylance et al., Pt, Au, Cu, and Zn electrodes were employed as working electrodes for the electrochemical conversion of HMF to HD [162]. The LSV tests presented in Fig. 12 revealed that the Pt electrode exhibited a more positive onset potential, followed by Au, Cu, and Zn electrodes. Due to the prevalence of water reduction on the Pt surface, the addition of HMF did not cause any changes in the onset potential or reduction current [162]. On the Au and Cu electrodes, the reduction of HMF took place prior to the HER. Notably, the addition of HMF led to significant changes in the onset potential and current distribution on the Zn electrode [162]. Analysis of the products demonstrated that the main product generated on the Pt electrode was H_2, along with a minor amount of DHMF, while HD was not detected [162]. On the Au and Cu electrodes, DHMF and HD were detected, respectively, although the FE value for HD was only 4 %. Notably, the Zn electrode exhibited high selectivity, with FE values of 72.4 % for HD and less than 1 % for DHMF [162]. Roylance et al. emphasized that the reduction of HMF to HD necessitates proton consumption. Consequently, the use of an unbuffered weakly acidic solution during the electrolysis can result in a rapid increase in local pH at the working electrode [162]. Fluctuations in pH throughout the electrolysis process can continuously impact yield, selectivity, and the type of products obtained. Therefore, it is crucial to employ buffered solutions to maintain a constant pH and accurately evaluate the effects of pH on the electrochemical process [162].

To enhance the efficient conversion of HMF without interference from HER, it is essential to choose catalysts that excel in HMF conversion but demonstrate limited activity for HER [187]. Ag is known to be electrochemically inert for HER, making it a potential candidate for HMF catalysis. Panigrahy et al. synthesized carbon-loaded silver nanoparticle aerogels (Ag-aerogel-CN_x) as catalysts for the ECH of HMF to HD [179]. The researchers found that the production of HD was significantly influenced by the cathodic potential and choice of the electrolyte. Higher FE values and suppression of undesired by-products such as H_2 could be achieved by adjusting the cathodic potential [179]. In a 0.5 M H_2SO_4 electrolyte, the Ag-aerogel-CN_x electrode achieved a remarkable FE of 78 % and HD selectivity of 77 % at −1.1 V vs. Ag/AgCl. The enhanced performance of Ag-aerogel-CN_x was attributed to its higher conductivity, smaller charge transfer resistance (R_{ct}), and larger electrochemically active surface area compared to pure Ag catalysts [179].

5.1.4. Electrochemical conversion of HMF to BHH

The electrochemical conversion of HMF leads to the formation of various compounds, such as DHMF, DMF, and HD [188–190]. Additionally, HMF can be electropolymerized to generate BHH, which exhibits favorable properties as a precursor for diesel or jet fuels [58]. The polymerization pathway for HMF is depicted in Fig. 10. Kloth et al. employed different carbon materials, including glassy carbon electrode (GC) and boron-doped diamond (BDD), as working electrodes for the conversion of HMF to BHH [58]. According to Kloth et al., the onset

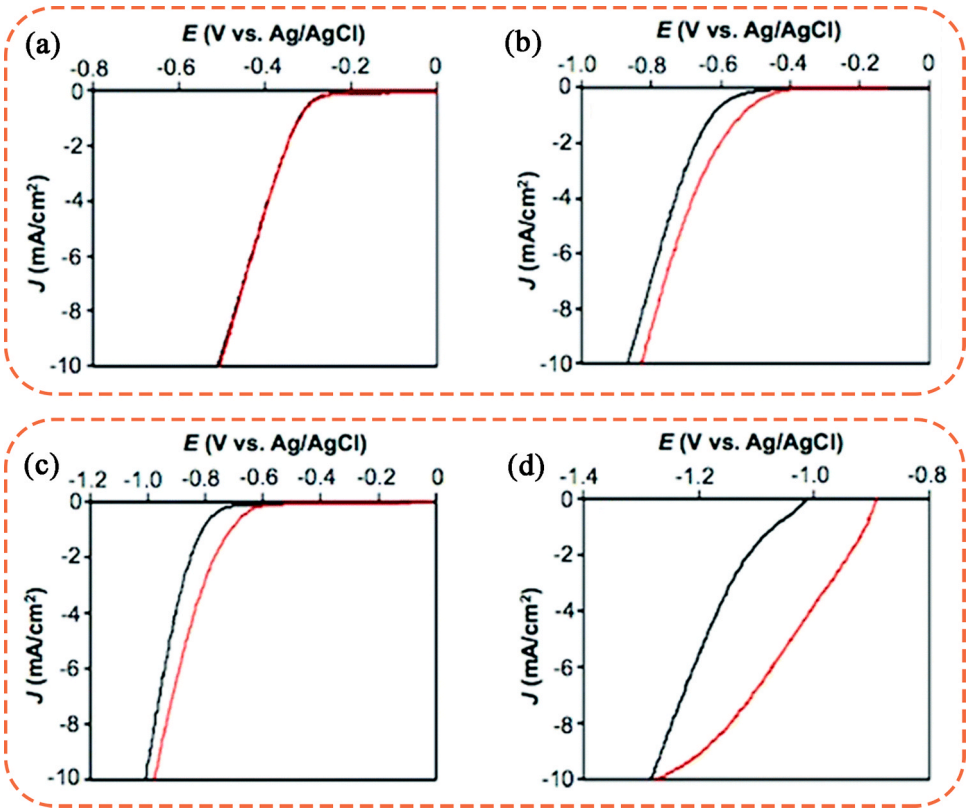

Fig. 12. LSVs of (a) Pt, (b) Au, (c) Cu and (d) Zn electrodes in 0.2 M sulfate buffer (pH 2.0) with (red) and without (black) 0.02 M HMF [162].

potential for HMF reduction on GC was significantly lower, and the selectivity of the generated products shifted from the electrogenerated hydrogenated dimerization product, BHH, to the ECH product, DHMF, with increasing overpotentials [58]. In contrast, regardless of the applied potential, the primary product at the BDD electrode was the dimerized BHH [58]. This can be attributed to the fact that GC is a sp^2 hybridized material, while BDD is a sp^3 hybridized material. On the GC, an increase in the initial HMF concentration resulted in the formation of ECH products and inhibited the HER, while simultaneously increasing the FE of BHH. However, an elevated HMF concentration reduced the selectivity of GC for BHH due to enhanced electrochemically induced HMF degradation processes. Notably, Kloth et al. demonstrated that inexpensive and straightforward graphite foils can also serve as active catalysts for HMF electro-hydrodimerization, enabling the convenient production of BHH as a green biofuel precursor [58].

5.2. *Effects of electrolyte pH on the electrochemical conversion of HMF*

The ECH of HMF, leading to DHMF, is significantly impacted by the pH of the electrolyte. In neutral environments, HMF undergoes direct hydrogenation through the interaction of HMF + 2 H_2O + 2e^- ⇌ DHMF + 2OH^-. However, in acidic conditions, the hydrogenation process involves hydrogen adsorption on the surface of metal electrodes, either sourced from H^+ ($H^+ + e^- \rightleftharpoons H_{ads}$) or H_2O ($H_2O + e^- \rightleftharpoons H_{ads} + OH^-$). Recent studies have highlighted the conversion of HMF to DHMF at varying pH conditions. Specifically, Kwon et al. investigated the catalytic performance of various metal electrodes in both neutral and acidic solutions [180]. The activation energy for HMF hydrogenation is low at acidic environments, subsequently facilitating furan ring hydrogenation to tetrahydrofuran. In contrast, under neutral conditions, the initial step of HMF reduction is non-catalytic and the activation energy is independent with the metal electrodes. It was noted that DHMTHF formation was absent in neutral solutions. Interestingly, metal electrodes manifest varying catalytic efficiencies towards HMF in either neutral or acidic conditions. In neutral conditions, Ag is emerged as the most effective catalyst for DHMF production, whereas, in acidic conditions, further conversion of DHMF to DHMTHF takes place. Kwon et al. categorized the metals into transition *d* metals and post-transition sp metals, and their onset potentials for HER and HMF hydrogenation in acidic and neutral environments are summarized in Fig. 13a, b [153,180]. Positive shifts in the onset potentials of HER and ECH of HMF were noted. In addition, the shifts in acidic (< 0.2 V vs. RHE) is more significant than in neutral (< 1.0 V vs. RHE) solutions.

Luna et al. conducted ECH of HMF in buffer solutions (pH = 9.2) [173,182–184], while Liu et al. reported a 98.2 % DHMF selectivity in alkaline boric acid buffer solutions [191]. In addition, Chadderdon et al. documented the conversion of HMF to DHMF under neutral conditions [174]. Panigrahy et al., examined how the electrolyte pH influences HD formation from HMF [179]. They explored various pH electrolytes, noting that in acidic conditions, adsorbed hydrogen played a crucial role in HMF hydrogenation. Roylance et al. identified a sulfate buffer solution with a pH = 2 as an optimal electrolyte for the conversion of HMF to HD [179], while Ji et al. using Ru_1Cu catalyst identified phosphate buffer solution (PBS) as a more favorable electrolyte than a boric acid buffer for HMF reduction [55].

It's essential to point out that the hydrogenation of HMF necessitates proton consumption. When weakly acidic electrolytes without buffering were used, the local pH at the working electrode rapidly increased during the electrolysis. Such pH fluctuations can alter yield, selectivity, and product distributions. To accurately evaluate the pH effects, buffer solutions are recommended to maintain consistent pH values. The widely utilized electrolytes for HMF reduction encompass PBS, carbonate buffer solution, sulfate buffer solution, and boric acid buffer solution. To achieve the desired product from HMF conversion, the optimal pH conditions should be tuned.

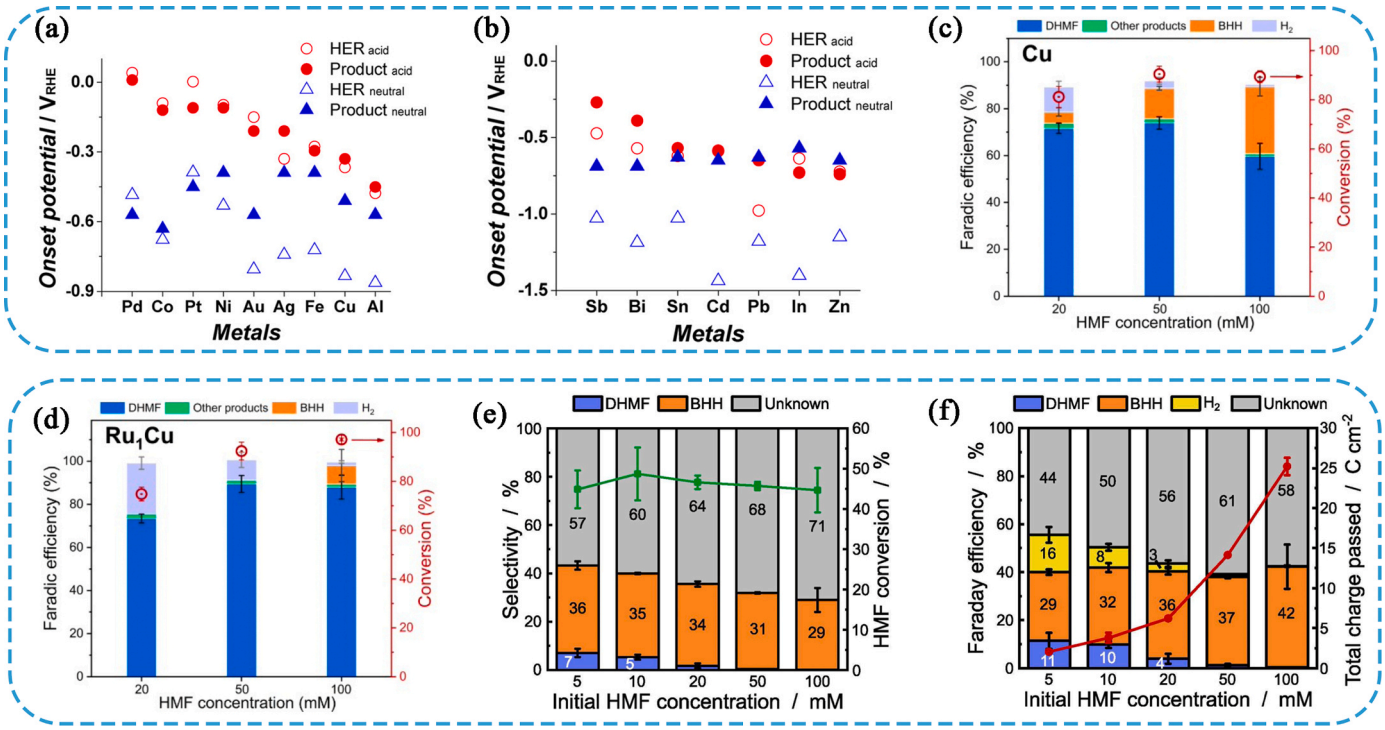

Fig. 13. Comparison of onset potentials of HER and HMF product formation on (a) transition d metals, and (b) post-transition *sp* metals in acidic and neutral conditions [153,180]. Product distributions and corresponding conversion of HMF over (c) Cu and (d) Ru_1Cu at various concentrations of HMF [55], (e) HMF conversion (line) and product selectivity (columns) and (f) total charge passed (line) and FE (columns) of the three major products BHH, DHMF, and H_2 [58].

5.3. Effects of initial HMF concentration on the electrochemical conversion of HMF

The initial concentration of HMF plays a crucial role in its ECH. Elevated HMF concentrations tend to inhibit the HER and favoring the ECH of HMF. However, it has been observed that higher HMF concentrations often lead to undesirable polymerization reactions, which negatively impact the selectivity and FE of the desired products. Generally, an initial HMF concentration around 0.02 M is found to be more suitable for the conversion of HMF to target products, such as DMHF. When the initial concentration exceeds 0.1 M, the formation of various by-products becomes prevalent, and both the reaction rate and FE of the target product significantly decrease. The increased surface coverage of HMF on the working electrode at higher concentrations, along with enhanced adsorption of HMF, leads to a shortage of available active sites for H_{ads} formation relative to adsorbed HMF (HMF_{ads}). Consequently, this inhibits the formation of BHMF by ECH. Moreover, higher initial HMF concentrations tend to promote dimerization and polymerization reactions of HMF molecules.

Luna et al. observed that higher concentrations of HMF do not significantly change the starting current in LSV tests but do lead to an increase in the Faraday current [182]. However, the increase in Faradaic current is not proportional to the starting concentration of HMF. This phenomenon might be related to the adsorption of HMF on the working electrode or the competition between HER and HMF reduction [182]. For instance, the selectivity of DHMF reached an acceptable 83 % in a 0.05 M HMF solution, but it dropped to only 13 % when the initial concentration of HMF was increased tenfold. The lower FE values are primarily due to the formation of by-products rather than the contribution of HER. Moreover, in more concentrated HMF solutions where the electrolysis process takes a long time to accumulate charge, the conversion of HMF to DHMF becomes less selective, leading to a significant decrease in productivity [182].

Roylance et al. investigated the effect of the starting concentration of HMF on the ECH of HMF in a 0.02 M solution buffered with borate (pH = 9.2) [172]. They found that at this concentration, the FE and selectivity remained above 89 % and 99 %, respectively, for the complete conversion of HMF to BHMF. Contrastingly, a 0.10 M HMF solution exhibited lower FE and selectivity values compared to the 0.02 M solution [172]. Similar results were observed by Chadderdon et al., who performed ECH with starting HMF concentrations of 0.005, 0.01, and 0.05 M [174]. Li et al. also investigated three different HMF concentrations (0.01, 0.02 and 0.03 M) and found that higher HMF concentrations slightly decrease the DHMF selectivity and FE while the HMF conversion remains mostly unchanged [175].

Ji et al. evaluated the catalytic properties of SSA in HMF at starting concentrations of 0.02, 0.05, and 0.1 M [55]. They observed that the formation of polymer BHH on the surface of the Cu electrode increased gradually with the initial concentration of HMF increased, resulting in lower FE values of 13.0 % and 28.5 % in 0.05 and 0.1 M HMF, respectively (Fig. 13c, d) [55]. However, the prepared Ru_1Cu SSA exhibited excellent ability to inhibit HMF dimerization, leading to high FE values of the target product DHMF even at higher starting concentrations of HMF (FE values of 89.4 % and 88.0 % in 0.05 and 0.1 M HMF, respectively) [55].

As higher HMF starting concentrations facilitates the dimerization of HMF to form BHH, Kloth et al. investigated the relationship between HMF starting concentration and BHH formation [58]. They confirmed a linear relationship between the rate of BHH formation and initial HMF concentration [58]. Moreover, regardless of the initial HMF concentration, the conversion of HMF remained quite stable at about 46 %, suggesting a dominant one-stage reaction kinetics behavior [58]. This finding indicates that the BHH formation mechanism is likely an outer-sphere reaction, as the inner-sphere mechanism at high HMF concentrations would result in a fractional order of reaction between 0 and 1 due to the limited availability of adsorption sites [58]. The results of Kloth et al. align with other reports, showing that both the selectivity and FE of DHMF formation decrease, and HER inhibition occurs when the initial HMF concentration increases. On the other hand, the FE of BHH increases with higher initial HMF concentrations

(Fig. 13e, f). Kloth et al. attributed the inhibition of DHMF and H_2 formation at high initial HMF concentrations to competition for protons in the fast outer-sphere dimerization reaction [58]. At elevated HMF concentrations, the faster formation of BHH depletes protons near the electrode surface, inhibiting the formation of H_{ads} and, and DHMF. Interestingly, the selectivity of BHH decreases with increasing initial HMF concentration, particularly in more concentrated HMF solutions [58]. For these opposing trends, Kloth et al. suggested that the formation of BHH might involve non-electrochemical reactions [58].

The initial concentration of HMF significantly affects its ECH, and an optimal concentration around 0.02 M is generally preferred to achieve higher selectivity and FE of the target product. Higher HMF concentrations tend to promote undesired side reactions, such as polymerization, leading to reduced selectivity and productivity. It is evident that careful consideration of the starting concentration is crucial for optimizing the ECH of HMF.

5.4. *Effects of applied potential on the electrochemical conversion of HMF*

The applied potential on the working electrode plays a crucial role in the electrochemical conversion of HMF. Typically, optimal applied potentials differ among various HMF conversion systems. Kown et al., investigated the effect of potential on the ECH of HMF differed using different electrodes [153]. At the Ni electrode, both DHMF and DMDHF were generated simultaneously. The selectivity of DHMF on the Ni electrode decreased with increasing cathodic potential higher than −0.35 V vs. RHE, while the yield of DMDHF increased gradually with more negative potentials [153]. On the Co electrode, the concentration of DHMF exceeded that of DMDHF when the applied potential was above −0.5 V vs. RHE. In contrast, at potentials below −0.5 V vs. RHE, the DMDMF concentration on the Co electrode surpassed DHMF [153]. Interestingly, the concentrations of DHMF and DMDHF on the Au electrode were almost the same and increased with higher overpotentials [153]. Additionally, Zhang et al. found that the BHMF yield gradually increased as the applied potential of the working electrode became more negative [178]. However, after reaching −1.9 V vs. Ag/AgCl, the BHMF yield hardly increased. The most suitable potential for HMF hydrogenation, considering BHMF yield, by-product production, and FE, was determined to be −1.9 V vs. Ag/AgCl [178].

The magnitude of the electrolysis potential demonstrates a direct relationship with the surface coverage of H_{ads} on the active site of an electrode. However, there is a limited influence of the applied potential on the hydrogenation kinetics between HMF_{ads} and H_{ads} [178]. At −1.3 V vs. Ag/AgCl, the FE was close to 100 %, assuming a small H_{ads} surface coverage, indicating that the reaction between HMF_{ads} and H_{ads} was more competitive than H_2 precipitation. When the electrolytic potential decreased from −1.3 V to −1.9 V vs. Ag/AgCl, the surface coverage of H_{ads} increased, leading to an increase in the rate of the hydrogenation reaction between HMF_{ads} and H_{ads} [178]. However, at −1.9 V vs. Ag/AgCl, the rate of HMF hydrogenation remained unchanged, either because the surface coverage of H_{ads} became saturated or because HMF_{ads} adsorption became rate-limiting [178]. There was a further decline in the FE values under more negative potentials. The absence of significant by-product formation suggests that this decrease in FE values stems from competitive interactions between the HER and the hydrogenation process of HMF [178].

Roylance et al. studied the effect of applied potential on HMF hydrogenation and identified three potential intervals based on product analysis [172]. In the first interval (−1.1 to −1.0 V vs. Ag/AgCl), DHMF formation was much less than consumed HMF, implying that the consumed HMF was partially used for other reactions. The competitive reactions between HMF molecules were suggested in this potential interval [172] (blue arrows in Fig. 14). Additionally, the mechanism of HMF reduction in this interval did not involve the formation of H_{ads}, which is the first step in H_2 formation [172]. In the second interval (−1.6 to −1.1 V vs. Ag/AgCl), increasing overpotential led to a significant increase in both FE and selectivity for DHMF formation, approaching 100 % [172]. This indicated that the reaction between HMF molecules was significantly weakened in this potential region, and H_{ads} likely formed on the electrode surface [172]. A new mechanism involving generated H_{ads} was proposed in this potential interval (read arrows in Fig. 14). As the coverage of H_{ads} on the electrode surface increased, the rate of DHMF formation increased, effectively inhibiting HMF-HMF reactions [172]. The third overpotential region was below −1.6 V vs. Ag/AgCl, where HER competed with DHMF formation, reducing the FE for DHMF [172]. However, since there was no competing reaction that consumed HMF in this potential region, the selectivity of DHMF remained high [172]. Chadderdon et al. concluded that the selectivity for DHMF and other products depended on the precise control of the cathodic potential [174]. The FE for DHMF increased, while the DHMF selectivity decreased with more negative potentials of the Ag/C working electrode. At −1.3 V vs. Ag/AgCl, Ag/C achieved the maximum FE value of 96.2 % for DHMF [174].

Roylance et al. identified −1.2 V vs. Ag/AgCl as the optimal applied potential for the highest FE of HD selectivity (72.4 %), FE decreased at more negative potentials due to the HER competition [162]. Panigrahy et al. also divided the reduction potential into three intervals and found that the second interval (−1.3 to −1.1 V vs. Ag/AgCl) achieved the highest FE and selectivity for HD, while potentials below −1.3 V led to increased HER [179]. Kloth et al. observed that with decreasing potential, the Volmer process accelerated, leading to increased H_{ads} coverage and enhanced DHMF and H_2 production [58]. At low overpotentials, however, DHMF and H_2 formation remained minimal, suggesting an outer-sphere mechanism for the HMF dimerization reaction

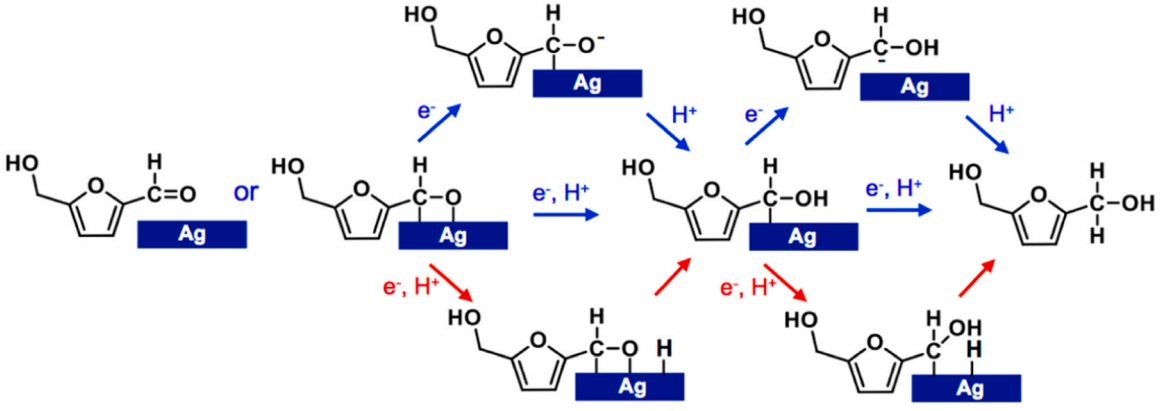

Fig. 14. Plausible HMF hydrogenation mechanisms. Blue arrows represent hydrogenation pathways that do not involve the formation of H_{ads}. Red arrows indicate additional pathways available when the formation of H_{ads} is enabled [172].

without H_{ads} involvement [58]. Overall, the applied potential significantly influences the electrochemical conversion of HMF, and careful control of the potential is necessary to achieve desired selectivity and product yields in the hydrogenation process.

5.5. Mechanisms of the ECH of HMF

The transformation of HMF to DHMF predominantly involves the hydrogenation of its aldehyde group. Conversely, producing DMF necessitates both hydrogenation and hydrogenolysis, which breaks the C-O bond of both the aldehyde and alcohol groups of HMF. Lee et al. investigated the HMF reduction utilizing Ag and Ni electrodes in a pH = 9.2 buffer solution. Analytical findings showed that the Ag electrode primarily promoted aldehyde hydrogenation, resulting exclusively in DHMF without DMF. The Ni electrode, however, supported both hydrogenolysis and hydrogenation, leading to the synthesis of MFA and DHMF, respectively. Nonetheless, a notable variance existed between the produced MFA and DHMF and the consumed HMF. This incongruity was ascribed to humins formation during HMF conversion, accounting for a 14.6 % yield [192]. Remarkably, only DMF formation was evident on the Ni electrode, and Ag demonstrated superior HMF conversion. Interaction studies revealed that HMF showed weak affinity to the Ag (100) surface, evidenced by minimal intramolecular bond length changes in HMF_{ads} relative to its unbound state. In contrast, HMF exhibited significant adsorption to the Ni (100) surface, leading to notable elongation in its aldehyde and alcohol bonds. The elongation of these bonds indicates considerable weakening. Lee et al. suggest that robust HMF adsorption and resultant bond weakening on the electrode surface, as observed with Ni, are pivotal for hydrogenolysis [192]. Probing other metals (Ti, W, Fe, Co, Cu, Cd, and In) revealed that Cu, Co, and Fe mirrored the behavior of Ni, producing MFA, DHMF, and limited DMF. W and Ti predominantly yielded humins, whereas Cd and In aligned with the behavior of Ag, largely producing DHMF. Notably, In secured the highest DHMF yield at 98.8 %, with no HMF degradation or humins production [192].

Three potential pathways delineating the conversion of HMF to MFA, each encompassing distinct hydrogenation and hydrogenolysis mechanisms, have been proposed [147,192]. In the first pathway (Fig. 15a, route 1), the C═O bond undergoes hydrogenation, subsequently followed by the hydrogenolysis of the alcohol C-O bond, with producing DHMF as an intermediate. Notably, empirical evaluations using DHMF as the primary molecule revealed no hydrogenolysis products on metal electrodes, thereby casting doubt on the likelihood of route 1. The second pathway (Fig. 15a, route 2) is characterized by the hydrolysis of the aldehyde C═O bond, transitioning it into a methyl group. During this 4-electron reduction process, HMF remains bound to the metal surface, ensuring no intermediate products were released into the solution. Lee et al. endorsed this pathway, employing DFT calculations to illustrate a

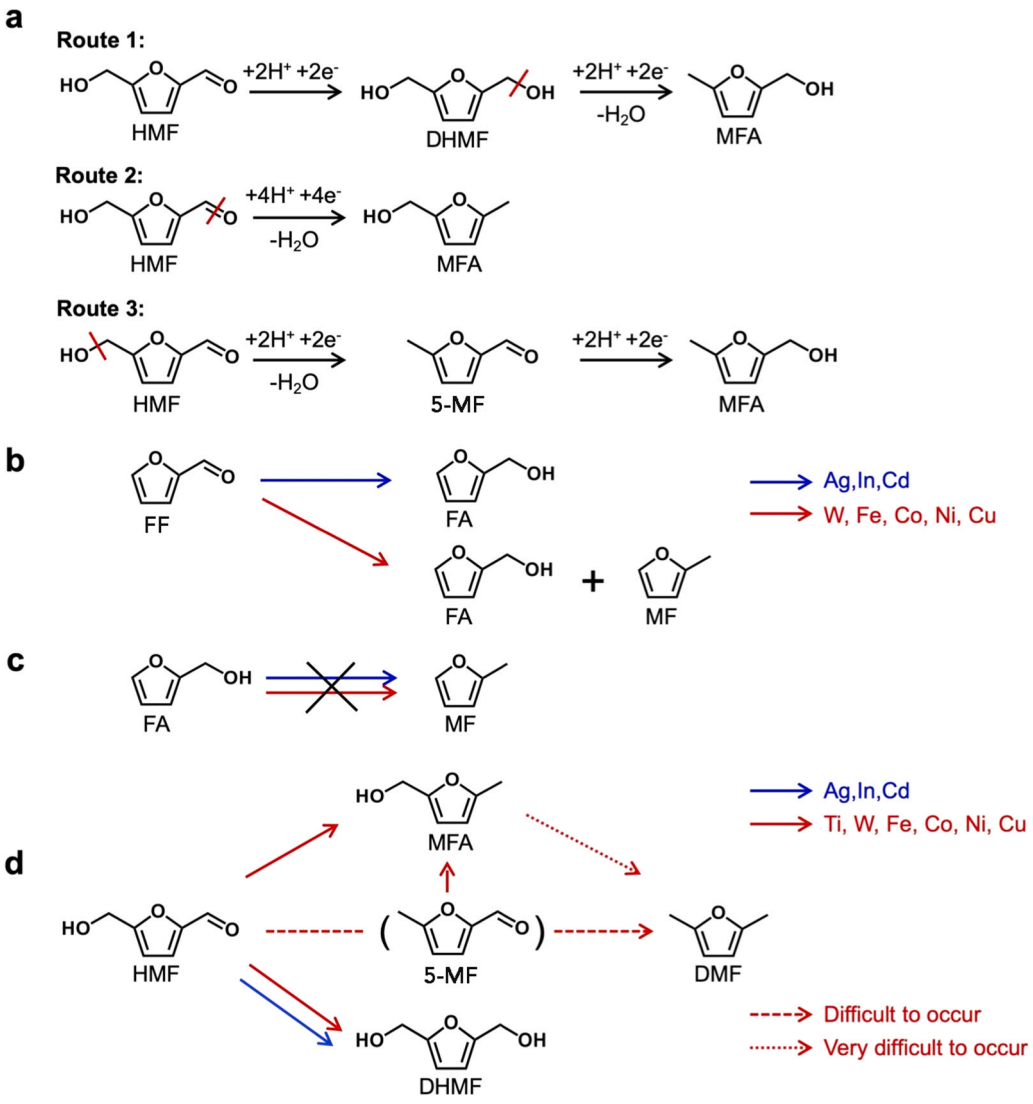

Fig. 15. Electrochemical conversion pathways: (a) HMF to MFA; (b) FF to FA or MF; (c) FA to MF; (d) HMF to DMF or DHMF [192].

pronounced alteration in the aldehyde C═O bond length compared to the alcohol C-O bond upon the adsorption of HMF on metal surfaces capable of hydrogenolysis. This suggests a predominant conversion of HMF to MFA via route 2. The third pathway (Fig. 15a, route 3) commences with the hydrogenation of the alcohol C-O bond, followed by the aldehyde C═O bond hydrogenation, resulting in the intermediate product, 5-MF. Lee et al. reported no detection of 5-MF, possibly due to its swift conversion into MFA or DMF [192]. Yet, Yuan et al. presented evidence of 5-MF contributing to DMF production during reduction, corroborating the viability of route 3 [88].

Lee et al. emphasized the preference for route 2 through the comparative analysis of reduction products of FF and FA using metals with hydrogenolysis ability (W, Fe, Co, Ni, Cu) versus those primarily selective for hydrogenation (In, Cd, Ag). The results revealed that FF, when reduced by hydrogenolysis-capable metals, produced both MF (hydrogenolysis product) and FA (hydrogenation product). Conversely, high hydrogenation-selective metals solely produced FA [192]. In FA reduction across all metals, hydrogenolysis products were absent. This lends credence to the assertion that aldehyde C═O groups undergo hydrogenolysis more readily than alcohol C-O bonds. Hence, HMF primarily transmutes to MFA via aldehyde C═O bond hydrogenolysis (Fig. 15a, route 2). However, the possibility of route 3 cannot be categorically negated. Yuan et al. speculated that HMF's inherent aldehyde group might facilitate the hydrogenolysis of its alcohol C-O bond more effectively than in FA. While MFA is the terminal product, 5-MF isn't, suggesting the hydrogenolysis of alcohol group is more elusive than that of the aldehyde group. Moreover, the presence of other substituents on the furan ring could influence the hydrogenolysis of the alcohol group. The majority of DMF generated during HMF reduction is not via MFA formation but through alternate mechanisms. A plausible pathway suggests that the aldehyde group facilitates the activation of the alcohol C-O bond, prompting its hydrogenolysis prior to that of the aldehyde C═O bond. The emergent 5-MF can then proceed to MFA formation via hydrogenation (route 3) or DMF through hydrogenolysis. Conversion pathways from HMF to DMF are illustrated in Fig. 15d.

In contrast to investigation focused solely on pH = 9.2 by Lee et al., Yuan et al. studied the interplay between the reaction pathway of HMF and the pH of electrolyte. According to Yuan et al., two possible ways in which hydrogen atoms can be added to HMF or its intermediate derivatives during the reduction sequence [147]. The first mechanism is the direct PCET. This mode involves the concurrent transfer of both a proton and an electron from the electrode to the organic species within the solution. The second mechanism is hydrogen atom transfer (HAT), wherein H_{ads} are translocated to the organic matter [147,187]. In processes governed by the HAT mechanism, the consumption of H_{ads} from the active sites on the electrode surface can be regeneration via reduction of the protons present in the solution. Throughout this HAT process, the system does not acquire a distinct pair of a H^+/e^-, thus no reduction current is generated. This contrasts with the PCET mechanism, where the system does acquire both a proton and an electron. The PCET route can lead to the formation of all intermediate hydrogenation products, the HAT mechanism selectively engenders a subset of these products.

The feasibility of HAT depends partly on the distance between the electrode surface and the organic atoms that receive H_{ads}. As elucidated by Yuan et al., the proximity of the oxygen atom within the aldehyde group of HMF to the surface of the Cu electrode facilitates the facile migration of H_{ads} from the Cu surface to the oxygen atom through the HAT process, culminating in the creation of HMF-H_O. Comparative examination of the reaction pathways reveals that the HMF-H_O pathway features a diminished energy barrier in comparison to the competing HMF-H_C route (0.47 eV versus 0.62 eV). Similarly, the reaction pathway for 5-MF hydrogenation via the 5-MF-H_O mechanism presents a lower energy barrier than the 5-MF-H_C pathway (0.49 eV versus 0.65 eV). Notably, while HMF-H_C and 5-MF-H_C are anticipated to be primarily fashioned through PCET, the possibility of the HAT pathway remains extant [88]. The kinetics of the PCET route are notably swayed by the pH of the electrode, given the direct influence of proton concentration on PCET kinetics. In contrast, the requisite H_{ads} coverage for the HAT mechanism remains relatively invariant, attributed to the compensatory adjustments offered by the RHE scale to variations in proton concentration. Therefore, the equilibrium coverage remains consistent regardless of pH, as long as the same potential is applied. The actual coverage of H_{ads} might vary with pH if pH engenders disparate effects on the kinetics of H_{ads} generation via the Volmer step, and the kinetics of H_{ads} consumption via Tafel/Heyrovsky steps and reactions with the organic species. Nonetheless, this disparity in coverage remains notably smaller than the orders of magnitude difference in proton concentration achieved by modulating pH by a few units. The pH-dependence of PCET kinetics, influenced by proton concentration, is poised to vary significantly more compared to the pH impact on HAT kinetics, which hinges on H_{ads} coverage. Therefore, the propensity for HMF_{ads} to undergo reactions with H_{ads} via HAT is accentuated at high pH, whereas this likelihood diminishes under acidic conditions, attributing to the heightened prominence of PCET kinetics [147].

DHMF synthesis encompasses two primary routes, with HMF-H_O intermediary formation through either HAT or PCET, as depicted in Fig. 16. From a thermodynamic standpoint, HMF-H_C exhibits superior stability relative to HMF-H_O. The formation of HMF-H_C from PCET would not be kinetically hindered under low pH conditions, and thus the formation of HMF-H_C may dominate. HAT is kinetically more favorable than PCET under high pH conditions, leading to a considerable extent of HMF-H_O formation, which can only be converted to DHMF [88].

To produce 5-MF, hydrogenolysis of the alcohol group in HMF is required, occurring in two steps (Fig. 17). The first step involves the addition of H to the oxygen atom of the alcohol group, followed by the loss of H_2O and the formation of a C-Metal bond on the surface of the electrode. This results in the formation of a surface intermediate called dehyHMF* [147]. The introduction of H to the O atom of the alcohol group using the HAT mechanism faces kinetic challenges, evidenced by a potential barrier of 0.78 eV. Hence, dehyHMF* predominantly forms through PCET, making acidic conditions preferable for this reaction. The second step in the formation of 5-MF involves the addition of another H to the carbon of dehyHMF*. As dehyHMF* can only be converted to 5-MF, the second step does not significantly impact the selectivity. Instead, it is the first step that determines the amount of 5-MF produced. Since the first step requires PCET, it is facilitated only at lower pHs, resulting in more 5-MF (as well as other products produced by 5-MF reduction, such as MFA and DMF) being produced at lower pHs.

There are three possible pathways for the formation of MFA (Fig. 18). In the first pathway, the C-O bond in HMF-H_C can be cleaved by concerted hydride and proton transfer (CHPT) to form MFA* and OH* [147]. In a subsequent step, OH* will be further reduced to H_2O by either HAT or PCET. PCET to the C portion of HMF-H_C, leading to the formation of MFA* and O*, is not considered feasible due to the thermodynamic barrier of forming MFA* + O*. As both PCET and CHPT are kinetically promoted at low pHs, pathway 1 can only facilitate MFA production under low pH conditions. In the second pathway (Fig. 18, pathway 2), 5-MF-H_O is first generated from 5-MF via HAT or PCET and is subsequently converted to MFA. In the third pathway (Fig. 18, pathway 3), 5-MF-H_C is first generated from 5-MF via PCET and then converted to MFA via either PCET or HAT. Both pathways 2 and 3 require 5-MF, which is more readily formed at low pHs. Consequently, MFA production via pathways 2 and 3 is also increased at low pHs [147].

Regarding DMF formation, it is associated with 5-MF. 5-MF-H_C generated by PCET can be further converted to DMF* and OH* by CHPT (Fig. 19). The OH* produced in the pathway of Fig. 19 is then further reduced to H_2O by either HAT or PCET. As PCET and CHPT are only favored to occur at low pHs, DMF formation also occurs to a considerable extent only under low pH conditions [147].

The conversion of HMF to HD involves three main steps: hydrogenolysis (substitution of the alcohol group with a terminal hydrogen), conversion of the formyl group to a terminal alkane, and ring opening.

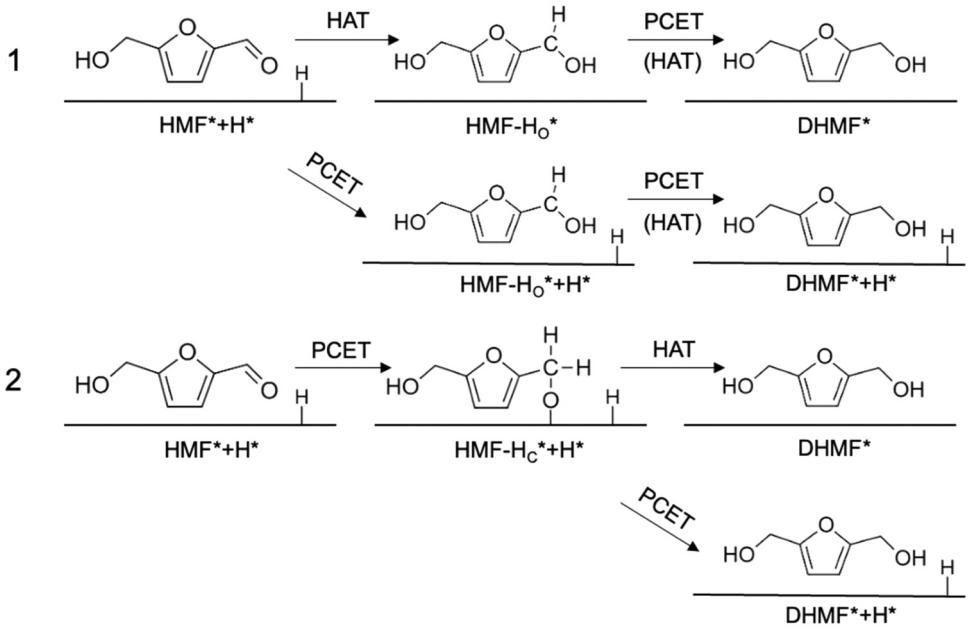

Fig. 16. Proposed pathways of HMF to DHMF [147].

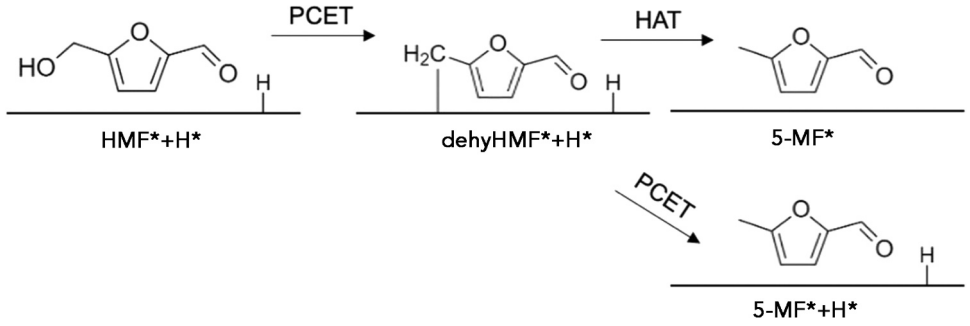

Fig. 17. Proposed pathways of HMF to 5-MF [147].

Zn was reported to have exceptional ability to reduce HMF to HD due to its capacity for Clemmensen reductions [162]. The Clemmensen reductions reduce aldehydes or ketones to their corresponding hydrocarbons, consuming 4 protons and 1 electron while removing 1 H_2O (Fig. 20a). Remarkably, during the conversion of HMF to HD on Zn in acidic media, DMF was not detected, suggesting that the formation of DMF and the hydrolysis of DMF to HD do not occur independently. Instead, acid-catalyzed ring opening and Clemmensen reduction of the furan ring synergistically led to the direct reductive ring opening of HMF to HD. Roylance et al. conducted a reduction of 5-MF under the same conditions to investigate the necessity of HMF hydrogenolysis step for reductive ring opening. The emergence of HD indicated that the absence of an alcohol group does not hinder the reductive opening of the furan ring. Hence, hydrogenolysis of HMF to 5-MF is a separate step that likely occurs prior to reductive ring opening [162]. This implies that the hydrogenolysis of HMF to 5-MF is a separate step that likely occurs prior to reductive ring opening [162]. Comparing Fig. 20c with Fig. 20a and b, the predictive model shares similarities with the Clemmensen reduction and ring opening mechanisms. Steps 1, 2, 3, and 7 are associated with Clemmensen reduction, while steps 4–6 are associated with ring opening [162]. Similarly, during the conversion of DMF to HD, one of the carbonyl oxygens of HD is derived from the furan oxygen of 5-MF, and the other carbonyl oxygen is derived from water, while the formyl group of 5-MF is converted to the terminal alkyl group by Clemmensen reduction. When HMF undergoes hydrogenolysis prior to ring opening, the subsequent reduction steps are identical to those of 5-MF [162].

6. Discussion

The ECH process is related to many experimental parameters that encompass applied potentials, catalyst particle sizes, substrate concentrations, electrolyte pHs, and the potentials. The tendency of a metal towards HER is governed by its hydrogen adsorption energy [193–197]. Metals can be classified into three categories based on their HER overpotentials: high, medium, and low. It's important to note that overpotential isn't an intrinsic catalyst property. While one might assume metals with high HER overpotentials are more conducive for ECH, it's crucial to understand that the activities of HER and ECH are intertwined yet distinct [198,199]. Metals exhibit varied efficiencies for ECH of LA, FF, and HMF. For instance, Pb is a prevalent choice for ECH of LA, whereas Cu is favorable for ECH of FF. For HMF ECH, Cu and Ag are commonly reported. Interestingly, both Pb and Cu are metals with high HER overpotentials. Moreover, while Cu shows significant activity for ECH of FF and HMF, its efficacy dwindles for ECH of LA [200–202]. The structural features, like the presence of a furan ring adjacent to the carbonyl group in FF and HMF, which is absent from LA molecules, could affect the activity. The impact of neighboring groups near the carbonyls offers a promising research avenue for future studies.

The ECH of LA, FF, and HMF fundamentally revolves around carbonyl-group reduction. Two typical reduction mechanisms exist. The

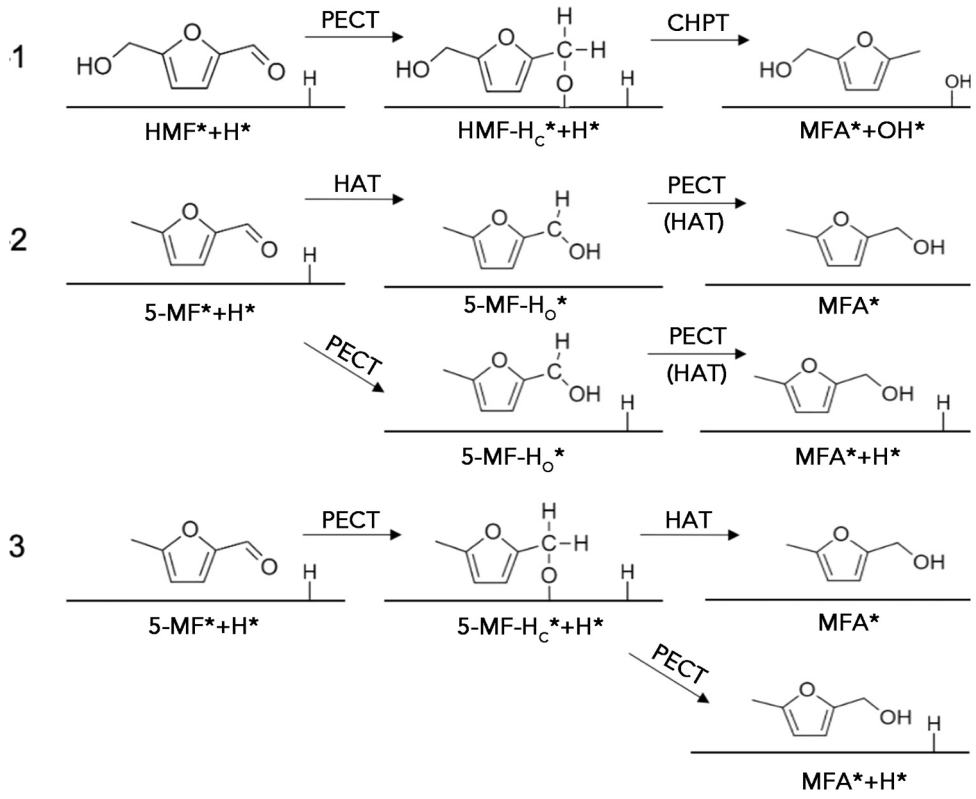

Fig. 18. Proposed pathways of HMF to MFA [147].

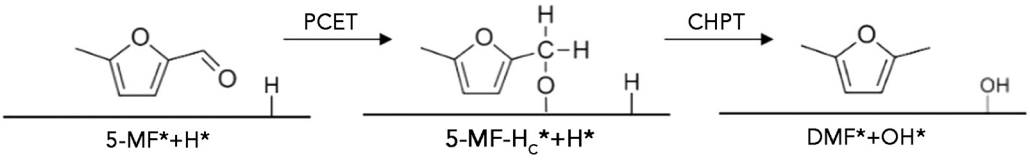

Fig. 19. Proposed pathways of 5-MF to DMF [147].

first involves proton reduction, forming H_{ads} that subsequently react with adsorbed LA, FF, and HMF. The second entails direct reduction of these carbonyls, regardless of the adsorption state on the electrode. Direct organic reduction, bypassing H_{ads}, necessitates elevated overpotentials and primarily takes place on electrodes with high HER overpotentials [203–205]. Conversely, dimerization processes take place through radical coupling.

Although the potential for ECH is theoretically advantageous over the HER, the reaction kinetics of ECH may be slower. Negatively shifts on the potential often accelerate the ECH process, either by enriching H_{ads} species and facilitating direct organic reduction. To achieve desired currents and reaction rates, the applied potential should surpass the thermodynamic redox potential. However, an excessive overpotential could skew the balance towards HER, thereby diminishing the FE of ECH. It's also observed that undesired byproducts could be produced at much lower potentials.

Effectively moderating HER remains pivotal for optimizing LA, FF, and HMF conversion. This review presents findings on the interplay between ECH and HER. Nonetheless, directly comparing diverse reports remains challenging due to the variations in reaction conditions and the dearth of uniform kinetic and thermodynamical metrics. Still, it's evident that the performance of the electrode materials is strongly related with factors like pHs and applied cathodic potentials. Each catalytic system demands an in-depth understanding, especially regarding the metal's interaction with carbonyl-containing molecules.

7. Conclusions and perspective

The ECH of carbonyl-containing short-chain organics is a complex process. A central challenge in this area is improving the selectivity and efficiency of the reactions to yield the desired products. The development of novel catalysts is thus essential, especially for the ECH of LA, FF, and HMF to fuels and valuable derivatives. Potential directions for seeking high-performance catalysts for ECH processes lie in the exploration of advanced catalysts, such as three-dimensional organometallic frameworks, single atomic alloys, and high-entropy alloys.

The nature of interactions between functional groups close to the carbonyls appears pivotal for understanding the ECH mechanism of carbonyl-containing short-chain organics. Among the monometallic catalysts, Pb and In catalysts have shown potential application for ECH of LA, whereas Cu has been noteworthy for FF production. Ag has exhibited exciting results for the ECH of HMF. Intriguingly, the reduction of various carbonyl-containing substances is highly dependent on the molecular structures. Current hypotheses suggest this variance might be due to the interaction of nearby functional groups with the carbonyls, but a thorough and definitive mechanism is not yet established. Therefore, deeper exploration on the mechanisms involved in the reduction of LA, FF, and HMF is essential for future studies.

The development of continuous reactors offers significant potential applications for electrochemical catalysis, acting as a bridge between lab research and large-scale applications. Continuous reactors, provide

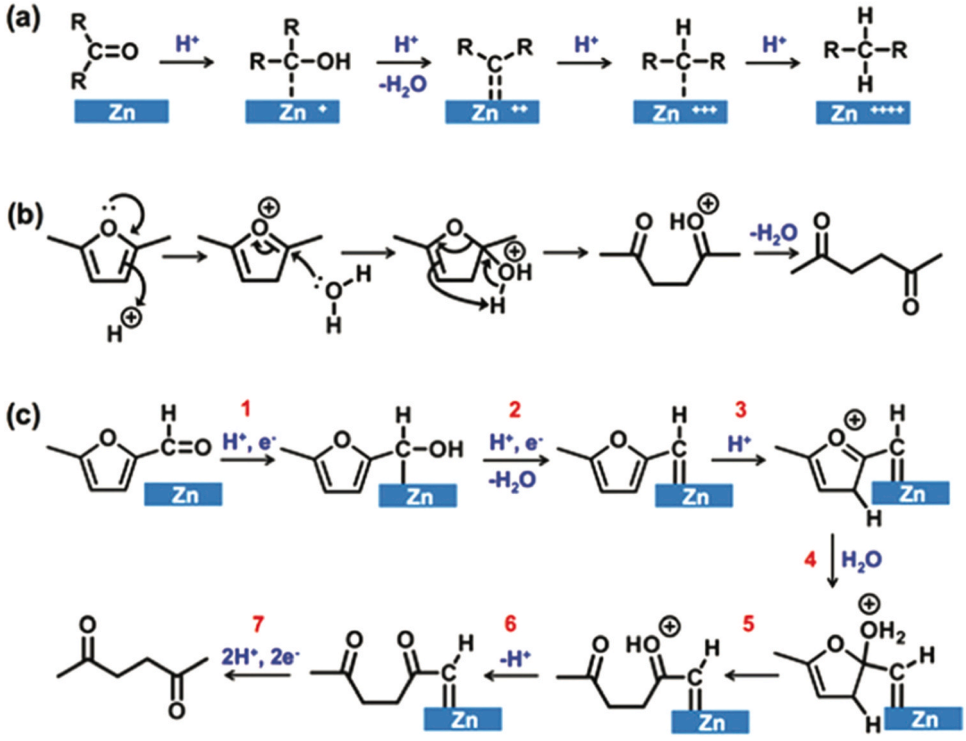

Fig. 20. (a) A general mechanism of Clemmensen reduction on Zn. Zn is used as the electron source and the (+) charges on Zn represent how many electrons are used in each step. (b) a ring-opening mechanism of DMF to HD by hydrolysis. (c) a predictive model for the reduction of 5-MF to HD constructed by combining mechanisms shown in (a) and (b) [162].

advantages over batch reactors, particularly in terms of reducing substrate residence time and enhancing substrate diffusion. While there have been significant progresses in developing lab-scale continuous reactors, challenges still persist. The prototypes often prove too expensive for wide application or too complex for straightforward industrial use. Additionally, adjusting reaction parameters to maximize energy efficiency is crucial, as it can influence production costs and revenue at an industrial level. Hence, the discourse on electrochemical evaluation must deeply integrate energy efficiency considerations.

Future research should also focus on value-added reactions that utilize the anode effectively. Typically, while the substrate undergoes reduction at the cathode, an oxygen evolution reaction occurs at the anode. Replacing this reaction with processes such as HMF or glycerol oxidation might enhance the value of the overall product. Lastly, refining the electrolyte composition is of utmost importance. The search for electrolytes that combine high conductivity with cost-effectiveness and environmental safety is ongoing. Although some researchers have delved into electrolyte optimization, current methods often involve blending aqueous electrolytes with different proportions of methanol or acetonitrile. More in-depth research in this domain is needed.

CRediT authorship contribution statement

Yunfei Zhang: Writing – original draft. **Yi Shen:** Writing – review & editing, Supervision, Funding acquisition.

Declaration of Competing Interest

The authors declare that they have no known competing financial interests or personal relationships that could have appeared to influence the work reported in this paper.

Data Availability

Data will be made available on request.

Acknowledgments

The project was financially supported by the National Natural Science Foundation of China (22279035) and a research grant (204-A021001) from the China-Singapore International Joint Research Institute.

Appendix A. Supporting information

Supplementary data associated with this article can be found in the online version at doi:10.1016/j.apcatb.2023.123576.

References

[1] C.O. Tuck, E. Pérez, I.T. Horváth, R.A. Sheldon, M. Poliakoff, Valorization of biomass: deriving more value from waste, Science 337 (2012) 695–699, https://doi.org/10.1126/science.1218930.
[2] X. Huang, K. Liu, W.L. Vrijburg, X. Ouyang, A. Iulian Dugulan, Y. Liu, M.W.G. M. Tiny Verhoeven, N.A. Kosinov, E.A. Pidko, E.J.M. Hensen, Hydrogenation of levulinic acid to γ-valerolactone over Fe-Re/TiO_2 catalysts, Appl. Catal. B: Environ. 278 (2020), 119314, https://doi.org/10.1016/j.apcatb.2020.119314.
[3] D.R. Chaffey, T. Bere, T.E. Davies, D.C. Apperley, S.H. Taylor, A.E. Graham, Conversion of levulinic acid to levulinate ester biofuels by heterogeneous catalysts in the presence of acetals and ketals, Appl. Catal. B: Environ. 293 (2021), 120219, https://doi.org/10.1016/j.apcatb.2021.120219.
[4] R. Weingarten, Wm.C. Conner, G.W. Huber, Production of levulinic acid from cellulose by hydrothermal decomposition combined with aqueous phase dehydration with a solid acid catalyst, Energy Environ. Sci. 5 (2012) 7559, https://doi.org/10.1039/c2ee21593d.
[5] J.Q. Bond, A.A. Upadhye, H. Olcay, G.A. Tompsett, J. Jae, R. Xing, D.M. Alonso, D. Wang, T. Zhang, R. Kumar, A. Foster, S.M. Sen, C.T. Maravelias, R. Malina, S.R. H. Barrett, R. Lobo, C.E. Wyman, J.A. Dumesic, G.W. Huber, Production of renewable jet fuel range alkanes and commodity chemicals from integrated catalytic processing of biomass, Energy Environ. Sci. 7 (2014) 1500–1523, https://doi.org/10.1039/C3EE43846E.

[6] Y. Yang, Z. Du, Y. Huang, F. Lu, F. Wang, J. Gao, J. Xu, Conversion of furfural into cyclopentanone over Ni–Cu bimetallic catalysts, Green. Chem. 15 (2013) 1932, https://doi.org/10.1039/c3gc37133f.
[7] Y. Wang, M. Zhang, Y. Liu, Z. Zheng, B. Liu, M. Chen, G. Guan, K. Yan, Recent advances on transition-metal-based layered double hydroxides nanosheets for electrocatalytic energy conversion, Adv. Sci. 10 (2023), 2207519, https://doi.org/10.1002/advs.202207519.
[8] J.B. Binder, A.V. Cefali, J.J. Blank, R.T. Raines, Mechanistic insights on the conversion of sugars into 5-hydroxymethylfurfural, Energy Environ. Sci. 3 (2010) 765, https://doi.org/10.1039/b923961h.
[9] A.G. Laurenza, O. Losito, M. Casiello, C. Fusco, A. Nacci, V. Pantone, L. D'Accolti, Valorization of cigarette butts for synthesis of levulinic acid as top value-added chemicals, Sci. Rep. 11 (2021), 15775, https://doi.org/10.1038/s41598-021-95361-4.
[10] N. Luo, T. Montini, J. Zhang, P. Fornasiero, E. Fonda, T. Hou, W. Nie, J. Lu, J. Liu, M. Heggen, L. Lin, C. Ma, M. Wang, F. Fan, S. Jin, F. Wang, Visible-light-driven coproduction of diesel precursors and hydrogen from lignocellulose-derived methylfurans, Nat. Energy 4 (2019) 575–584, https://doi.org/10.1038/s41560-019-0403-5.
[11] J.Q. Bond, D.M. Alonso, D. Wang, R.M. West, J.A. Dumesic, Integrated catalytic conversion of γ-valerolactone to liquid alkenes for transportation fuels, Science 327 (2010) 1110–1114, https://doi.org/10.1126/science.1184362.
[12] H.G. Cha, K.S. Choi, Combined biomass valorization and hydrogen production in a photoelectrochemical cell, Nat. Chem. 7 (2015) 328–333, https://doi.org/10.1038/nchem.2194.
[13] Y. Song, W. Xie, Y. Song, H. Li, S. Li, S. Jiang, J.Y. Lee, M. Shao, Bifunctional integrated electrode for high-efficient hydrogen production coupled with 5-hydroxymethylfurfural oxidation, Appl. Catal. B: Environ. 312 (2022), 121400, https://doi.org/10.1016/j.apcatb.2022.121400.
[14] L. Jiang, G. Xu, Y. Fu, A nitrogen-doped carbon modified nickel catalyst for the hydrogenation of levulinic acid under mild conditions, Green. Chem. 23 (2021) 7065–7073, https://doi.org/10.1039/D1GC01732B.
[15] H. Zhao, J.E. Holladay, H. Brown, Z.C. Zhang, Metal chlorides in ionic liquid solvents convert sugars to 5-hydroxymethylfurfural, Science 316 (2007) 1597–1600, https://doi.org/10.1126/science.1141199.
[16] M. Suastegui, J.E. Matthiesen, J.M. Carraher, N. Hernandez, N.R. Quiroz, A. Okerlund, E.W. Cochran, Z. Shao, J.P. Tessonnier, Combining metabolic engineering and electrocatalysis: application to the production of polyamides from sugar, Angew. Chem. Int. Ed. 55 (2016) 2368–2373, https://doi.org/10.1002/anie.201509653.
[17] D.M. Alonso, S.H. Hakim, S. Zhou, W. Won, O. Hosseinaei, J. Tao, V. Garcia-Negron, A.H. Motagamwala, M.A. Mellmer, K. Huang, C.J. Houtman, N. Labbé, D. P. Harper, C.T. Maravelias, T. Runge, J.A. Dumesic, Increasing the revenue from lignocellulosic biomass: Maximizing feedstock utilization, Sci. Adv. 3 (2017), e1603301, https://doi.org/10.1126/sciadv.1603301.
[18] K. Zhang, Q. Meng, H. Wu, T. Yuan, S. Han, J. Zhai, B. Zheng, C. Xu, W. Wu, M. He, B. Han, Levulinic acid hydrogenation to γ-valerolactone over single Ru atoms on a TiO_2 @nitrogen doped carbon support, Green. Chem. 23 (2021) 1621–1627, https://doi.org/10.1039/D0GC04108D.
[19] K. Gu, D. Wang, C. Xie, T. Wang, G. Huang, Y. Liu, Y. Zou, L. Tao, S. Wang, Defect-rich high-entropy oxide nanosheets for efficient 5–hydroxymethylfurfural electrooxidation, Angew. Chem. Int Ed. 60 (2021) 20253–20258, https://doi.org/10.1002/anie.202107390.
[20] J.S. Luterbacher, J.M. Rand, D.M. Alonso, J. Han, J.T. Youngquist, C. T. Maravelias, B.F. Pfleger, J.A. Dumesic, Nonenzymatic sugar production from biomass using biomass-derived γ-valerolactone, Science 343 (2014) 277–280, https://doi.org/10.1126/science.1246748.
[21] X. Liu, Y. Jiang, J. Huang, W. Zhong, B. He, P. Jin, Y. Chen, Bifunctional PdPt bimetallenes for formate oxidation-boosted water electrolysis, Carbon Energy (2023), https://doi.org/10.1002/cey2.367.
[22] Z. Zhao, R. Bababrik, W. Xue, Y. Li, N.M. Briggs, D.T. Nguyen, U. Nguyen, S. P. Crossley, S. Wang, B. Wang, D.E. Resasco, Solvent-mediated charge separation drives alternative hydrogenation path of furanics in liquid water, Nat. Catal. 2 (2019) 431–436, https://doi.org/10.1038/s41929-019-0257-z.
[23] T. Wang, L. Tao, X. Zhu, C. Chen, W. Chen, S. Du, Y. Zhou, B. Zhou, D. Wang, C. Xie, P. Long, W. Li, Y. Wang, R. Chen, Y. Zou, X.Z. Fu, Y. Li, X. Duan, S. Wang, Combined anodic and cathodic hydrogen production from aldehyde oxidation and hydrogen evolution reaction, Nat. Catal. 5 (2021) 66–73, https://doi.org/10.1038/s41929-021-00721-y.
[24] H. Liu, X. Cao, X. Tang, X. Zeng, Y. Sun, X. Ke, L. Lin, Choline chloride-promoted efficient solvent-free hydrogenation of biomass-derived levulinic acid to γ-valerolactone over Ru/C, Green. Chem. 23 (2021) 1983–1988, https://doi.org/10.1039/D1GC00100K.
[25] Y. He, B. Zhu, F. Wang, J. Xiong, M.A. Akram, L. Feng, Tuning the adsorption behaviors of non-noble electrocatalysts to boost valorization of 5-hydroxymethylfurfural, J. Mater. Chem. A 11 (2023) 14284–14293, https://doi.org/10.1039/D3TA01609A.
[26] Y. Xiao, C. Shen, W. Zhang, M. Zhang, H. Zhang, T. Shao, Z. Xiong, Y. Ding, S. Hao, L. Liu, Y. Chen, J. Li, Electrocatalytic biomass upgrading of furfural using transition-metal borides via density functional theory investigation, Small 19 (2023), 2205876, https://doi.org/10.1002/smll.202205876.
[27] Y. Xiao, C. Shen, Z. Xiong, Y. Ding, L. Liu, W. Zhang, Y.A. Wu, Comprehensive study addressing the challenge of efficient electrocatalytic biomass upgrading of 5–(hydroxymethyl)furfural (HMF) with a CH_3NH_2 ionic liquid on metal-embedded Mo_2B_2 MBene nanosheets, Small (2023), 2302271, https://doi.org/10.1002/smll.202302271.
[28] J. Wu, L. Xu, Y. Li, C. Dong, Y. Lu, T.T.T. Nga, Z. Kong, S. Li, Y. Zou, S. Wang, Anodic cross-coupling of biomass platform chemicals to sustainable biojet fuel precursors, J. Am. Chem. Soc. 144 (2022) 23649–23656, https://doi.org/10.1021/jacs.2c11153.
[29] Y. Liu, C. Gu, L. Chen, W. Zhou, Y. Liao, C. Wang, L. Ma, Ru–MnO_x interaction for efficient hydrodeoxygenation of levulinic acid and its derivatives, ACS Appl. Mater. Interfaces 15 (2023) 4184–4193, https://doi.org/10.1021/acsami.2c22045.
[30] E. Lam, J.H. Chong, E. Majid, Y. Liu, S. Hrapovic, A.C.W. Leung, J.H.T. Luong, Carbocatalytic dehydration of xylose to furfural in water, Carbon 50 (2012) 1033–1043, https://doi.org/10.1016/j.carbon.2011.10.007.
[31] Z. Mukadam, S. Liu, A. Pedersen, J. Barrio, S. Fearn, M. S.Ch. Sarma, S.B. Titirici, I.E.L. Scott, K. Stephens, S. Chan, Mezzavilla, Furfural electrovalorisation using single-atom molecular catalysts, Energy Environ. Sci. 16 (2023) 2934–2944, https://doi.org/10.1039/D3EE00551H.
[32] X. Pan, X. Zhang, G. Huang, S. Mei, J. Huang, J. Chen, W. Liu, H. Yu, Promoting electrocatalytic hydrogenation of 5-hydroxymethylfurfural using buffer electrolytes as proton-donating motifs: theoretical predictions and experimental validations, Appl. Catal. B: Environ. 323 (2023), 122191, https://doi.org/10.1016/j.apcatb.2022.122191.
[33] K. Li, J. Chen, Y. Yan, Y. Min, H. Li, F. Xi, J. Liu, P. Chen, Quasi-homogeneous carbocatalysis for one-pot selective conversion of carbohydrates to 5-hydroxymethylfurfural using sulfonated graphene quantum dots, Carbon 136 (2018) 224–233, https://doi.org/10.1016/j.carbon.2018.04.087.
[34] W. Luo, M. Sankar, A.M. Beale, Q. He, C.J. Kiely, P.C.A. Bruijnincx, B. M. Weckhuysen, High performing and stable supported nano-alloys for the catalytic hydrogenation of levulinic acid to γ-valerolactone, Nat. Commun. 6 (2015), 6540, https://doi.org/10.1038/ncomms7540.
[35] S. Van De Vyver, J. Thomas, J. Geboers, S. Keyzer, M. Smet, W. Dehaen, P. A. Jacobs, B.F. Sels, Catalytic production of levulinic acid from cellulose and other biomass-derived carbohydrates with sulfonated hyperbranched poly(arylene oxindole)s, Energy Environ. Sci. 4 (2011) 3601, https://doi.org/10.1039/c1ee01418h.
[36] H. Lin, J. Strull, Y. Liu, Z. Karmiol, K. Plank, G. Miller, Z. Guo, L. Yang, High yield production of levulinic acid by catalytic partial oxidation of cellulose in aqueous media, Energy Environ. Sci. 5 (2012) 9773, https://doi.org/10.1039/c2ee23225a.
[37] S. Liu, K. Wang, H. Yu, B. Li, S. Yu, Catalytic preparation of levulinic acid from cellobiose via Brønsted-Lewis acidic ionic liquids functional catalysts, Sci. Rep. 9 (2019), 1810, https://doi.org/10.1038/s41598-018-38051-y.
[38] P. Nilges, T.R. dos Santos, F. Harnisch, U. Schröder, Electrochemistry for biofuel generation: electrochemical conversion of levulinic acid to octane, Energy Environ. Sci. 5 (2012) 5231–5235, https://doi.org/10.1039/C1EE02685B.
[39] T.R. dos Santos, P. Nilges, W. Sauter, F. Harnisch, U. Schröder, Electrochemistry for the generation of renewable chemicals: electrochemical conversion of levulinic acid, RSC Adv. 5 (2015) 26634–26643, https://doi.org/10.1039/C4RA16303F.
[40] X. Zhang, T. Liu, Y. Zhou, L. Zhang, X. Zhou, J. Feng, A. Wang, A transformative strategy to realize hydrogen production with electricity output through ultra-low potential furfural oxidation on hollow PdCu alloy networks, Appl. Catal. B: Environ. 328 (2023), 122530, https://doi.org/10.1016/j.apcatb.2023.122530.
[41] Q. Yang, D. Gao, C. Li, S. Wang, X. Hu, G. Zheng, G. Chen, Highly dispersed Pt on partial deligandation of Ce-MOFs for furfural selective hydrogenation, Appl. Catal. B: Environ. 328 (2023), 122458, https://doi.org/10.1016/j.apcatb.2023.122458.
[42] S. Gyergyek, M. Grilc, B. Likozar, D. Makovec, Electro-hydrogenation of biomass-derived levulinic acid to γ-valerolactone via the magnetic heating of a Ru nanocatalyst, Green. Chem. 24 (2022) 2788–2794, https://doi.org/10.1039/D2GC00102K.
[43] J.B. Binder, R.T. Raines, Simple chemical transformation of lignocellulosic biomass into furans for fuels and chemicals, J. Am. Chem. Soc. 131 (2009) 1979–1985, https://doi.org/10.1021/ja808537j.
[44] Y. Zhang, B. Wang, L. Qin, Q. Li, Y. Fan, A non-noble bimetallic alloy in the highly selective electrochemical synthesis of the biofuel 2,5-dimethylfuran from 5-hydroxymethylfurfural, Green. Chem. 21 (2019) 1108–1113, https://doi.org/10.1039/C8GC03689F.
[45] C. Yang, C. Zhuang, Z. Zhai, X. Zhao, D. Huang, D. Tian, C. Min, J. Zhao, Y. Wang, Phase regulation of Ni-based catalyst promotes selective hydrogenation of furfural: Effect of glycerol and Zn content, Appl. Catal. B: Environ. 334 (2023), 122854, https://doi.org/10.1016/j.apcatb.2023.122854.
[46] Y. Qi, B. Liu, X. Qiu, X. Zeng, Z. Luo, W. Wu, Y. Liu, L. Chen, X. Zu, H. Dong, X. Lin, Y. Qin, Simultaneous oxidative cleavage of lignin and reduction of furfural via efficient electrocatalysis by P-doped $CoMoO_4$, Adv. Mater. 35 (2023), 2208284, https://doi.org/10.1002/adma.202208284.
[47] Y. Zheng, R. Zhang, L. Zhang, Q. Gu, Z. Qiao, A resol-assisted cationic coordinative co-assembly approach to mesoporous ABO_3 perovskite oxides with rich oxygen vacancy for enhanced hydrogenation of furfural to furfuryl alcohol, Angew. Chem. Int. Ed. 60 (2021) 4774–4781, https://doi.org/10.1002/anie.202012416.
[48] H. Zhang, X. Gu, C. Canlas, A.J. Kropf, P. Aich, J.P. Greeley, J.W. Elam, R. J. Meyers, J.A. Dumesic, P.C. Stair, C.L. Marshall, Atomic layer deposition overcoating: tuning catalyst selectivity for biomass conversion, Angew. Chem. Int. Ed. 53 (2014) 12132–12136, https://doi.org/10.1002/anie.201407236.
[49] A. Turkin, S. Eyley, G. Preegel, W. Thielemans, E. Makshina, B.F. Sels, How trace impurities can strongly affect the hydroconversion of biobased 5-

hydroxymethylfurfural, ACS Catal. 11 (2021) 9204–9209, https://doi.org/10.1021/acscatal.1c01949.
[50] X. Pang, H. Bai, H. Zhao, W. Fan, W. Shi, Efficient electrocatalytic oxidation of 5-hydroxymethylfurfural coupled with 4-nitrophenol hydrogenation in a water system, ACS Catal. 12 (2022) 1545–1557, https://doi.org/10.1021/acscatal.1c04880.
[51] B. Hu, L. Warczinski, X. Li, M. Lu, J. Bitzer, M. Heidelmann, T. Eckhard, Q. Fu, J. Schulwitz, M. Merko, M. Li, W. Kleist, C. Hättig, M. Muhler, B. Peng, Formic acid-assisted selective hydrogenolysis of 5–hydroxymethylfurfural to 2,5–dimethylfuran over bifunctional pd nanoparticles supported on N-doped mesoporous carbon, Angew. Chem. Int. Ed. 60 (2021) 6807–6815, https://doi.org/10.1002/anie.202012816.
[52] P. Zhou, G. Hai, G. Zhao, R. Li, X. Huang, Y. Lu, G. Wang, CeO_2 as an "electron pump" to boost the performance of Co_4N in electrocatalytic hydrogen evolution, oxygen evolution and biomass oxidation valorization, Appl. Catal. B: Environ. 325 (2023), 122364, https://doi.org/10.1016/j.apcatb.2023.122364.
[53] X. Kong, Y. Zhu, Z. Fang, J.A. Kozinski, I.S. Butler, L. Xu, H. Song, X. Wei, Catalytic conversion of 5-hydroxymethylfurfural to some value-added derivatives, Green. Chem. 20 (2018) 3657–3682, https://doi.org/10.1039/C8GC00234G.
[54] E. Kang, D.W. Chae, B. Kim, Y.G. Kim, Efficient preparation of DHMF and HMFA from biomass-derived HMF via a Cannizzaro reaction in ionic liquids, J. Ind. Eng. Chem. 18 (2012) 174–177, https://doi.org/10.1016/j.jiec.2011.11.020.
[55] K. Ji, M. Xu, S. Xu, Y. Wang, R. Ge, X. Hu, X. Sun, H. Duan, Electrocatalytic hydrogenation of 5–hydroxymethylfurfural promoted by a Ru_1Cu single-atom alloy catalyst, Angew. Chem. Int Ed. 61 (2022), https://doi.org/10.1002/anie.202209849.
[56] R. Alamillo, M. Tucker, M. Chia, Y. Pagán-Torres, J. Dumesic, The selective hydrogenation of biomass-derived 5-hydroxymethylfurfural using heterogeneous catalysts, Green. Chem. 14 (2012) 1413, https://doi.org/10.1039/c2gc35039d.
[57] C. Moreau, M.N. Belgacem, A. Gandini, Recent catalytic advances in the chemistry of substituted furans from carbohydrates and in the ensuing, Polymers 27 (2004) 11–30, https://doi.org/10.1023/B:TOCA.0000013537.13540.0e.
[58] R. Kloth, D.V. Vasilyev, K.J.J. Mayrhofer, I. Katsounaros, Electroreductive 5–Hydroxymethylfurfural Dimerization on Carbon Electrodes, ChemSusChem 14 (2021) 5245–5253, https://doi.org/10.1002/cssc.202101575.
[59] P. Nilges, U. Schröder, Electrochemistry for biofuel generation: production of furans by electrocatalytic hydrogenation of furfurals, Energy Environ. Sci. 6 (2013) 2925, https://doi.org/10.1039/c3ee41857j.
[60] M. Yang, Y. Li, C. Dong, S. Li, L. Xu, W. Chen, J. Wu, Y. Lu, Y. Pan, Y. Wu, Y. Luo, Y. Huang, S. Wang, Y. Zou, Correlating the valence state with the adsorption behavior of a Cu-based electrocatalyst for furfural oxidation with anodic hydrogen production reaction, Adv. Mater. (2023), 2304203, https://doi.org/10.1002/adma.202304203.
[61] Z. Yu, N. Ji, J. Xiong, Y. Han, X. Li, R. Zhang, Y. Qiao, M. Zhang, X. Lu, Ultrafine ruthenium clusters shell-embedded hollow carbon spheres as nanoreactors for channel microenvironment-modulated furfural tandem hydrogenation, Small 18 (2022), 2201361, https://doi.org/10.1002/smll.202201361.
[62] F. Wan, B. Yang, J. Zhu, D. Jiang, H. Zhang, Q. Zhang, S. Chen, C. Zhang, Y. Liu, Z. Fu, The transfer hydrogenation of high concentration levulinic acid to γ-valerolactone catalyzed by glucose phosphate carbamide zirconium, Green. Chem. 23 (2021) 3428–3438, https://doi.org/10.1039/D1GC00209K.
[63] A. Bunrit, T. Butburee, M. Liu, Z. Huang, K. Meeporn, C. Phawa, J. Zhang, S. Kuboon, H. Liu, K. Faungnawakij, F. Wang, Photo–thermo-dual catalysis of levulinic acid and levulinate ester to γ-valerolactone, ACS Catal. 12 (2022) 1677–1685, https://doi.org/10.1021/acscatal.1c04959.
[64] J.B.G. Filho, R.D.F. Rios, C.G.O. Bruziquesi, D.C. Ferreira, H.F.V. Victória, K. Krambrock, M.C. Pereira, L.C.A. Oliveira, A promising approach to transform levulinic acid into γ-valerolactone using niobic acid photocatalyst and the accumulated electron transfer technique, Appl. Catal. B: Environ. 285 (2021), 119814, https://doi.org/10.1016/j.apcatb.2020.119814.
[65] S. Li, M. Dong, J. Yang, X. Cheng, X. Shen, S. Liu, Z. Wang, X. Gong, H. Liu, B. Han, Selective hydrogenation of 5-(hydroxymethyl)furfural to 5-methylfurfural over single atomic metals anchored on Nb2O5, Nat. Commun. 12 (2021), 584, https://doi.org/10.1038/s41467-020-20878-7.
[66] X. Liu, S. Ye, G. Lan, P. Su, X. Zhang, C.A.H. Price, Y. Li, J. Liu, Atomic pyridinic nitrogen sites promoting levulinic acid hydrogenations over double-shelled hollow Ru/C nanoreactors, Small 17 (2021), 2101271, https://doi.org/10.1002/smll.202101271.
[67] I.K.M. Yu, F. Deng, X. Chen, G. Cheng, Y. Liu, W. Zhang, J.A. Lercher, Impact of hydronium ions on the Pd-catalyzed furfural hydrogenation, Nat. Commun. 13 (2022), 7154, https://doi.org/10.1038/s41467-022-34608-8.
[68] Y. Qiu, J.A. Lopez-Ruiz, G. Zhu, M.H. Engelhard, O.Y. Gutiérrez, J.D. Holladay, Electrocatalytic decarboxylation of carboxylic acids over RuO_2 and Pt nanoparticles, Appl. Catal. B: Environ. 305 (2022), 121060, https://doi.org/10.1016/j.apcatb.2021.121060.
[69] Y. Zhou, T.J.A. Slater, X. Luo, Y. Shen, A versatile single-copper-atom electrocatalyst for biomass valorization, Appl. Catal. B: Environ. 324 (2023), 122218, https://doi.org/10.1016/j.apcatb.2022.122218.
[70] X. Deng, G. Xu, Y. Zhang, L. Wang, J. Zhang, J. Li, X. Fu, J. Luo, Understanding the roles of electrogenerated Co^{3+} and Co^{4+} in selectivity-tuned 5–hydroxymethylfurfural oxidation, Angew. Chem. Int Ed. 60 (2021) 20535–20542, https://doi.org/10.1002/anie.202108955.
[71] X. Huang, J. Song, M. Hua, Z. Xie, S. Liu, T. Wu, G. Yang, B. Han, Enhancing the electrocatalytic activity of CoO for the oxidation of 5-hydroxymethylfurfural by introducing oxygen vacancies, Green. Chem. 22 (2020) 843–849, https://doi.org/10.1039/C9GC03698A.
[72] J. Zhang, P. Yu, G. Zeng, F. Bao, Y. Yuan, H. Huang, Boosting HMF oxidation performance via decorating ultrathin nickel hydroxide nanosheets with amorphous copper hydroxide islands, J. Mater. Chem. A 9 (2021) 9685–9691, https://doi.org/10.1039/D0TA11678E.
[73] X. Zhang, M. Han, G. Liu, G. Wang, Y. Zhang, H. Zhang, H. Zhao, Simultaneously high-rate furfural hydrogenation and oxidation upgrading on nanostructured transition metal phosphides through electrocatalytic conversion at ambient conditions, Appl. Catal. B: Environ. 244 (2019) 899–908, https://doi.org/10.1016/j.apcatb.2018.12.025.
[74] X. Huang, J. Song, M. Hua, B. Chen, Z. Xie, H. Liu, Z. Zhang, Q. Meng, B. Han, Robust selenium-doped carbon nitride nanotubes for selective electrocatalytic oxidation of furan compounds to maleic acid, Chem. Sci. 12 (2021) 6342–6349, https://doi.org/10.1039/D1SC01231B.
[75] Y. Zhou, Y. Shen, H. Li, Mechanistic study on electro-oxidation of 5-hydroxymethylfurfural and water molecules via operando surface-enhanced Raman spectroscopy coupled with an Fe^{3+} probe, Appl. Catal. B: Environ. 317 (2022), 121776, https://doi.org/10.1016/j.apcatb.2022.121776.
[76] L. Guo, X. Zhang, L. Gan, L. Pan, C. Shi, Z. Huang, X. Zhang, J. Zou, Advances in selective electrochemical oxidation of 5–hydroxymethylfurfural to produce high-value chemicals, Adv. Sci. 10 (2023), 2205540, https://doi.org/10.1002/advs.202205540.
[77] T. Ali, H. Wang, W. Iqbal, T. Bashir, R. Shah, Y. Hu, Electro-synthesis of organic compounds with heterogeneous catalysis, Adv. Sci. 10 (2023), 2205077, https://doi.org/10.1002/advs.202205077.
[78] L. Xin, Z. Zhang, J. Qi, D.J. Chadderdon, Y. Qiu, K.M. Warsko, W. Li, Electricity storage in biofuels: selective electrocatalytic reduction of levulinic acid to valeric acid or γ-valerolactone, ChemSusChem 6 (2013) 674–686, https://doi.org/10.1002/cssc.201200765.
[79] F. Wang, M. Xu, L. Wei, Y. Wei, Y. Hu, W. Fang, C.G. Zhu, Fabrication of La-doped TiO_2 film electrode and investigation of its electrocatalytic activity for furfural reduction, Electrochim. Acta 153 (2015) 170–174, https://doi.org/10.1016/j.electacta.2014.11.203.
[80] Z. Li, S. Kelkar, C.H. Lam, K. Luczek, J.E. Jackson, D.J. Miller, C.M. Saffron, Aqueous electrocatalytic hydrogenation of furfural using a sacrificial anode, Electrochim. Acta 64 (2012) 87–93, https://doi.org/10.1016/j.electacta.2011.12.105.
[81] X.H. Chadderdon, D.J. Chadderdon, J.E. Matthiesen, Y. Qiu, J.M. Carraher, J. P. Tessonnier, W. Li, Mechanisms of furfural reduction on metal electrodes: distinguishing pathways for selective hydrogenation of bioderived oxygenates, J. Am. Chem. Soc. 139 (2017) 14120–14128, https://doi.org/10.1021/jacs.7b06331.
[82] S. Chen, R. Wojcieszak, F. Dumeignil, E. Marceau, S. Royer, How catalysts and experimental conditions determine the selective hydroconversion of furfural and 5-hydroxymethylfurfural, Chem. Rev. 118 (2018) 11023–11117, https://doi.org/10.1021/acs.chemrev.8b00134.
[83] F.W.S. Lucas, Y. Fishler, A. Holewinski, Tuning the selectivity of electrochemical levulinic acid reduction to 4-hydroxyvaleric acid: a monomer for biocompatible and biodegradable plastics, Green. Chem. 23 (2021) 9154–9164, https://doi.org/10.1039/D1GC02826J.
[84] S.Y. Lee, H.U. Kim, T.U. Chae, J.S. Cho, J.W. Kim, J.H. Shin, D.I. Kim, Y.S. Ko, W. D. Jang, Y. Jang, A comprehensive metabolic map for production of bio-based chemicals, Nat. Catal. 2 (2019) 18–33, https://doi.org/10.1038/s41929-018-0212-4.
[85] O.O. James, S. Maity, L.A. Usman, K.O. Ajanaku, O.O. Ajani, T.O. Siyanbola, S. Sahu, R. Chaubey, Towards the conversion of carbohydrate biomass feedstocks to biofuels via hydroxylmethylfurfural, Energy Environ. Sci. 3 (2010) 1833, https://doi.org/10.1039/b925869h.
[86] S. Esposito, B. Silvestri, C. Rossano, V. Vermile, C. Imparato, M. Manzoli, B. Bonelli, V. Russo, E.M. Gaigneaux, A. Aronne, M. Di Serio, The role of metallic and acid sites of Ru-Nb-Si catalysts in the transformation of levulinic acid to γ-valerolactone, Appl. Catal. B: Environ. 310 (2022), 121340, https://doi.org/10.1016/j.apcatb.2022.121340.
[87] E. Hayashi, Y. Yamaguchi, K. Kamata, N. Tsunoda, Y. Kumagai, F. Oba, M. Hara, Effect of MnO_2 crystal structure on aerobic oxidation of 5-hydroxymethylfurfural to 2,5-furandicarboxylic acid, J. Am. Chem. Soc. 141 (2019) 890–900, https://doi.org/10.1021/jacs.8b09917.
[88] L. Shen, Q. Zheng, Y. Liu, J. Wu, Z. Lu, T. Tu, Efficient hydrogenation of levulinic acid catalysed by spherical NHC-Ir assemblies with atmospheric pressure of hydrogen, Green. Chem. (2021).
[89] A. Bhattacherjee, K. Schnorr, S. Oesterling, Z. Yang, T. Xue, R. De Vivie-Riedle, S. R. Leone, Photoinduced heterocyclic ring opening of furfural: distinct open-chain product identification by ultrafast X-ray transient absorption spectroscopy, J. Am. Chem. Soc. 140 (2018) 12538–12544, https://doi.org/10.1021/jacs.8b07155.
[90] H. Olcay, A.V. Subrahmanyam, R. Xing, J. Lajoie, J.A. Dumesic, G.W. Huber, Production of renewable petroleum refinery diesel and jet fuel feedstocks from hemicellulose sugar streams, Energy Environ. Sci. 6 (2013) 205–216, https://doi.org/10.1039/C2EE23316A.
[91] C. Ver Elst, R. Vroemans, M. Bal, S. Sergeyev, C. Mensch, B.U.W. Maes, Synthesis of levulinic acids from muconic acids in hot water, Angew. Chem. Int. Ed. (2023), e202309597, https://doi.org/10.1002/anie.202309597.
[92] R.J.M. Bisselink, M. Crockatt, M. Zijlstra, I.J. Bakker, E. Goetheer, T.M. Slaghek, D.S. vanEs, Identification of more benign cathode materials for the electrochemical reduction of levulinic acid to valeric acid, ChemElectroChem 6 (2019) 3285–3290, https://doi.org/10.1002/celc.201900734.

[93] Y. Du, X. Chen, J. Qi, P. Wang, C. Liang, Synthesis of valeric acid by selective electrocatalytic hydrogenation of biomass-derived levulinic acid, Catalysts 10 (2020) 692, https://doi.org/10.3390/catal10060692.
[94] S. Shao, Y. Yang, K. Sun, S. Yang, A. Li, F. Yang, X. Luo, S. Hao, Y. Ke, Electron-rich ruthenium single-atom alloy for aqueous levulinic acid hydrogenation, ACS Catal. 11 (2021) 12146–12158, https://doi.org/10.1021/acscatal.1c03004.
[95] Y. Wang, H. Wu, J. Wang, K. Zhang, Y. Liu, Z. Wei, Highly efficient and recyclable nitrogen-doped mesoporous carbon-supported Ru catalyst for the reductive amination of levulinic acid/esters to pyrrolidones, ACS Sustain. Chem. Eng. 10 (2022) 17274–17285, https://doi.org/10.1021/acssuschemeng.2c05579.
[96] W. Gu, A. Pei, S. Zhang, F. Jiang, Y. Jia, Q. Qin, R. Du, Z. Li, R. Liu, Y. Qiu, K. Yan, Y. Zhao, C. Liang, G. Chen, Atomic-interface effect of single-atom Ru/CoO_x for selective electrooxidation of 5-hydroxymethylfurfural, ACS Appl. Mater. Interfaces 15 (2023) 28036–28043, https://doi.org/10.1021/acsami.3c03430.
[97] M. Zhu, X. Du, Y. Zhao, B. Mei, Q. Zhang, F. Sun, Z. Jiang, Y. Liu, H. He, Y. Cao, Ring-opening transformation of 5-hydroxymethylfurfural using a golden single-atomic-site palladium catalyst, ACS Catal. 9 (2019) 6212–6222, https://doi.org/10.1021/acscatal.9b00489.
[98] D. Chandra, Y. Inoue, M. Sasase, M. Kitano, A. Bhaumik, K. Kamata, H. Hosono, M. Hara, A high performance catalyst of shape-specific ruthenium nanoparticles for production of primary amines by reductive amination of carbonyl compounds, Chem. Sci. 9 (2018) 5949–5956, https://doi.org/10.1039/C8SC01197D.
[99] Q. Yang, Y. Jiang, H. Zhuo, E.M. Mitchell, Q. Yu, Recent progress of metal single-atom catalysts for energy applications, Nano Energy 111 (2023), 108404, https://doi.org/10.1016/j.nanoen.2023.108404.
[100] Y. Zhang, Y. Shen, Electrodeposition synthesis of free-standing metal/carbon felts electrodes for electrocatalytic hydrogenation of levulinic acid, Int. J. Hydrog. Energy 47 (2022) 22763–22774, https://doi.org/10.1016/j.ijhydene.2022.05.080.
[101] Y. Zhang, X. Wang, Y. Shen, High-performance bimetallic In-Pb for electrocatalytic hydrogenation of levulinic acid, Fuel 342 (2023), 127787, https://doi.org/10.1016/j.fuel.2023.127787.
[102] J. Luo, H. Yun, A.V. Mironenko, K. Goulas, J.D. Lee, M. Monai, C. Wang, V. Vorotnikov, C.B. Murray, D.G. Vlachos, P. Fornasiero, R.J. Gorte, Mechanisms for high selectivity in the hydrodeoxygenation of 5-hydroxymethylfurfural over PtCo nanocrystals, ACS Catal. 6 (2016) 4095–4104, https://doi.org/10.1021/acscatal.6b00750.
[103] Y. Nakagawa, K. Takada, M. Tamura, K. Tomishige, Total hydrogenation of furfural and 5-hydroxymethylfurfural over supported Pd–Ir alloy catalyst, ACS Catal. 4 (2014) 2718–2726, https://doi.org/10.1021/cs500620b.
[104] T. Yuan, M. Chu, K. Zhang, S. Jia, S. Han, J. Zhai, H. Wang, T. Xue, H. Wu, Efficient electrocatalytic reduction of levulinic acid to valeric acid on a nanocrystalline PbO-In_2O_3 catalyst, ChemistrySelect 7 (2022), https://doi.org/10.1002/slct.202201624.
[105] N.L.N. Broge, A.D. Bertelsen, F. Søndergaard-Pedersen, B.B. Iversen, Facile solvothermal synthesis of Pt–Ir–Pd–Rh–Ru–Cu–Ni–Co high-entropy alloy nanoparticles, Chem. Mater. 35 (2023) 144–153, https://doi.org/10.1021/acs.chemmater.2c02842.
[106] S. Ganguly, S. Paul, D. Khurana, T.S. Khan, P.K. Giri, C. Loha, S. Ghosh, Ternary Ni–Co–Se nanostructure for electrocatalytic oxidative value addition of biomass platform chemicals, ACS Appl. Energy Mater. 6 (2023) 5331–5341, https://doi.org/10.1021/acsaem.3c00313.
[107] H. Wu, J. Song, C. Xie, Y. Hu, P. Zhang, G. Yang, B. Han, Surface engineering in PbS via partial oxidation: towards an advanced electrocatalyst for reduction of levulinic acid to γ-valerolactone, Chem. Sci. 10 (2019) 1754–1759, https://doi.org/10.1039/C8SC03161D.
[108] Y. Qiu, L. Xin, D.J. Chadderdon, J. Qi, C. Liang, W. Li, Integrated electrocatalytic processing of levulinic acid and formic acid to produce biofuel intermediate valeric acid, Green. Chem. 16 (2014) 1305–1315, https://doi.org/10.1039/C3GC42254B.
[109] Y. Lu, C. Dong, Y. Huang, Y. Zou, Z. Liu, Y. Liu, Y. Li, N. He, J. Shi, S. Wang, Identifying the geometric site dependence of spinel oxides for the electrooxidation of 5–hydroxymethylfurfural, Angew. Chem. Int. Ed. 59 (2020) 19215–19221, https://doi.org/10.1002/anie.202007767.
[110] A.S. Touchy, S.M.A. Hakim Siddiki, K. Kon, K. Shimizu, Heterogeneous Pt catalysts for reductive amination of levulinic acid to pyrrolidones, ACS Catal. 4 (2014) 3045–3050, https://doi.org/10.1021/cs500757k.
[111] J. Liu, S. Tao, Selective electroreduction of levulinic acid by controlling the crystalline structure of PbO on electrodes, Appl. Surf. Sci. 616 (2023), 156464, https://doi.org/10.1016/j.apsusc.2023.156464.
[112] A. Phanopoulos, A.J.P. White, N.J. Long, P.W. Miller, Catalytic transformation of levulinic acid to 2-methyltetrahydrofuran using ruthenium– *N*-triphos complexes, ACS Catal. 5 (2015) 2500–2512, https://doi.org/10.1021/cs502025t.
[113] O. Mamun, E. Walker, M. Faheem, J.Q. Bond, A. Heyden, Theoretical investigation of the hydrodeoxygenation of levulinic acid to γ-valerolactone over Ru(0001), ACS Catal. 7 (2017) 215–228, https://doi.org/10.1021/acscatal.6b02548.
[114] T. Sekine, A. Yamura, K. Sugino, Mechanism of hydrocarbon formation in the electrolytic reduction of acetone in aqueous sulfuric acid, J. Electrochem. Soc. 112 (1965) 439, https://doi.org/10.1149/1.2423564.
[115] Y.J. Yeon, H.Y. Park, Y.J. Yoo, Enzymatic reduction of levulinic acid by engineering the substrate specificity of 3-hydroxybutyrate dehydrogenase, Bioresour. Technol. 134 (2013) 377–380, https://doi.org/10.1016/j.biortech.2013.01.078.
[116] M.A. Tike, V.V. Mahajani, Kinetics of Liquid-Phase Hydrogenation of Furfuryl Alcohol to Tetrahydrofurfuryl Alcohol over a Ru/TiO2 Catalyst, Ind. Eng. Chem. Res 46 (2007) 3275–3282, https://doi.org/10.1021/ie061137m.
[117] N. Shan, M.K. Hanchett, B. Liu, Mechanistic insights evaluating Ag, Pb, and Ni as electrocatalysts for furfural reduction from first-principles methods, J. Phys. Chem. C 121 (2017) 25768–25777, https://doi.org/10.1021/acs.jpcc.7b0677.
[118] S.K. Green, J. Lee, H.J. Kim, W.B. Kim, G.W. Huber, The electrocatalytic hydrogenation of furanic compounds in a continuous electrocatalytic membrane reactor, Green. Chem 15 (2013) 1869–1879, https://doi.org/10.1039/C3GC00090G.
[119] S. Sitthisa, T. Sooknoi, Y. Ma, P.B. Balbuena, D.E. Resasco, Kinetics and mechanism of hydrogenation of furfural on Cu/SiO_2 catalysts, J. Catal. 277 (2011) 1–13, https://doi.org/10.1016/j.jcat.2010.10.005.
[120] L. Gao, X. Wen, S. Liu, D. Qu, Y. Ma, J. Feng, Z. Zhong, H. Guan, L. Niu, Nickel-vanadium-cobalt ternary layered double hydroxide for efficient electrocatalytic upgrading of 5-hydroxymethylfurfural to 2,5-furancarboxylic acid at low potential, J. Mater. Chem. A 10 (2022) 21135–21141, https://doi.org/10.1039/D2TA03016K.
[121] W. Xu, C. Yu, J. Chen, Z. Liu, Electrochemical hydrogenation of biomass-based furfural in aqueous media by Cu catalyst supported on N-doped hierarchically porous carbon, Appl. Catal. B: Environ. 305 (2022), 121062, https://doi.org/10.1016/j.apcatb.2022.121062.
[122] J.A. Lopez-Ruiz, E. Andrews, S.A. Akhade, M.S. Lee, K. Koh, U. Sanyal, S.F. Yuk, A.J. Karkamkar, M.A. Derewinski, J. Holladay, V.A. Glezakou, R. Rousseau, O. Y. Gutiérrez, J.D. Holladay, Understanding the role of metal and molecular structure on the electrocatalytic hydrogenation of oxygenated organic compounds, ACS Catal. 9 (2019) 9964–9972, https://doi.org/10.1021/acscatal.9b02921.
[123] B. Zhao, M. Chen, Q. Guo, Y. Fu, Electrocatalytic hydrogenation of furfural to furfuryl alcohol using platinum supported on activated carbon fibers, Electrochimica Acta 135 (2014) 139–146, https://doi.org/10.1016/j.electacta.2014.04.164.Electrocatalytic hydrogenation of furfural to furfuryl alcohol using platinum supported on activated carbon fibers, Electrochimica Acta. (2014).
[124] P. Parpot, A.P. Bettencourt, G. Chamoulaud, K.B. Kokoh, E.M. Belgsir, Electrochemical investigations of the oxidation–reduction of furfural in aqueous medium application to electrosynthesis, Electrochim. Acta 49 (2004) 397–403, https://doi.org/10.1016/j.electacta.2003.08.021.
[125] A.M.S. Lucho, R.S. Goncalves, Effect of light on the electrocatalytic reduction of furfural on copper electrode in N,N-dimethylformamide, Catal. Commun 4 (2003) 641–645, https://doi.org/10.1016/j.catcom.2003.10.007.
[126] J.V. Steen, F. Boissou, M. Luhmer, C.B. Herman, S. Baranton, C. Coutanceau, T. Doneux, Furfural electroreduction in choline-glycerol deep eutectic solvent, J. Electroanal. Chem 933 (2023), 117269, https://doi.org/10.1016/j.jelechem.2023.117269.
[127] J.T. Brosnahan, Z. Zhang, Z. Yin, S. Zhang, Electrocatalytic reduction of furfural with high selectivity to furfuryl alcohol using AgPd alloy nanoparticles, 13 (2021) 2312–2316, doi:10.1039/d0nr07676g.
[128] R.J. Dixit, K. Bhattacharyya, V.K. Ramani, S. Basu, Electrocatalytic hydrogenation of furfural using non-noble-metal electrocatalysts in alkaline medium, Green. Chem 23 (2021) 4201–4212, https://doi.org/10.1039/D1GC00579K.
[129] S. Jung, E.J. Biddinger, Electrocatalytic Hydrogenation and Hydrogenolysis of Furfural and the Impact of Homogeneous Side Reactions of Furanic Compounds in Acidic Electrolytes, 4 (2016) 6500-6508, doi: 10.1021/acssuschemeng.6b01314.
[130] S. Jung, A.N. Karaiskakis, E.J. Biddinger, Enhanced activity for electrochemical hydrogenation and hydrogenolysis of furfural to biofuel using electrodeposited Cu catalysts, Catal. Today 323 (2019) 26–34, https://doi.org/10.1016/j.cattod.2018.09.011.
[131] L. Liu, Mechanism and kinetics of the electrocatalytic hydrogenation of furfural to furfuryl alcohol, J. Electroanal. Chem 804 (2017) 248–253, https://doi.org/10.1016/j.jelechem.2017.09.021.
[132] X. Li, J. Hu, T. Yang, X. Yang, J. Qu, C.M. Li, Efficient photocatalytic H_2-evolution coupled with valuable furfural-production on exquisite 2D/2D $LaVO_4$/g-C_3N_4 heterostructure, Nano Energy 92 (2022), 106714, https://doi.org/10.1016/j.nanoen.2021.106714.
[133] G. Chamoulaud, D. Floner, C. Moinet, C. Lamy, E.M. Belgsir, Biomass conversion II: simultaneous electrosyntheses of furoic acid and furfuryl alcohol on modified graphite felt electrodes, Electrochim. Acta 46 (2001) 2757–2760, https://doi.org/10.1016/S0013-4686(01)00507-2.
[134] D. Chu, Y. Hou, J. He, M. Xu, Y. Wang, S. Wang, J. Wang, L. Zha, Nano TiO_2 film electrode for electrocatalytic reduction of furfural in ionic liquids, J. Nanopart. Res. 7 (2009) 1805–1809, https://doi.org/10.1007/s11051-009-9610-5.
[135] P. Zhan, X. Liu, S. Zhang, Q. Zhu, H. Zhao, C. Ren, J. Zhang, L. Lu, D. Cai, P. Qin, Electroenzymatic reduction of furfural to furfuryl alcohol by an electron mediator and enzyme orderly assembled biocathode, ACS Appl. Mater. Interfaces 15 (2023) 12855–12863, https://doi.org/10.1021/acsami.3c00320.
[136] T. Lenk, V. Rueß, J. Gresch, U. Schröder, Exploring the electrochemical ring hydrogenation of furanic compounds, Green. Chem. 25 (2023) 3077–3085, https://doi.org/10.1039/D3GC00515A.
[137] R.S. Delima, M.D. Stankovic, B.P. MacLeod, A.G. Fink, M.B. Rooney, A. Huang, R. P. Jansonius, D.J. Dvorak, C.P. Berlinguette, Selective hydrogenation of furfural using a membrane reactor, Energy Environ. Sci. 15 (2022) 215–224, https://doi.org/10.1039/D1EE02818A.
[138] X. Li, L. Cong, Y. Wu, N. Lin, F. Liu, D. Xin, F. Han, J. Yang, W. Chen, H. Lin, Strategies for controlling gas evolution reactions to boost the divergent paired

electrochemical upgrading of furfural in acidic environment, Chem. Eng. J. 470 (2023), 144093, https://doi.org/10.1016/j.cej.2023.144093.
[139] X. Shang, Y. Yang, Y. Sun, Electrohydrodimerization of biomass-derived furfural generates a jet fuel precursor, Green. Chem. 22 (2020) 5395–5401, https://doi.org/10.1039/D0GC01720E.
[140] A.S. May, E.J. Biddinger, Strategies to control electrochemical hydrogenation and hydrogenolysis of furfural and minimize undesired side reactions, ACS Catal. 10 (2020) 3212–3221, https://doi.org/10.1021/acscatal.9b05531.
[141] M.D. Stankovic, J.F. Sperryn, R.S. Delima, C.C. Rupnow, M.B. Rooney, M. Stolar, C.P. Berlinguette, Electrochemical production of methyltetrahydrofuran, a biofuel for diesel engines, Energy Environ. Sci. 16 (2023) 3453–3461, https://doi.org/10.1039/D3EE01079A.
[142] Z. Yu, N. Ji, J. Xiong, X. Li, R. Zhang, L. Zhang, X. Lu, Ruthenium-nanoparticle-loaded hollow carbon spheres as nanoreactors for hydrogenation of levulinic acid: explicitly recognizing the void-confinement effect, Angew. Chem. Int. Ed. 60 (2021) 20786–20794, https://doi.org/10.1002/anie.202107314.
[143] Y. Kwon, K.J.P. Schouten, M.T.M. Koper, Electrocatalytic conversion of furanic compounds, ACS Catal 6 (2016) 6704–6717, https://doi.org/10.1021/acscatal.6b01861.
[144] J. Zhao, P.D. Tran, Y. Chen, J.S.C. Loo, J. Barber, Z.J. Xu, Achieving high electrocatalytic efficiency on copper: a low-cost alternative to platinum for hydrogen generation in water, ACS Catal. 5 (2015) 4115–4120, https://doi.org/10.1021/acscatal.5b00556.
[145] X. Chen, L. Zhang, B. Zhang, X. Guo, X. Mu, Highly selective hydrogenation of furfural to furfuryl alcohol over Pt nanoparticles supported on g-C_3N_4 nanosheets catalysts in water, Sci. Rep. 6 (2016), 28558, https://doi.org/10.1038/srep28558.
[146] W. Tolek, N. Nanthasanti, B. Pongthawornsakun, P. Praserthdam, J. Panpranot, Effects of TiO_2 structure and Co addition as a second metal on Ru-based catalysts supported on TiO_2 for selective hydrogenation of furfural to FA, Sci. Rep. 11 (2021), 9786, https://doi.org/10.1038/s41598-021-89082-x.
[147] X. Yuan, K. Lee, M.T. Bender, J.R. Schmidt, K. Choi, Mechanistic differences between electrochemical hydrogenation and hydrogenolysis of 5–hydroxymethylfurfural and their pH dependence, ChemSusChem 15 (2022), https://doi.org/10.1002/cssc.202200952.
[148] F.M.A. Geilen, T. vomStein, B. Engendahl, S. Winterle, M.A. Liauw, J. Klankermayer, W. Leitner, Highly selective decarbonylation of 5-(hydroxymethyl)furfural in the presence of compressed carbon dioxide, Angew. Chem. Int. Ed. 50 (2011) 6831–6834, https://doi.org/10.1002/anie.201007582.
[149] Y. Yang, T. Mu, Electrochemical oxidation of biomass derived 5-hydroxymethylfurfural (HMF): pathway, mechanism, catalysts and coupling reactions, Green. Chem. 23 (2021) 4228–4254, https://doi.org/10.1039/D1GC00914A.
[150] I. Scodeller, S. Mansouri, D. Morvan, E. Muller, K. deOliveiraVigier, R. Wischert, F. Jérôme, Synthesis of renewable *meta* -Xylylenediamine from biomass-derived furfural, Angew. Chem. Int. Ed. 57 (2018) 10510–10514, https://doi.org/10.1002/anie.201803828.
[151] S. Song, V. Fung Kin Yuen, L. Di, Q. Sun, K. Zhou, N. Yan, Integrating biomass into the organonitrogen chemical supply chain: production of pyrrole and D-proline from furfural, Angew. Chem. Int. Ed. 59 (2020) 19846–19850, https://doi.org/10.1002/anie.202006315.
[152] A. Ranoux, K. Djanashvili, I.W.C.E. Arends, U. Hanefeld, 5-Hydroxymethylfurfural synthesis from hexoses is autocatalytic, ACS Catal. 3 (2013) 760–763, https://doi.org/10.1021/cs400099a.
[153] Y. Kwon, Y.Y. Birdja, S. Raoufmoghaddam, M.T.M. Koper, Electrocatalytic hydrogenation of 5-hydroxymethylfurfural in acidic solution, ChemSusChem 8 (2015) 1745–1751, https://doi.org/10.1002/cssc.201500176.
[154] M. Kim, Y. Su, A. Fukuoka, E.J.M. Hensen, K. Nakajima, Aerobic oxidation of 5–(hydroxymethyl)furfural cyclic acetal enables selective furan-2,5–dicarboxylic acid formation with CeO_2-supported gold catalyst, Angew. Chem. Int. Ed. 57 (2018) 8235–8239, https://doi.org/10.1002/anie.201805457.
[155] S. Li, X. Sun, Z. Yao, X. Zhong, Y. Cao, Y. Liang, Z. Wei, S. Deng, G. Zhuang, X. Li, J. Wang, Biomass valorization via paired electrosynthesis over vanadium nitride-based electrocatalysts, Adv. Funct. Mater. 29 (2019), 1904780, https://doi.org/10.1002/adfm.201904780.
[156] S. Xu, P. Zhou, Z. Zhang, C. Yang, B. Zhang, K. Deng, S. Bottle, H. Zhu, Selective oxidation of 5-hydroxymethylfurfural to 2,5-furandicarboxylic acid using O_2 and a photocatalyst of co-thioporphyrazine bonded to g-C_3N_4, J. Am. Chem. Soc. 139 (2017) 14775–14782, https://doi.org/10.1021/jacs.7b08861.
[157] M.C. Allen, A.J. Hoffman, T. Liu, M.S. Webber, D. Hibbitts, T.J. Schwartz, Highly Selective Cross-Etherification of 5-Hydroxymethylfurfural with Ethanol, ACS Catal. 10 (2020) 6771–6785, https://doi.org/10.1021/acscatal.0c01328.
[158] G. Piao, S.H. Yoon, H.G. Cha, D.S. Han, H. Park, Porous dendritic BiSn electrocatalysts for hydrogenation of 5-hydroxymethylfurfural, J. Mater. Chem. A. 10 (2022) 24006–24017, https://doi.org/10.1039/D2TA05969J.
[159] S.R. Kubota K.S. Choi Electrochemical Valorization of Furfural to Maleic Acid 6 2018 9596 9600 doi: 10.1021/acssuschemeng.8b02698.
[160] M.D. Stankovic, J.F. Sperryn, R.S. Delima, C.C. Rupnow, M.B. Rooney, M. Stolar, C.P. Berlinguette, Electrochemical production of methyltetrahydrofuran, a biofuel for diesel engines, Energy Environ. Sci. 16 (2023) 3453–3461, https://doi.org/10.1039/D3EE01079A.
[161] R. Kawasumi, S. Narita, K. Miyamoto, K. Tominaga, R. Takita, M. Uchiyama, One-step conversion of levulinic acid to succinic acid using I_2/*t*-BuOK system: the iodoform reaction revisited, Sci. Rep. 7 (2017), 17967, https://doi.org/10.1038/s41598-017-17116-4.
[162] J.J. Roylance, K.-S. Choi, Electrochemical reductive biomass conversion: direct conversion of 5-hydroxymethylfurfural (HMF) to 2,5-hexanedione (HD) via reductive ring-opening, Green. Chem. 18 (2016) 2956–2960, https://doi.org/10.1039/C6GC00533K.
[163] X. Wu, S. Xie, H. Zhang, Q. Zhang, B.F. Sels, Y. Wang, Metal sulfide photocatalysts for lignocellulose valorization, Adv. Mater. 33 (2021), 2007129, https://doi.org/10.1002/adma.202007129.
[164] J.C. Serrano-Ruiz, J.A. Dumesic, Catalytic routes for the conversion of biomass into liquid hydrocarbon transportation fuels, Energy Environ. Sci. 4 (2011) 83–99, https://doi.org/10.1039/C0EE00436G.
[165] Y. Román-Leshkov, J.N. Chheda, J.A. Dumesic, Phase modifiers promote efficient production of hydroxymethylfurfural from fructose, Science 312 (2006) 1933–1937, https://doi.org/10.1126/science.1126337.
[166] Z. An, J. Li, Recent advances in the catalytic transfer hydrogenation of furfural to furfuryl alcohol over heterogeneous catalysts, Green. Chem. 24 (2022) 1780–1808, https://doi.org/10.1039/D1GC04440K.
[167] Y. Hioki, M. Costantini, J. Griffin, K.C. Harper, M.P. Merini, B. Nissl, Y. Kawamata, P.S. Baran, Overcoming the limitations of Kolbe coupling with waveform-controlled electrosynthesis, Science 380 (2023) 81–87, https://doi.org/10.1126/science.adf4762.
[168] W. Liu, L. Dang, Z. Xu, H. Yu, S. Jin, G.W. Huber, Electrochemical oxidation of 5-hydroxymethylfurfural with NiFe Layered Double Hydroxide (LDH) nanosheet catalysts, ACS Catal. 8 (2018) 5533–5541, https://doi.org/10.1021/acscatal.8b01017.
[169] S. Barwe, J. Weidner, S. Cychy, D.M. Morales, S. Dieckhöfer, D. Hiltrop, J. Masa, M. Muhler, W. Schuhmann, Electrocatalytic oxidation of 5-(hydroxymethyl) furfural using high-surface-area nickel boride, Angew. Chem. Int. Ed. 57 (2018) 11460–11464, https://doi.org/10.1002/anie.201806298.
[170] Y. Qiu, L. Xin, Y. Li, I.T. McCrum, F. Guo, T. Ma, Y. Ren, Q. Liu, L. Zhou, S. Gu, M. J. Janik, W. Li, BCC-phased PdCu alloy as a highly active electrocatalyst for hydrogen oxidation in alkaline electrolytes, J. Am. Chem. Soc. 140 (2018) 16580–16588, https://doi.org/10.1021/jacs.8b08356.
[171] Y. Liu, L. Li, J. Wang, Y. Fei, N. Liu, G. Wu, Effect of carbon nanotube addition in two sizing agents on interfacial properties of carbon fiber/polycarbonate composites, N. Carbon Mater. 36 (2021) 639–648, https://doi.org/10.1016/S1872-5805(21)60035-5.
[172] J.J. Roylance, T.W. Kim, K.S. Choi, Efficient and selective electrochemical and photoelectrochemical reduction of 5-hydroxymethylfurfural to 2,5-bis(hydroxymethyl)furan using water as the hydrogen source, ACS Catal. 6 (2016) 1840–1847, https://doi.org/10.1021/acscatal.5b02586.
[173] G. Sanghez De Luna, P.H. Ho, A. Sacco, S. Hernández, J.J. Velasco-Vélez, F. Ospitali, A. Paglianti, S. Albonetti, G. Fornasari, P. Benito, AgCu bimetallic electrocatalysts for the reduction of biomass-derived compounds, ACS Appl. Mater. Interfaces 13 (2021) 23675–23688, https://doi.org/10.1021/acsami.1c02896.
[174] X.H. Chadderdon, D.J. Chadderdon, T. Pfennig, B.H. Shanks, W. Li, Paired electrocatalytic hydrogenation and oxidation of 5-(hydroxymethyl)furfural for efficient production of biomass-derived monomers, Green. Chem. 21 (2019) 6210–6219, https://doi.org/10.1039/C9GC02264C.
[175] H. Li, T. Zhang, M. Peng, Q. Zhang, J. Liu, J. Zhang, Y. Fu, W. Li, Highly selective electrocatalytic hydrogenation of 5-hydroxymethylfurfural to 2,5-dihydroxymethylfuran over AgCu nanoalloys, Int. J. Hydrog. Energy 47 (2022) 28904–28914, https://doi.org/10.1016/j.ijhydene.2022.06.211.
[176] X. Yue, W. Zhao, S. Wang, Y. Zou, Selective electrocatalytic hydrogenation of 5-hydroxymethyl- furfural to 2,5-dihydroxymethylfuran on bimetallic PdCu alloy, Chin. J. Struct. Chem. 41 (2022) 2205063–2205069, https://doi.org/10.14102/j.cnki.0254-5861.2022-0074.
[177] Z. Zhao, X. Luo, J. Peng, S. Wang, T. Guo, H. Zheng, Complementary metal–semiconductor interactions on Ag-TiO_2 NT heterojunction for the efficient electrochemical reduction of 5-hydroxymethylfurfural, Sustain. Energy Fuels 6 (2022) 5281–5289, https://doi.org/10.1039/D2SE01101H.
[178] L. Zhang, F. Zhang, F.C. Michel, A.C. Co, Efficient electrochemical hydrogenation of 5–hydroxymethylfurfural to 2,5–bis(hydroxymethyl)furan on Ag-displaced nanotextured Cu catalysts, ChemElectroChem 6 (2019) 4739–4749, https://doi.org/10.1002/celc.201900640.
[179] S. Panigrahy, R. Mishra, P. Panda, M. Kempasiddaiah, S. Barman, Carbon-supported Ag nanoparticle aerogel for electrocatalytic hydrogenation of 5-(hydroxymethyl)furfural to 2,5-hexanedione under acidic conditions, ACS Appl. Nano Mater. 5 (2022) 8314–8323, https://doi.org/10.1021/acsanm.2c01388.
[180] Y. Kwon, E. deJong, S. Raoufmoghaddam, M.T.M. Koper, Electrocatalytic hydrogenation of 5-hydroxymethylfurfural in the absence and presence of glucose, ChemSusChem 6 (2013) 1659–1667, https://doi.org/10.1002/cssc.201300443.
[181] B. Muchharla, M. Dikshit, U. Pokharel, R. Garimella, A. Adedeji, K. Kumar, W. Cao, H. Elsayed-Ali, K.K. Sadasivuni, N.A. Al-Dhabi, S. Kumar, B. Kumar, Reduced metal nanocatalysts for selective electrochemical hydrogenation of biomass-derived 5-(hydroxymethyl)furfural to 2,5-bis(hydroxymethyl)furan in ambient conditions, Front. Chem. 11 (2023), 1200469, https://doi.org/10.3389/fchem.2023.1200469.
[182] G. Sanghez De Luna, P.H. Ho, A. Lolli, F. Ospitali, S. Albonetti, G. Fornasari, P. Benito, Ag electrodeposited on Cu Open-Cell foams for the selective electroreduction of 5–hydroxymethylfurfural, ChemElectroChem 7 (2020) 1238–1247, https://doi.org/10.1002/celc.201902161.
[183] G.S. de Luna A. Sacco S. Hernandez F. Ospitali S. Albonetti G. Fornasari P. Benito Insights into the electrochemical reduction of 5–Hydroxymethylfurfural at high current densities 15 2022 doi: 10.1002/cssc.202102504.
[184] G.S. De Luna, P. Zeller, E. Öztuna, F. Maluta, A. Canciani, F. Ospitali, P.H. Ho, A. Paglianti, A. Knop-Gericke, G. Fornasari, J.J. Velasco-Vélez, P. Benito, In situ

development of a 3D Cu-CeO_2 catalyst selective in the electrocatalytic hydrogenation of biomass furanic compounds, ACS Catal. 13 (2023) 12737–12745, https://doi.org/10.1021/acscatal.3c03363.
[185] W. Zhang, Y. Qi, Y. Zhao, W. Ge, L. Dong, J. Shen, H. Jiang, C. Li, Rh-dispersed Cu nanowire catalyst for boosting electrocatalytic hydrogenation of 5-hydroxymethylfurfural, Sci. Bull. 68 (2023) 2190–2199, https://doi.org/10.1016/j.scib.2023.07.036.
[186] M. Li, T. Zheng, D. Lu, S. Dai, X. Chen, X. Pan, D. Dong, R. Weng, G. Xu, F. Wang, Facet effect on the reconstructed Cu-catalyzed electrochemical hydrogenation of 5-hydroxymethylfurfural (HMF) towards 2,5-bis(hydroxymethy)furan (BHMF), J. Energy Chem. 84 (2023) 101–111, https://doi.org/10.1016/j.jechem.2023.05.003.
[187] M.T. Bender, X. Yuan, M.K. Goetz, K.S. Choi, Electrochemical hydrogenation, hydrogenolysis, and dehydrogenation for reductive and oxidative biomass upgrading using 5-hydroxymethylfurfural as a model system, ACS Catal. 12 (2022) 12349–12368, https://doi.org/10.1021/acscatal.2c03606.
[188] M.V. Morales, J.M. Conesa, A. Guerrero-Ruiz, I. Rodríguez-Ramos, Tunable selectivity of Ni catalysts in the hydrogenation reaction of 5-hydroxymethylfurfural in aqueous media: role of the carbon supports, Carbon 182 (2021) 265–275, https://doi.org/10.1016/j.carbon.2021.06.007.
[189] L. Bui, H. Luo, W.R. Gunther, Y. Román-Leshkov, Domino reaction catalyzed by zeolites with brønsted and lewis acid sites for the production of γ-valerolactone from furfural, Angew. Chem. Int. Ed. 52 (2013) 8022–8025, https://doi.org/10.1002/anie.201302575.
[190] G. Meng, K. Ji, W. Zhang, Y. Kang, Y. Wang, P. Zhang, Y. Wang, J. Li, T. Cui, X. Sun, T. Tan, D. Wang, Y. Li, Tandem catalyzing the hydrodeoxygenation of 5-hydroxymethylfurfural over a Ni_3Fe intermetallic supported Pt single-atom site catalyst, Chem. Sci. 12 (2021) 4139–4146, https://doi.org/10.1039/D0SC05983H.
[191] H. Liu, T.H. Lee, Y. Chen, E.W. Cochran, W. Li, Paired electrolysis of 5-(hydroxymethyl)furfural in flow cells with a high-performance oxide-derived silver cathode, Green. Chem. 23 (2021) 5056–5063, https://doi.org/10.1039/D1GC00988E.
[192] D.K. Lee, S.R. Kubota, A.N. Janes, M.T. Bender, J. Woo, J.R. Schmidt, K. Choi, The impact of 5–hydroxymethylfurfural (HMF)-metal interactions on the electrochemical reduction pathways of HMF on various metal electrodes, ChemSusChem 14 (2021) 4563–4572, https://doi.org/10.1002/cssc.202101037.
[193] R. Zhu, A. Chatzidimitriou, B. Liu, D.J. Kerwood, J.Q. Bond, Understanding the Origin of maleic anhydride selectivity during the oxidative scission of levulinic acid, ACS Catal. 10 (2020) 1555–1565, https://doi.org/10.1021/acscatal.9b04289.
[194] N. Heidary, N. Kornienko, Electrochemical biomass valorization on gold-metal oxide nanoscale heterojunctions enables investigation of both catalyst and reaction dynamics with *operando* surface-enhanced Raman spectroscopy, Chem. Sci. 11 (2020) 1798–1806, https://doi.org/10.1039/D0SC00136H.
[195] R.S. Delima, M.D. Stankovic, B.P. MacLeod, A.G. Fink, M.B. Rooney, A. Huang, R. P. Jansonius, D.J. Dvorak, C.P. Berlinguette, Selective hydrogenation of furfural using a membrane reactor, Energy Environ. Sci. 15 (2022) 215–224, https://doi.org/10.1039/D1EE02818A.
[196] J. Zheng, X. Chen, X. Zhong, S. Li, T. Liu, G. Zhuang, X. Li, S. Deng, D. Mei, J. G. Wang, Hierarchical porous NC@CuCo nitride nanosheet networks: highly efficient bifunctional electrocatalyst for overall water splitting and selective electrooxidation of benzyl alcohol, Adv. Funct. Mater. 27 (2017), 1704169, https://doi.org/10.1002/adfm.201704169.
[197] X. Lu, K. Wu, B. Zhang, J. Chen, F. Li, B. Su, P. Yan, J. Chen, W. Qi, Highly efficient electro-reforming of 5–hydroxymethylfurfural on vertically oriented nickel nanosheet/carbon hybrid catalysts: structure–function relationships, Angew. Chem. Int. Ed. 60 (2021) 14528–14535, https://doi.org/10.1002/anie.202102359.
[198] S.A. Akhade, N. Singh, O.Y. Gutiérrez, J. Lopez-Ruiz, H. Wang, J.D. Holladay, Y. Liu, A. Karkamkar, R.S. Weber, A.B. Padmaperuma, M.-S. Lee, G.A. Whyatt, M. Elliott, J.E. Holladay, J.L. Male, J.A. Lercher, R. Rousseau, V.A. Glezakou, Electrocatalytic hydrogenation of biomass-derived organics: a review, Chem. Rev. 120 (2020) 11370–11419, https://doi.org/10.1021/acs.chemrev.0c00158.
[199] F.W.S. Lucas, R.G. Grim, S.A. Tacey, C.A. Downes, J. Hasse, A.M. Roman, C. A. Farberow, J.A. Schaidle, A. Holewinski, Electrochemical routes for the valorization of biomass-derived feedstocks: from chemistry to application, ACS Energy Lett. (2021) 1205–1270, https://doi.org/10.1021/acsenergylett.0c02692.
[200] K. Li, Y. Sun, Electrocatalytic upgrading of biomass-derived intermediate compounds to value-added products, Chem. A Eur. J. 24 (2018) 18258–18270, https://doi.org/10.1002/chem.201803319.
[201] L. Zhang, T.U. Rao, J. Wang, D. Ren, S. Sirisommboonchai, C. Choi, H. Machida, Z. Huo, K. Norinaga, A review of thermal catalytic and electrochemical hydrogenation approaches for converting biomass-derived compounds to high-value chemicals and fuels, Fuel Process. Technol. 226 (2022), 107097, https://doi.org/10.1016/j.fuproc.2021.107097.
[202] S. Kar, Q. Zhou, Y. Ben-David, D. Milstein, Catalytic furfural/5-hydroxymethyl furfural oxidation to furoic acid/furan-2,5-dicarboxylic acid with H_2 production using alkaline water as the formal oxidant, J. Am. Chem. Soc. 144 (2022) 1288–1295, https://doi.org/10.1021/jacs.1c10908.
[203] T. Peng, T. Zhuang, Y. Yan, J. Qian, G.R. Dick, J. Behaghel De Bueren, S.F. Hung, Y. Zhang, Z. Wang, J. Wicks, F.P. Garcia De Arquer, J. Abed, N. Wang, A. Sedighian Rasouli, G. Lee, M. Wang, D. He, Z. Wang, Z. Liang, L. Song, X. Wang, B. Chen, A. Ozden, Y. Lum, W.R. Leow, M. Luo, D.M. Meira, A.H. Ip, J. S. Luterbacher, W. Zhao, E.H. Sargent, Ternary alloys enable efficient production of methoxylated chemicals via selective electrocatalytic hydrogenation of lignin monomers, J. Am. Chem. Soc. 143 (2021) 17226–17235, https://doi.org/10.1021/jacs.1c08348.
[204] Y. Feng, K. Yang, R.L. Smith, X. Qi, Metal sulfide enhanced metal–organic framework nanoarrays for electrocatalytic oxidation of 5-hydroxymethylfurfural to 2,5-furandicarboxylic acid, J. Mater. Chem. A 11 (2023) 6375–6383, https://doi.org/10.1039/D2TA09426F.
[205] J. Du, D. Xiang, K. Zhou, L. Wang, J. Yu, H. Xia, L. Zhao, H. Liu, W. Zhou, Electrochemical hydrogen production coupled with oxygen evolution, organic synthesis, and waste reforming, Nano Energy 104 (2022), 107875, https://doi.org/10.1016/j.nanoen.2022.107875.